THE INFLUENCE OF WATER COMPOSITION ON THE PITTING BEHAVIOUR OF NEWLY DEVELOPED CORROSION RESISTANT STEELS

by

M. H. COTTERRELL

A thesis submitted to the Faculty of Engineering, University of Cape Town in fulfilment of the degree of Master of Science in Applied Science.

Department of Materials Engineering, University of Cape Town

February 1988

ACKNOWLEDGEMENTS

I would like to express my appreciation to the following people who have helped me during this research project:

My supervisor, Professor Colin Allen, whose encouragement, help and guidance helped to make the project a rewarding experience.

Mr. Robert Noel for being an able supervisor before leaving to work in Mauritius.

Mrs. Penny Park-Ross for her capable assistance in the laboratory, and in proof reading the final thesis.

Mr. Nick Dreze, Mr. Glen Newins and Reg Hendricks for their technical expertise in the workshop.

Mr. James Petersen for his photographic expertise and willing help in many areas of work.

Mrs. Helgard Bohm for her technical assistance and for the help in preparing the graphics used in this thesis.

Mr. Dave Dean for his electronics expertise and help in the development and maintenance of equipment.

All my fellow students.

This thesis was based the results of the collaborative programme of work undertaken as part of the research and development programme of the Research Organization of the Chamber of Mines of South Africa.

I would like to thank the Chamber of Mines Research Organization and the CSIR for their financial support for the project.

ABSTRACT

The mechanisation of the working stopes in South African gold mines has required the introduction of a fundamentally new technology, hydro-power, in which machines are powered hydraulically using mine water fed from above ground. Mine water is aggressive and has a variable acidity and pH, and contains high concentrations of sulphate, chloride and nitrate ions.

In order to minimise the pitting corrosion of piping and stoping machinery a compromise between selecting a suitable corrosion resistant material and treating the mine water to an acceptable level of corrosiveness is being sought.

A potentiodynamic polarization technique has been used to determine the pitting corrosion behaviour of the martensitic stainless steel AISI 431. The results were used to design a shortened testing programme to determine the pitting corrosion behaviour of the newly developed corrosion resisting steels, Alloy 1210, 3CR12 and Alloy 825. Experimental E-pH diagrams were constructed for Alloy 1210, 3CR12 and Alloy 825 and compared with an existing E-pH diagram for AISI 431. Alloy 1210 and 3CR12 showed a larger active range than AISI 431, while Alloy 825 was only passive over a small potential range above pH 6.

The presence of chloride ions was found to cause localized breakdown of the passive layer and result in pitting corrosion in each of the alloys. The chloride concentration at which the breakdown of passivity changed from being uniform (transpassivity) to localized (pitting) was defined as the critical chloride concentration, $[Cl^-]_{crit}$. The corrosion potential, the pitting or breakdown potential and the protection potential have been plotted as a function of the chloride concentration for solutions with various ratios of sulphate to nitrate for each of the alloys and additionally at a range of pH values for AISI 431.

In the case of AISI 431 increasing sulphate and nitrate concentrations inhibited pitting corrosion by increasing the $[Cl^-]_{crit}$, and nitrate was found to be a more efficient inhibitor than sulphate. Sulphates and nitrates were found to act synergistically in inhibiting pitting corrosion and thereby increasing the $[Cl^-]_{crit}$. In sulphate plus nitrate solutions, increasing the pH increased the $[Cl^-]_{crit}$, while decreasing the pH decreased the $[Cl^-]_{crit}$.

In the case of Alloy 1210 and 3CR12 sulphates plus nitrates inhibited pitting corrosion and by increasing the sulphate concentration in nitrate solutions the $[Cl^-]_{crit}$ was increased. For 3CR12, increasing the sulphate concentration above 1000 ppm resulted in no further increase of the $[Cl^-]_{crit}$. The $[Cl^-]_{crit}$ was increased for Alloy 825 with increasing sulphate concentrations in nitrate solutions, however the increased sulphate concentration reduced the stability of the passive layer and increased the rate of general corrosion.

AISI 431 showed the best pitting corrosion resistance, Alloy 825 showed the worst and Alloy 1210 and 3CR12 showed a similar pitting corrosion resistance. The results have been discussed in terms of their practical application to the real mine water environment. Attention has been drawn to the complexity of the variables in real mine water and the importance of using the experimentally determined finding with caution.

TABLE OF CONTENTS

CHAPTER 1

INTRODUCTION

1.1 AIMS AND OBJECTIVES

Corrosion and abrasion either acting individually or synergistically constitutes a major component of the cost of plant maintenance and replacement in the gold mining industry in South Africa. Considerable effort is currently being made by the Chamber of Mines Research Organization (C.O.M.R.O.) to develop new engineering materials, resistant to both corrosion and abrasion, which can be universally utilised for pipe work and in the mechanisation of mining operations. However, there is little quantitative information available on the corrosion behaviour of these newly developed stainless type steels in mine water. This present work is an attempt to assess the pitting corrosion behaviour of these steels in solutions containing a range of corrosive and inhibitive ions which are normally found in mine waters.

The specific objectives of this study were :

(1) To continue in the evaluation of the effect of ions commonly encountered in mine water that Capendale (1985) began, by establishing the effect of sulphate ions and the interactive effect of sulphate plus nitrate ions and pH, on the pitting corrosion behaviour of AISI 431 in chloride solutions.

(2) To develop a shortened testing programme to determine the pitting corrosion behaviour of other alloys based upon the experimental results and findings obtained from the extensive testing of AISI 431.

(3) To use the developed testing programme to determine the pitting corrosion behaviour of three development alloys, namely Alloy 1210, 3CR12 and Alloy 825.

(4) To attempt to elucidate the mechanisms contributing to pitting behaviour in these alloys.

1.2 THE HYDRO-POWER CONCEPT

The mechanisation of the working stopes has also required the introduction of a fundamentally new technology in which the machines are powered hydraulically using mine water fed from the surface. 'Hydro-power' is the term applied to the concept of using high pressure water for a dual purpose in deep level mining, namely, for cooling the

workings and for powering machinery on the stopes. The existing large quantities of chilled water used to cool the mines are now being used as a source of energy to drive water-powered hydraulic machinery. This means that one energy distribution system provides both hydraulic and cooling power to the mining areas - thus satisfying both needs. The simplicity of such a system, together with the reduction in energy losses (inherent in any power system when converting energy from one state to another) make it an attractive proposition. A pilot hydro-power system has been employed at Kloof gold mine and has demonstrated the feasibility of the hydro-power concept (C.O.M.R.O. Information leaflet no. 4,(1986)). A schematic diagram of the pilot hydro-power system is shown below in figure 1.1.

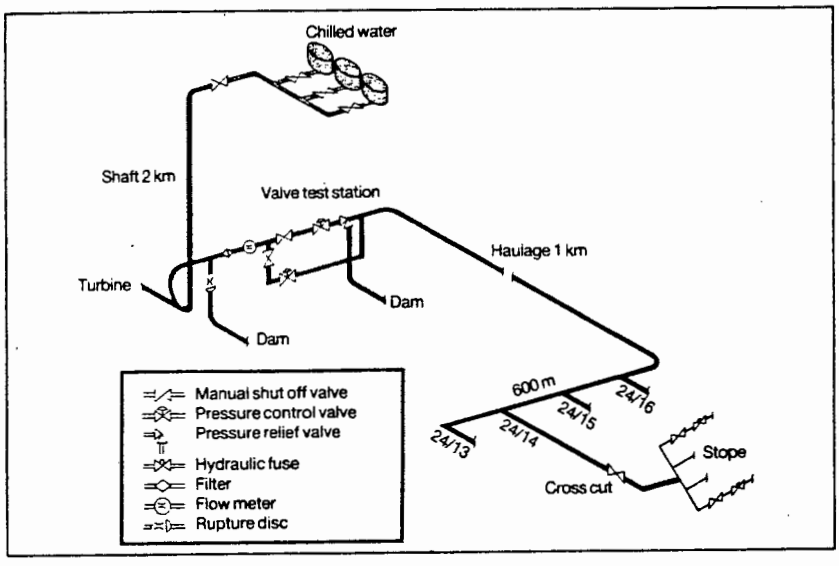

Figure 1.1 : Schematic diagram of the pilot hydro-power system at Kloof gold mine. The system utilizes the hydrostatic head in an existing 2000 m shaft column and distributes pressure at a pressure of 17 MPa to three production stopes. (after C.O.M.R.O. Information leaflet no. 4, (1986))

Figure 1.2 shows the typical water requirements for both cooling and machine powering for a working panel which is 35 m long. It can be seen that at a depth of 1500 m, a surplus of hydraulic power is available.

The development of hydraulically powered hand held rockdrills to replace pneumatic machines used traditionally in stoping is the single most promising approach to improving productivity in conventional gold mining. While rockdrills operating on emulsions of 98% water are in an advanced stage of development, those operating on plain water are still the subject of much development and are at a prototype form at this stage. It is necessary to utilize the very latest developments in materials technology to ensure that components have sufficient resistance to corrosion, impact, cavitation erosion, and sliding wear when lubricated by water (Brown and Wymer, (1986)).

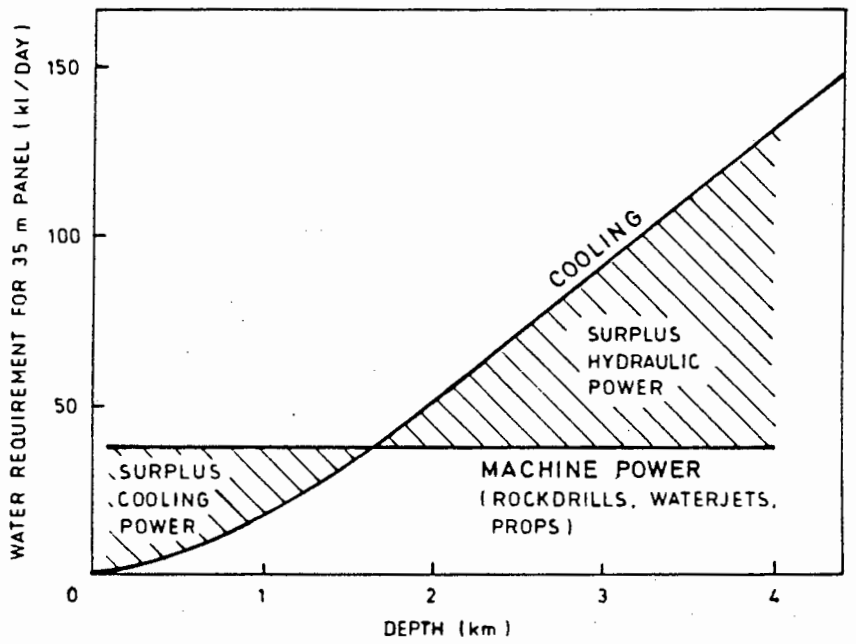

Figure 1.2 : The graph shows the typical water requirements for both cooling and machine powering. (after C.O.M.R.O. Information leaflet no. 4, 1986)

1.3 WATER TREATMENT AND THE HYDRO-POWER WATER CYCLE

The South African gold-mining industry uses 4000 litres of water per second. The high cost of obtaining water from the surface and the vast consumption has necessitated the use of fissure water and the recycling of water wherever possible. The hydro-power concept requires that water be recycled continuously in order that sufficient water is available to maintain the system. Unfortunately, recycling leads to contamination of the water. These sources of contamination are shown in figure 1.3.

For instance oxidation of pyrite ore by chemical and bacterial action results in the reduction of pH and an increase of the sulphate concentration. Lime is added to the water to increase the pH, and this increases the total dissolved solids (T.D.S.) further. The nitrate concentration is increased by the mixing of blasting fumes and products with the water. The chloride concentration is increased due to the mixing of the mine water with fissure water. In addition, the T.D.S. is further increased due to evaporation, which is estimated at 10 percent per cycle.

Water treatment practices commonly used for the treatment of mine service waters include (White, (1985)) :

(i) Biocidal treatment to avoid biological fouling,
(ii) Sterilisation for potability,
(iii) Water conditioning for neutralisation and clarification,
(iv) Sequestration or anti-fouling for the prevention of scale,
(v) Addition of corrosion inhibitors.
(vi) Filtration of abrasive solid particles.

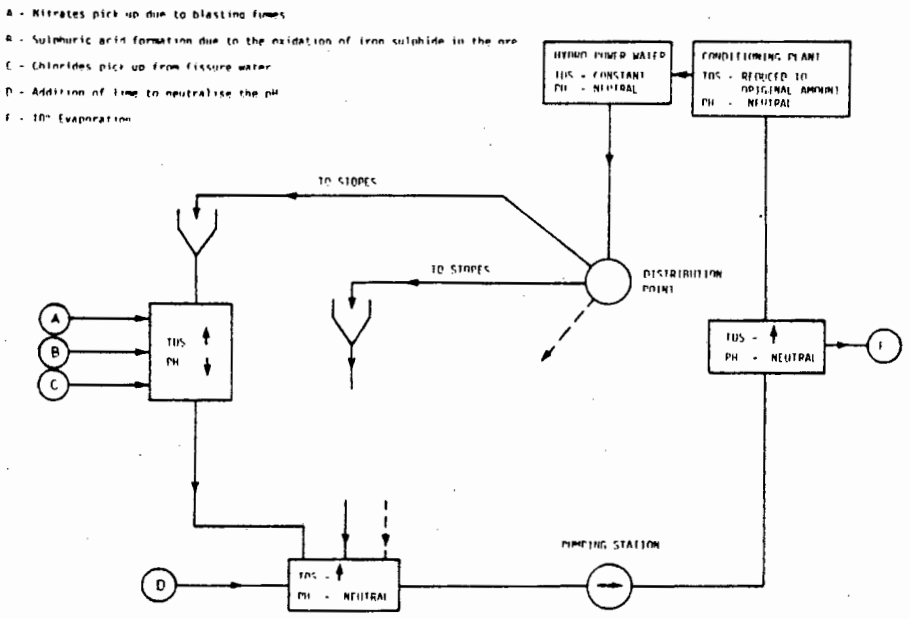

Figure 1.3 : The hydro-power water cycle indicating sources of water contamination (after Capendale, (1985))

The type of water treatment selected is determined by the intended use for the water after it has been treated. The water treatment required in a hydro-power system would clearly be dependent on the materials utilised in the system. It would be necessary, for example, to maintain aggressive ion/inhibitive ion ratio at a level that would avoid corrosion problems within the system. Likewise, the pH and other variables would have to be carefully controlled.

1.4 CORROSIVITY OF MINE WATERS

Rawat (1976) summarised the factors affecting the corrosivity of mine waters as follows :

(a) dissolved gasses (oxygen, nitrogen, carbon dioxide, ammonia, sulphurous gasses etc.),

(b) mineral constituents, including hardness salts, sodium salts (chloride, sulphate, nitrate, bicarbonate, etc.), salts of heavy metals, and silica,

(c) organic matter of animal and vegetable origin, and

(d) microbiological forms, various types of algae, and slime forming bacteria.

A survey of the water in gold mines conducted by the Chamber of Mines indicated that the composition of the waters varied widely from one mine to another. Furthermore variations were found in the composition of water sampled at different points in a particular mine as well as in samples taken from the same point at different times (Capendale, (1985)). Appendix A gives a complete analysis of a wide range of mine waters. Table 1.1 lists the average concentrations of the predominant ions expected to influence the corrosion resistance of stainless steels, together with the pH, conductivity and total dissolved solids of some selected mines. All of the mines are in the Orange Free State or the Transvaal.

Table 1.1 : Mine water compositions (Chamber of Mines Research Organization, (1983))

MINE	pH	CONDUCTIVITY mS/m	TOTAL DISSOLVED SOLIDS (ppm)	Cl^- (ppm)	SO_4^{2-} (ppm)	NO_3^- (ppm)	Na^+ (ppm)
Mine A	6.0	252	1944	85	1035	258	263
Mine B	6.5	490	3038	1203	265	144	790
Mine C	6.1	614	3790	1865	153	65	1040
Mine D	6.5	255	2184	39	82	327	20
Mine E	6.3	700	4975	1812	821	228	1130
Mine F	5.8	1200	10870	2766	2008	1650	1520
Mine G	6.3	192	4180	1220	901	191	900
Mine H	7.6	175	1820	103	677	188	104
Mine I	6.9	240	2824	36	1586	10	70
Mine J	6.5	850	6756	1564	2176	1185	1480

1.4.1 Dissolved Gases

The oxygen reduction reaction is the predominant cathodic reaction leading to the corrosion of ferrous metals in nearly neutral solutions. Thus the concentration of oxygen has a strong influence on the rate of corrosion. Oxygen concentrations were found to be generally above 5 mg/l in circulating mine water, which is close to 100% saturation. At this level it is assumed that the corrosion reaction will be controlled by the rate of oxygen diffusion to the surface of the metal and not the bulk oxygen concentration in the water (Higginson and White, (1983)). Low concentrations of oxygen were found in fissure water, which had high sulphide concentrations. Stagnant water will have low oxygen concentrations.

1.4.2 Aggressive and Inhibitive Ions

Chloride ions are acknowledged to be a major contributor in the corrosion of mild steel and the localized breakdown of passive layers on stainless steel. The chloride ion concentration is increased by the combination of fissure water into the mine water. Higginson and White (1983) report that sulphate and nitrate ions increase the corrosion rate of mild steel, although their synergistic effect together with chloride ions was not documented. However sulphate and nitrate ions are widely accepted as having an inhibitive effect on the localised breakdown of passivity of stainless steel in the presence of chloride.

1.4.3 Organic Matter

The types of organic matter vary widely, and they may be in suspension, or in colloidal or true solution. Very rapid rates of corrosion of mild steel may result when abstracted organic acids are present in soft water.

1.4.4 Microbial matter

Bacterial action on metals has been classified into the following types (Moreau and Brison, (1972)) :

(i) Those that inhibit corrosion
(ii) Those that cause limited attack, and
(iii) Those that catalyse corrosion reactions.

Thiobacillus species produce H_2SO_4, which increases the corrosivity of the water through the oxidation of sulphur. Ferrobacillus ferro-oxydans are usually present with thiobacillus and can cause the accelerated oxidation of pyrite at low pH values. This increases the corrosivity of the water.

CHAPTER 2

LITERATURE REVIEW

2.1 INTRODUCTION

Stainless steels derive their outstanding corrosion resistance from the presence of a passive oxide layer on the surface. The passive layer is chromium rich and generally it is accepted that for the layer to form more than 12% chromium is required in the alloy. However, the excellent corrosion resistance of stainless steels is often undermined by the localised breakdown of the passive layer by pitting corrosion, in environments that contain aggressive anions such as chloride ions. To evaluate the usefulness of a stainless steel in an aggressive environment, it is therefore very important to establish the conditions under which pitting occurs.

Electrochemical techniques have been developed that are capable of defining the conditions under which a given metal/environment system is likely to exhibit pitting (Sedriks, (1979)). Normally, polarization curves are obtained by changing the potential of the metal from negative to positive potentials and measuring the current densities that result from the cathodic and anodic processes. A schematic polarization curve is shown in figure 2.1. The diagram can be divided into four distinct regions of potential: the cathodic region, the active region, the passive region, and the transpassive region. A polarization scan is described below:

The polarization scan begins in the cathodic region where the specimen is polarized to a potential more active than the free corrosion potential, E_{corr}, of the specimen. In this region the predominant reaction is the reduction of some species in solution such as the reduction of hydrogen in the hydrogen evolution reaction (HER) or the oxygen reduction reaction (ORR).

The specimen is polarized in the positive direction and the potential is plotted against the polarization current density. The current density approaches zero at the corrosion potential where the cathodic and anodic reactions occur at the same rate. Above the corrosion potential, active dissolution of the metal occurs and the current density increases rapidly until a value, i_{crit}, is reached, which corresponds with the primary passivation potential, E_{pp}. The potential range between the corrosion potential and the primary passivation potential is known as the active region.

Increasing the potential from the primary passivation potential causes film forming oxidation reactions to reduce the polarization current density to a value of i_{pass}, where corrosion occurs at an extremely slow rate. The potential at which the passive layer becomes stable is known as the Flade potential, E_F. The passive film, in the form of a protective oxide film is stable until the breakdown potential, E_{br}, is reached. The region between the primary passivation potential and the breakdown potential is the passive potential range.

The breakdown potential is characterised by a sharp increase in the polarization current density as the passive layer no longer protects the specimen surface. Corrosion occurs by transpassive dissolution, but in the presence of aggressive anions may break down at a lower potential, E_p, by localized corrosion in the form of pitting corrosion. The range above the breakdown potential is referred to as the transpassive region.

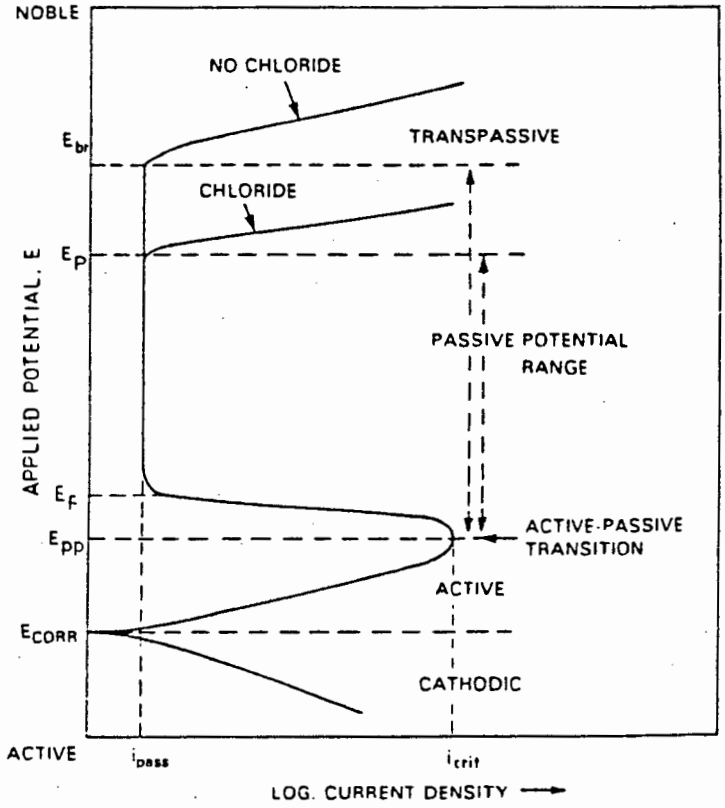

Figure 2.1 : A schematic polarization curve for a stainless steel in a sulphuric acid solution showing the cathodic region, the active region, the passive region, and the transpassive region.

In the event of localized breakdown by pitting corrosion, reversal of the scan after a specified current density is reached, causes a hysteresis loop to form. The loop meets the passive region of the polarization scan at the protection potential, E_{prot}. The protection potential is the potential below which pits repassivate, and therefore will no longer propagate.

The parameters E_{corr}, E_{pp}, E_F, E_{br}, and E_{prot} are obtained from experimentally determined polarization scans for particular metal/environment combinations.

2.1.1 The Corrosion Potential

The corrosion potential, E_{corr}, is dependant on the oxidising species' concentration in solution. Increasing the oxidizer concentration (oxygen, Fe^{2+}, Cu^{2+}) moves the corrosion potential in the noble direction. For this reason most polarization scans that are run on stainless steel in aerated solutions do not show an active to passive transition since the cathodic curve intersects the anodic curve in the passive region above the active to passive transition.

2.1.2 The Breakdown Potential

Breakdown of the passive layer of stainless steel may occur transpassively or locally by pitting corrosion. In the absence of aggressive ions breakdown occurs transpassively at a potential E_{br}. Aggressive ions such as the chloride ion cause breakdown by pitting corrosion at a potential E_p. E_p occurs at more active potentials than E_{br}, and the value of E_p or E_{br} is dependent on the material/environment combination. Inhibitive anions such as nitrate ions shift E_p to more noble values until complete inhibition may occur at sufficiently high inhibitor concentrations resulting in transpassive breakdown at E_{br}. The larger the potential range between E_p and E_{corr}, the higher the resistance of an alloy to pitting corrosion. Therefore if E_{corr} is close to E_p, pitting may result due to small increases in the oxidising power of the solution thereby raising the free corrosion potential above E_p. Since the value of E_{corr} of stainless steel in oxygenated chloride solutions may not change significantly from alloy to alloy, it has become customary to equate pitting resistance simply with the absolute value of E_p, rather than $E_p - E_{corr}$ (Sedriks, (1979)). A schematic polarization curve showing the relationship between pitting corrosion and the potential range between E_p and E_{corr} is presented in figure 2.2. The hysteresis loop and the protection potential, E_{prot}, are also shown.

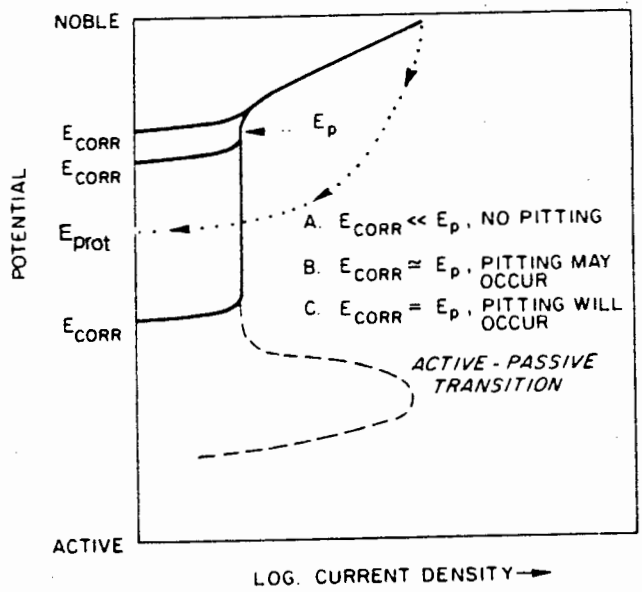

Figure 2.2 : Schematic polarization curve illustrating conditions under which pitting may or may not occur (after Sedriks).

2.1.3 The Protection Potential

A hysteresis loop will result if the scan direction is reversed after pitting corrosion has been initiated at E_p. The potential at which the loop intersects the passive region of the polarization curve, is known as the protection potential, E_{prot}. The protection potential is approximately equal to the potential inside the pit (Pourbaix (1970)) which is dependent on the composition of the solution inside the pit (Szklarska-Smialowska and Janik-Czachor (1971)). Existing pits will not propagate at potentials below E_{prot}, although this concept is controversial at present since some investigators feel that the value for E_{prot} is not a unique property of an alloy since the degree to which the pits are allowed to propagate will change the solution environment within the pits and therefore change the potential at which pits will repassivate (Syrett (1977)). However, Baboian and Haynes (1981) regard the protection potential as a better indication of a material's localized corrosion resistance than the breakdown potential, since they found the reproducibility of the reverse scan to be better than for the forward scan.

2.2 PITTING CORROSION MECHANISMS

2.2.1 Pit Initiation

In a review paper on pitting and crevice corrosion Kruger and Rhyne concluded that the following conditions were necessary for the initiation of localized corrosion by pitting:

(i) A critical potential E_p, usually called the pit nucleation or pitting potential, must be exceeded. There also exists a critical protection potential E_{prot} which is more active than E_p. Corrosion, once initiated, cannot be stopped at potentials more noble than E_{prot}.

(ii) There must be the presence of an aggressive species, particularly the chloride ion, in solution.

(iii) There is an induction period separating the initiation of the breakdown processes, by the introduction of conditions conducive to breakdown, and the completion of the process when pitting commences.

(iv) There must be breakdown of the surface film at localized sites.

Oldfield (1987) listed four general models which satisfy the above requirements:

2.2.1.1 Adsorbed ion displacement models

In these models anionic species such as Cl^- ions are adsorbed on to the passive film, either singly or in groups, and compete with oxygen in the passive film. Leckie and Uhlig (1966) proposed that adsorbed oxygen, rather than metal oxide is considered to make up the passive film. Whilst oxygen usually has a greater affinity for adsorption sites than chloride, as the potential of the alloy is shifted to more positive values, chloride ions are adsorbed into the double layer. At sufficient concentration, corresponding to the critical potential, E_p, chloride ions destroy the passive layer at favoured sites by displacing the adsorbed oxygen ions.

The anodic overvoltage for the dissolution of alloy ions is appreciably reduced at areas where chloride is in contact with the metal in place of oxygen, and therefore a pit forms by rapid dissolution of metal ions into solution. The preferred transport of chloride in ionic form and heavy-metal chlorides to the anodic

site ensures that the anode remains active. Since competitive adsorption is a slow process, it results in an incubation time prior to initiation.

The competitive adsorption theory explains why anions such as OH^-, NO^{3-}, SO_4^{2-} and ClO_4^- inhibit pitting, since they are also adsorbed onto the passive layer displacing chloride. For pitting to initiate, the anodic overvoltage has to be increased beyond the value which was required to induce pitting prior to the addition of the inhibitive anion. The more readily an anion adsorbs onto the passive surface, and the higher its affinity for the metal surface, the more effectively it excludes chloride and inhibits pitting. This model implies that E_p should be insensitive to pH changes below 7, since the H^+ ion does not competitively adsorb onto the passive surface. However, the OH^- ion has an affinity for the passive surface and acts as an inhibitor, thus E_p is sensitive to pH fluctuations in the alkaline region.

Kolotyrkin (1961) showed that the presence of aggressive anions only was not sufficient for pitting corrosion to occur. He observed that a potential above a certain critical value was necessary for pitting to initiate at a given concentration of aggressive ion. It was shown that the critical potential required for pitting could be obtained by polarization or by the addition of an oxidising agent to the solution.

Kolotyrkin proposed that the depassivation of the passive layer by chloride ions was reversible, and that two concurrent processes take place, namely the passivating adsorption of oxygen (from water molecules) and the activating adsorption of chloride ions. The position of the equilibrium depended not only on the electrode potential but also on the concentration of the halide ion at the surface of the metal. This indicates that pitting corrosion can occur in a previously non-aggressive environment if the concentration of the aggressive anion is increased or if the concentration of oxidising agent in solution is increased.

2.2.1.2 Ion migration or penetration models

These models assume that anions penetrate the passive film causing breakdown when the anion reaches the metal/film interface. These models range from those which assume the existence of pores in the passive film to those which assume penetration by migration through a pore-free film. Hoar, Mears and Rothwell (1965) and Richardson and Wood (1970) have proposed models falling into this range.

Heine, Keir and Pryor (1965) proposed a model for pitting corrosion by chloride penetration through the passive oxide layer of aluminium. They cautioned however, that until pertinent supporting data became available, these results should not be extrapolated to stainless steel. However this model does allow an explanation of many experimentally determined results for stainless steel.

In this model chloride ions are adsorbed into the oxide layer of the stainless steel during the incubation period prior to initiation. This creates additional current carriers and/or additional vacancies in the cation lattice and thus reduces the ionic resistance of the oxide film. This results in a reduction of the anodic polarization and allows rapid diffusion of metal ions into solution. Chloride ions are concentrated at certain selected areas such as grain boundaries, dislocations, inclusions and other areas where rapid exchange and substitution is expected. Penetration of chloride ions is expected to reach the oxide-metal interface. At the areas of highest chloride concentration, the resistance to the outward passage of metal ions will be lowest, and the oxide layer will be susceptible to enhanced dissolution. When metal ions pass through the oxide layer into solution, they will decrease the pH of the area if they precipitate as hydrated metal oxides. This can cause the localized attack to become macroscopic as the process becomes autocatalytic in nature.

2.2.1.3 Breakdown-repair models

Models in this group are based on chemically induced mechanical disruption of the passive film. Included in this set are the local acidification models, which propose that breakdown occurs via mechanical or electrochemical means followed by hydrolysis of metal ions to give a reduction in pH, and the salt film model, where a non-protective salt film is formed where the film breaks down.

Hoar (1967) proposed a mechanical mechanism for pitting initiation, in which anion adsorption replaces water, and the interfacial free energy of the oxide/solution interface is lowered due to mutually repulsive forces between charged particles. The interfacial tension is eventually reduced so far that a kind of "peptization" by interfacial energy occurs. This results in the adsorbed ions repelling one another and the oxide to which they are attached resulting in the formation of cracks. Any crack or area where the oxide layer has been damaged has additional anions attracted to it

and they too become adsorbed to its sides. The process is progressive localized breakdown of the passive layer, resulting in localized corrosion occurring.

Galvele (1976) proposed a model which relies on the breakdown of passivity by localised acidification at cracks in the oxide layer due to hydrolysis of metal ions. A critical pH has to be achieved for pitting initiation. The pitting potential is regarded as being the minimum potential at which the critical localized acidity can be maintained inside a pit. Galvele claims that this model has the advantage over other models since it can account for the effect of variables such as pH, ionic concentration and inhibitor concentration on the pitting potential. Support for the local acidification model was obtained by Keitelman and Galvele (1982) for pure iron in sodium sulphate solutions.

Galvele showed that the concentration of the metal ion, the hydrated metal ion and H^+ is related to the product of the depth x and the current density i of a unidirectional pit. This is illustrated in the figure 2.3, of species concentration C ($mol.l^{-1}$) vs xi ($A.cm^{-1}$)

The necessary acidification can be obtained in pits as small as 10^{-6} cm for $x.i$ values of 10^{-6} $A.cm^{-1}$. This means that cracks in the passive oxide film would provide a diffusion path sufficiently long to reach the critical pH if the potential applied to the metal was high enough. The existence of cracks in the passive oxide film is taken to be well documented by Galvele.

Janik-Czachor (1981) proposed that chloride ions agglomerate in solution, usually near inhomogeneities such as inclusions. The chloride ions are adsorbed onto the passive film and cause thinning of the film. At sufficiently high potentials the passive film is removed locally and replaced by a chloride salt film.

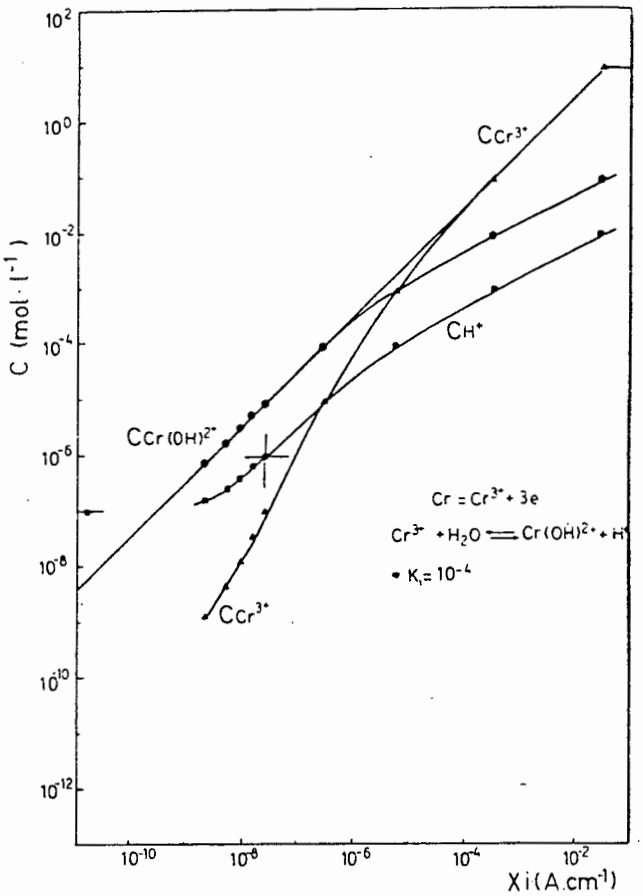

Figure 2.3 : Concentrations of Cr^{3+}, $Cr(OH)^{2+}$, and H^+ as a function of the product of the depth x and the current density i in a unidirectional pit (after Galvele).

2.2.1.4 Stochastic models

In these stochastic models pit initiation is treated as a random event which in some cases leads to the establishment of stable pits.

Williams, Westcott and Fleischmann (1984) used peak counting, passage time, spectral density, ensemble statistics and slope distribution analysis to recover parameters for a general stochastic model and judged their dependence upon experimental variables. They assumed that pitting corrosion was an unpredictable process with regard to the time of initiation and the place of attack. Figure 2.4 shows a typical ensemble of current transients for a stainless steel, illustrating the poor reproducibility of pitting initiation events.

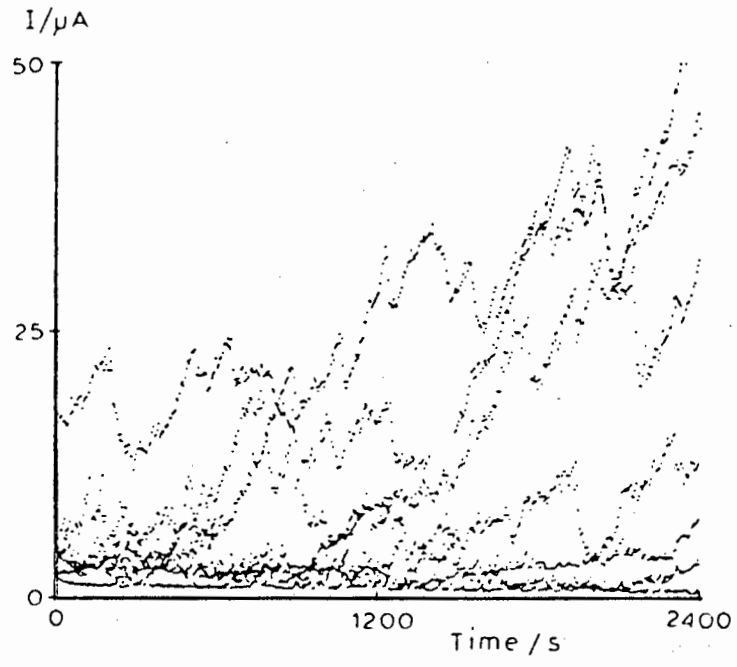

Figure 2.4 : Ensemble of current transients : 18Cr13Ni1Nb stainless steel, 5 cm^2, 0.028 M NaCl, deaerated solution, unstirred, +50 mV (SCE), potential transition made by 10 mV/sec ramp from the rest potential [-200 mV(SCE)] (after Williams et al).

The following assumptions were made:

(i) pits are randomly nucleated in space and time with a frequency, λ (s^{-1} cm^{-2}) and that each pit evolves with time according to a deterministic rule

(ii) events have a probability, μ (s^{-1}), of dying

(iii) events that survive beyond a critical age τ (s) do not die and are stable pits

(iv) the rate of nucleation of pits Λ (s^{-1} cm^{-2}) is:

$$\Lambda = \lambda e^{-\mu\tau}$$

(v) all pits evolve according to the deterministic law $i = C.u$, where u (s) is the age of the pit.

From these assumptions it is clear that pits are unstable when they first nucleate and only become stable after they have survived past the critical age. Birth, propagation and death of unstable pits will rapidly reach a stationary state, the system will be non-stationary only during the later phases of pitting.

Williams et al used the stochastic model of pitting corrosion to analyse an experimental time series, and to derive parameters which are interpreted in terms of a microscopic model. They found that the results supported a simple local acidification model for the initiation of pitting corrosion. Initiation of pitting corrosion

requires generation and maintenance of gradients of acidity and electrode potential on the scale of the surface roughness of the specimen. Fluctuations in the gradients, leading to the birth and death of events, arise because of fluctuations in the boundary layer thickness in the liquid at the metal surface. A pit is stable when its depth exceeds the thickness of the boundary layer. Local acidification could arise due to the hydrolysis of metal ions in solution, as a result of dissolution of the passive metal.
The parameters from the general model, λ, μ, and τ can be related to this model in the following way:

(i) the nucleation rate is determined by the time required to establish the critical pH

(ii) the death of an event is as a result of the local reduction of the hydrodynamic boundary layer thickness

(iii) the observed lifetimes relate to the fluctuations occurring in the hydrodynamic layer due to convection in the unstirred condition

Williams et al note that other models (Okada, 1985), for pitting initiation in which there is a transition between an unstable and stable state of pitting, also fall into their general stochastic theory. They emphasize the importance of local transport processes since this explains the significant effect of stirring, electrolyte conductivity, buffer capacity and surface roughness on pitting initiation, and the lack of dependence on the electrode potential once it has exceeded the pitting potential.

Oldfield (1987) notes that although the stochastic model is able to explain many observed phenomena, there is no single model which links the stochastic model to the fundamental modelling above. In his review paper, Sharland (1987) draws attention to the controversy as to whether the initiation of localized corrosion is truly a "rare event", in the statistical sense. He suggests that the randomness and poor reproducibility of experimental observations may be due to certain instabilities in the dynamics of the system. Sharland also draws attention to the fact that there are many theories regarding the interaction of halide ions with the passive film of metals and although some of the theories are purely speculative, many have been developed to explain certain experimental observations. He also emphasizes that none of the theories are able to explain all the features of film breakdown satisfactorily.

2.2.2 Pit Propagation

In the present study, pitting initiation is regarded as the important criterion for comparing the pitting corrosion resistance of the development alloys. Syrett (1977) proposed Pit Propagation Rate (PPR) curves to determine the propagation rate of pitting corrosion. Using this method he found a close correlation between experimentally determined propagation rates and those from long term immersion tests.

The nature of pit propagation is such that theories describing it are concerned mainly with geometry, mass transfer, and reaction kinetics. Oldfield (1987) divided propagation models into three groups.

2.2.2.1 Metal dissolution hydrolysis

In this approach the dissolution and hydrolysis of metal ions are considered as a function of pH and potential, and compared with the hydrogen evolution reaction.

In Galvele's (1976) model a potential is defined at which the rate of production of hydrogen ions via hydrolysis is equal to their rate of consumption via hydrogen evolution. Below this potential passivation is maintained; above it repassivation does not occur. Galvele proposes that the bulk solution acts as a supporting electrolyte for the metal ions and the hydrolysis products produced during pitting initiation. Transport by diffusion is the dominant mechanism.

2.2.2.2 Salt layer formation

In this approach it is assumed that a highly resistive film, probably a salt film, exists on a growing pit's surface. Vetter and Strehblow (1970) consider this film to be formed by the cations of the metal and the aggressive ion. The film is considered dense and poreless; the rate of pit growth is equivalent to the rate of salt film dissolution.

As a result of experimental work done on AISI 302 stainless steel in chloride solutions Frankel et al. (1987) concluded that metastable pits form at potentials below E_p, but repassivate as a result of the pit cover rupturing. At potentials equal to and higher than E_p, the pit cover remains intact long enough for a salt layer to precipitate on the pit surface and stabilize the pit growth. From experimental work conducted on titanium rods, Beck

(1973) proposed that there is a highly resistive salt layer on the titanium surface that accounts for the potential drop in propagating pits. It was speculated that the salt film comprised of TiX_4 or $TiOX_2$.

Alkire and Cangellari (1983) investigated the effect of different fluid velocities on the precipitated metal chloride salt covering the surface of a growing pit. It is postulated that the precipitated chloride salt prevents pit repassivation in the early stages of pit growth. They proposed that at sufficiently high fluid velocities the chloride salt would be washed away from the pit surface and allow the metal to repassivate.

2.2.2.3 Mass transfer control

In this group of models the mass transfer of species in and out of the pit are assumed to be corrosion controlling reactions. Although mass transfer by migration can occur, the assumption is usually made that it is by diffusion only.

Alkire, Ernsberger and Damon (1976) were able to estimate the conductivity variations required for auto-acceleration of dissolution rates for artificial copper pits. The conductivity variations arise due to concentration gradients caused by diffusion limited attack within the occluded region of the pit. Whereas it was thought that the cathodic processes associated with pits occurred on the exterior surfaces of the pit, Alkire and Siitari (1979) found that they can occur within the occluded region of the pit. The distribution of cathodic reaction was found to depend on the prevailing transport laws for the system.

In artificial pit studies Beck (1977) found that the observed current density for pits on iron in concentrated chloride solutions was limited by the rate of mass transfer of corrosion product out of the pit. By increasing the flow rate of solution at the pit surface, the current density increased to a limiting ohmic value.

2.3 FACTORS AFFECTING PITTING CORROSION

In his review on Test Techniques for Pitting and Crevice Corrosion, Oldfield (1987) cited the following factors as having an important affect on the pitting behaviour of stainless steel.

2.3.1 Alloy Composition

Alloy composition effects the stability of the protective film on the stainless steel. It also controls the maximum dissolution rate once propagation has occurred. Additionally, for a given passive current density the degree to which the pH is reduced in a pit is dependent on the alloy composition.

2.3.2 Passive Film Characteristics

The passive current and the film stability determine the alloy's resistance to pitting corrosion. The resistance to pitting is also affected by surface finish, surface preparation, heat treatment and cold working. For this reason caution should be exercised that laboratory testing is carried out on specimens that are prepared with the same surface finish and heat treatment as the in-service components will have.

2.3.3 Electrochemical Reactions

In practice the maximum possible corrosion propagation rate is not often attained, since it is modified by the rate of the oxygen reduction reaction on the area surrounding the corroding metal and the rate of hydrogen evolution on the corroding area, if the pH of the solution in this area is not low enough. These rate limiting reactions can hide large differences in the corrosion resistance between different alloys. Accordingly great care should be exercised before the addition of alternative oxidising species, since this can dramatically alter the given alloy/environment state.

2.3.4 Mass Transport

Mass transport occurs via migration, diffusion and convection, and all three play a major role in pitting corrosion. All three mechanisms must be carefully noted, since each may play a role in a particular situation.

2.3.5 Bulk Solution Environment

Temperature, flow rate and volume effects are important and must be recognised. Temperature increases may increase or decrease the rate of corrosion depending on the particular situation. Flow rate may effect the rate of oxygen reduction, thereby controlling the rate of reaction.

2.3.6 Bulk Solution Composition

Bulk solution ingredients such as Cl^- level, pH, pollutants, oxygen level etc. determine the basic corrosivity of a solution. It is emphasized that great care should be taken in using simulated or synthetic environments and relating results directly to the "real" environment.

2.4 THE INFLUENCE OF METALLURGICAL ASPECTS ON PITTING

Passivity is defined by the American Society for Testing and Materials as the state of a metal surface characterized by low corrosion rates in a potential region that is strongly oxidizing for the metal. A schematic polarization curve for a stainless steel in a sulphuric acid solution is shown in figure 2.5. The passive potential range is defined by the low current portion of the curve between the active-passive transition and the pitting or transpassive potential.

The resistance of an alloy to pitting corrosion in a particular solution can be related to the size of the passive potential range from a polarization scan performed in the solution in question.

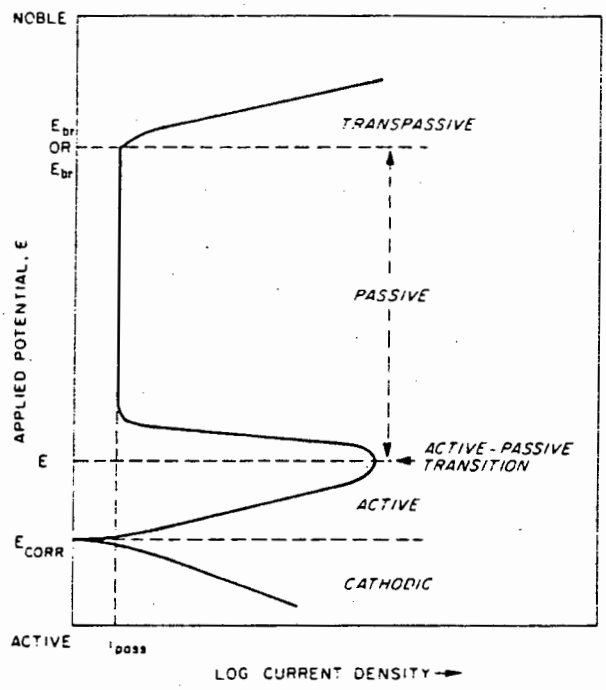

Figure 2.5 : A schematic polarization curve for a stainless steel in a sulphuric acid solution.

Sedriks (1984) noted that for commercially produced stainless steels a large number of metallurgical factors have a significant influence on passivity as is illustrated in figure 2.6.

Alloying elements in the solid solution, second phases, sigma, chi, manganese sulphides, carbides, and chromium and molybdenum depleted zones surrounding precipitates can all have a profound influence on both the maintenance and breakdown of passivity.

Sedriks suggested that a logical way to handle such a complex array of metallurgical variables is to examine how each variable affects passivity. In this way the information can be used in alloy development, fabrication, materials selection and heat and surface treatments.

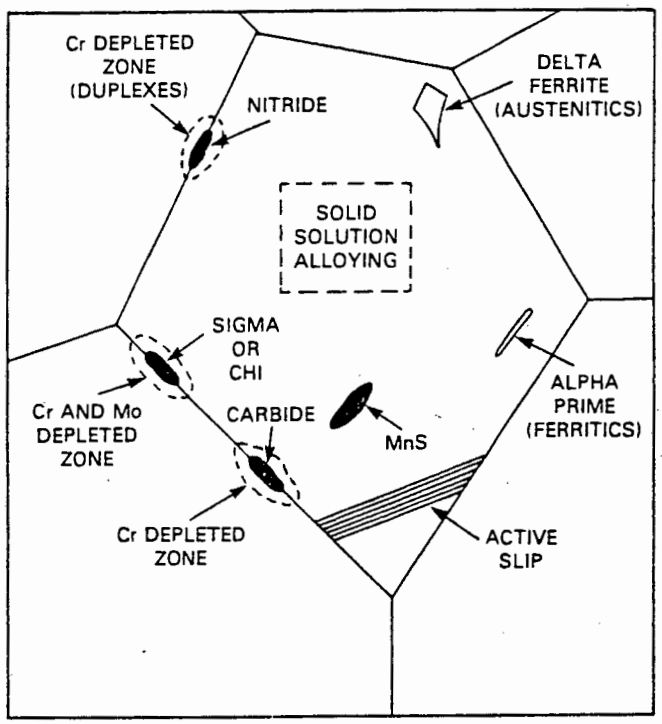

Figure 2.6 : Schematic of metallurgical variables affecting the passivation behaviour of stainless steels (after Sedriks).

2.4.1 Effects of Solid Solution Alloying

2.4.1.1 Chromium

Stainless steels derive their passive behaviour from alloying with chromium, by the formation of a passive oxide film on the surface of the steel. Auger Electron Spectroscopy (AES) revealed that increasing the chromium content in a Fe-Cr alloy leads to a decrease in the thickness of the passive layer and chromium enrichment of the layer with respect to the chromium concentration in the metal (Cieslak and Duquette, (1984)). Burstein and Marshall (1984) have shown that on freshly generated AISI 304L stainless steel surfaces in perchloric acid that repassivation occurs by the dissolution of the iron component of the newly developed passive layer while the chromium remains. Repassivation is complete when the outer surface of the oxide film contains no iron ions.

Pure chromium exhibits a wide passive potential range in chloride-free sulphuric acid solutions, of the order of 1.5 volts. Chloride ions reduce the noble extreme of the passive range from Eb_r to E_p., as shown in figure 2.1. Walker and Rowe (1969) found that the pitting potential of chromium still remained at relatively high noble values, as results from testing in chloride solutions of chromium plated stainless steels showed.

The addition of chromium moves the primary passivation potential (E_{pp} in figure 2.5) in the active direction, thus expanding the passive potential range, and reducing the passive current density (i_{pass} in figure 2.5). The effect of chromium content on the anodic polarization behaviour Fe-Ni-Cr alloys in chloride solutions is illustrated in figure 2.7.

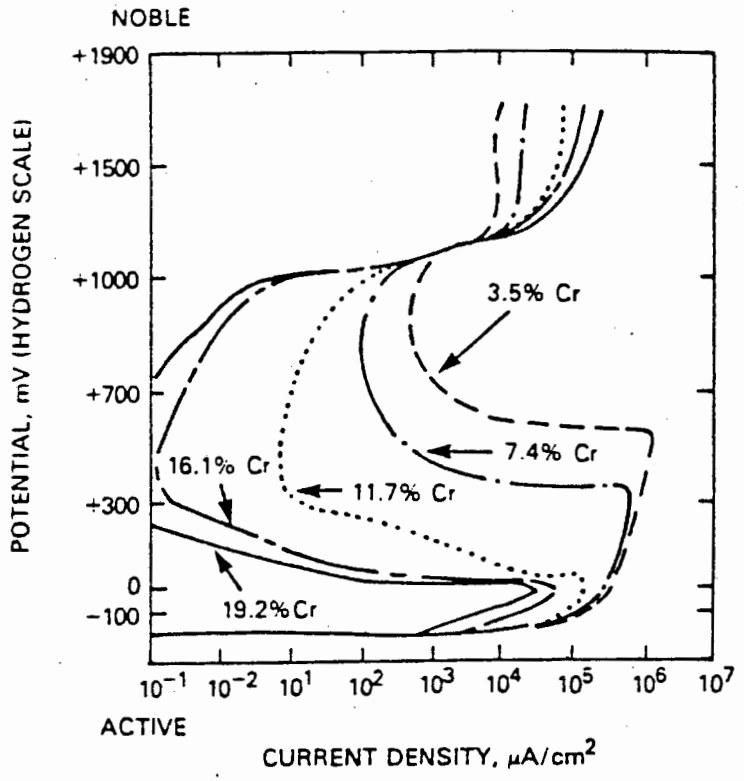

Figure 2.7 : Effect of chromium content of Fe-Ni-Cr alloys on their anodic polarization behaviour in 2N H_2SO_4 at 90°C. Nickel content in the range of 8.3% to 9.8% (after Osozawa and Engell).

2.4.1.2 Molybdenum

It is well known that for a given chromium content in a stainless steel the addition of molybdenum has a strong beneficial influence on passivity (Sedriks, (1984)). Molybdenum moves the pitting

potential in the noble direction, thereby extending the passive potential range. The mechanism by which molybdenum extends the passive potential range is not fully understood.

From AES studies on Fe-Cr and Fe-Cr-Mo stainless steels Cieslak and Duquette (1984) found that the passive film thickness and composition was basically unchanged by the addition of molybdenum. The beneficial effect of molybdenum on pitting corrosion resistance of stainless steels was attributed to the alteration of those sites in the film that are most susceptible to breakdown.

Marshall and Burstein (1984) investigated the effect of molybdenum on repassivation kinetics by comparing the repassivation behaviour of AISI 316 and 304. They found that the molybdenum aided the dissolution of the iron component of the oxide film during repassivation, causing the oxide film to become chromium enriched more rapidly than in the absence of molybdenum. They concluded that the constructive dissolution process accelerates the onset of passivity and thus improves the resistance to chloride induced pitting corrosion.

2.4.1.3 Nitrogen and Nitrogen-plus-Molybdenum

Sedriks (1984) reported that nitrogen additions to molybdenum-free austenitic stainless steels are beneficial to the development of passivity. Nitrogen moves the pitting potential in the noble direction thereby increasing the passive potential range. Additionally, in the presence of molybdenum, the beneficial effect of nitrogen on the pitting potential is increased. This synergistic effect is used in some proprietary commercial stainless steels.

The mechanistic role of nitrogen and molybdenum are still to be established. Sedricks (1984) noted that recent studies on a stainless steel containing 24.3Cr-19.9Ni-6.06Mo-0.44N-0.018C using Auger spectroscopy and X-ray photoelectron analyses found no molybdenum in the passive layer, and a seven fold enrichment of nitrogen on the metal side of the metal-film interface.

High levels of nitrogen necessitate high levels of manganese (e.g. 4%) to ensure solid solubility of nitrogen in the chromium-containing austenite. It is generally accepted that the detrimental effect of increased manganese is over ridden by the beneficial effect of the molybdenum-plus-nitrogen effect on the pitting potential.

2.4.1.4 Other Alloying Elements

Nickel, vanadium, silicon and tungsten have a beneficial effect on the pitting resistance when they are added to an alloy. The beneficial effect of nickel on the pitting potential is not pronounced. The effects of the various beneficial alloying elements on a schematic polarization scan can be seen in figure 2.8 below.

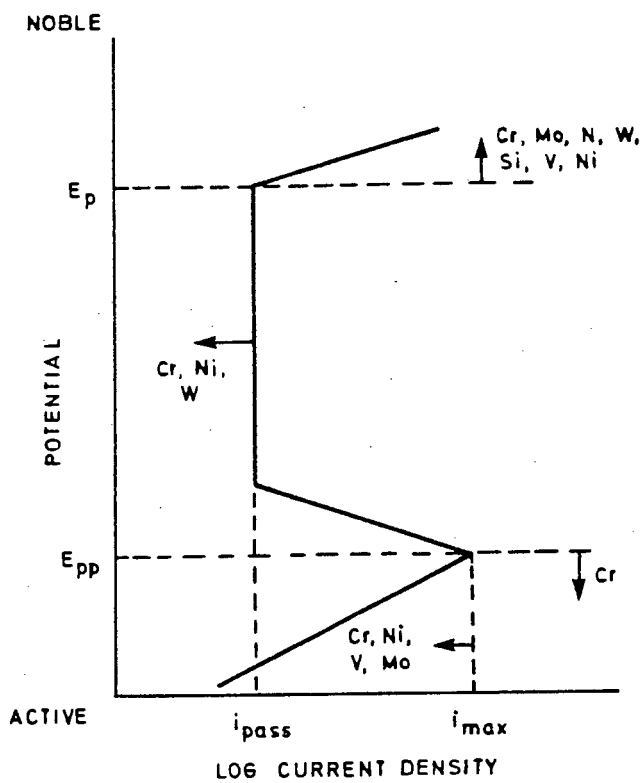

Figure 2.8 : Schematic summary of the effect of alloying elements in stainless steels on the anodic polarization curve (after Sedriks).

2.4.2 Effects of Microstructure

2.4.2.1 Carbides

Anodic polarization curves of the carbides of chromium, niobium and titanium in relation to the anodic polarization curve for Type 304L stainless steel in a sulphuric acid solution are shown in figure 2.9.

Sedriks (1984) notes that in aqueous chloride solutions, where the breakdown of passivity by pitting is of concern, it is the chromium depleted region surrounding the chromium carbide that provides the sites for the initiation of corrosive attack. Sensitised grain boundaries in austenitic and ferritic stainless steels are preferred sites for passivity breakdown by pitting initiation. The sensitization also reduces the passive potential range and increases the passive current density.

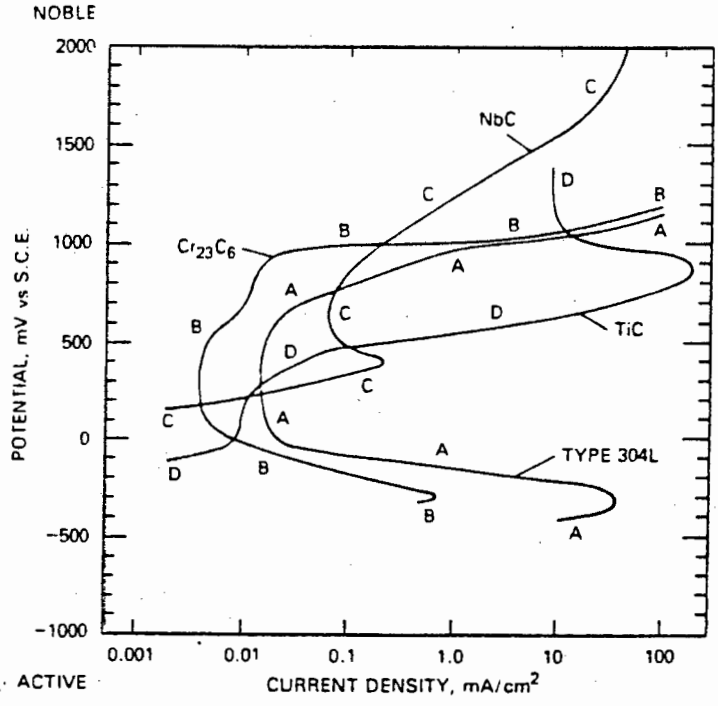

Figure 2.9 : Anodic polarization curves for solution annealed Type 304L stainless steel (A), $Cr_{23}N_6$ (B), NbC (C) and TiC (D) in boiling 3.4 N H_2SO_4 (after Kolotyrkin et al. and Aaltonen et al.).

2.4.2.2 Sigma and Chi

Sedriks (1983) reported that the presence of sigma or the similar intermetallic chi, moves the pitting potential in the active direction, thereby decreasing the passive potential range. Sedriks (1984) noted that Herbsleb and Schwaab (1982) found that sigma and chi generally contain higher chromium and molybdenum contents than the matrix. Sedriks therefore concludes that the corrosive attack is directed at the areas within the matrix surrounding the sigma and chi where chromium and molybdenum depletion has occurred.

2.4.2.3 Manganese Sulphide

Sedriks (1984) notes that it is well established that manganese sulphide inclusions are the most favourable sites for pit initiation in stainless steels. Cieslak (1986) reports that manganese sulphide inclusions are anodic to the matrix, and that the pit initiation resistance, as measured by the pitting potential, is controlled by the manganese sulphide geometry rather than the sulphide concentration. However, increased sulphide concentration will increase the probability that there will be inclusions that have the correct geometry for initiation to occur. Frankenthal and Pickering (1972) suggest that most pits in stainless steels are initiated at inclusions, and those that are not associated with inclusions do not grow to an appreciable size because the pit cavity is exposed to the bulk solution which facilitates repassivation.

2.4.2.4 Alpha Prime and Delta Ferrite

Delta ferrite in austenitic stainless steels and alpha prime in a ferritic stainless steels move the pitting potential in the active direction, thereby reducing the passive potential range.(Sedriks, (1984)). Sedriks refers to Dundas and Bond (1975) who proposed that delta ferrite in austenitic stainless steels may be associated with the depletion of the chromium and molybdenum from the surrounding austenitic matrix and that pitting attack may occur in the depleted austenite.

2.5 THE EFFECT OF AGGRESSIVE AND INHIBITIVE IONS

In industrial and natural waters chloride ions are the most common cause of pitting corrosion, however pitting corrosion depends not only on the concentration of chloride ions, but also on the concentration of non-aggressive anions, and more precisely on the ratio of aggressive to non-aggressive anions (Szklarska-Smialowska, (1971)). Leckie and Uhlig (1966) found that OH^-, NO_3^-, SO_4^{2-} and ClO_4^- inhibited the pitting corrosion of 18-8 stainless steel in chloride solutions with a decreasing efficiency as follows : $OH^- > NO_3^- > SO_4^{2-} > ClO_4^-$

2.5.1 Effect of Chloride Ions

The decrease of the pitting potential, E_p, with increasing chloride concentration is well established and has been reported by many authors. Pourbaix (1965) cites Brennert (1937) as being the first to report the effect. Pourbaix et al. (1963) showed that the pitting potential for AISI 410 stainless steel dropped progressively as the chloride concentration was increased from a 0.005 M to 0.10 M NaCl solution. Mankowski and Szklarska-Smialowska (1975) found that the chloride concentration within pits was much higher than that in the bulk solution. Verink and Pourbaix (1971) plotted E_p, E_{prot}, E_{corr} and E_{pp} of a 12% Cr alloy as a function of the log of the chloride ion concentration at a pH of 8.8. E_{corr}, E_{pp} and E_{prot} did not vary appreciably with increased chloride concentration, while E_p decreased very quickly after a certain concentration of chloride had been exceeded. Figure 2.10 shows that a chloride ion concentration of approximately 10^{-2} M was required for pitting corrosion to occur.

Leckie and Uhlig (1966) plotted the pitting potential against the log of the chloride ion concentration for an 18-8 stainless steel in a neutral solution, and found that there was a linear correlation between E_p and the chloride concentration at concentrations above 0.01 M given by the following equation :

$$E_p = -0.088 \log [Cl^-] + 0.168 \qquad \text{Equation 2.1}$$

Higginson (1984) found that E_p decreased linearly with the logarithm of increasing chloride concentration for AISI 304 and 316 in near neutral solutions. Atrens (1983) investigated the effect of increasing the chloride concentration on E_p and E_{prot} for a 12% Cr turbine blade material. He found that both E_p and E_{prot} decreased linearly with respect to the log of the chloride ion concentration. Results obtained at 80°C are shown in figure 2.11, where the slope of the E_p line is 183 mV per decade and the slope for the E_{prot} line is 143 mV per decade. E_{corr} values measured 1 to 5 minutes after immersion into the solution for air saturated and deaerated solutions are imposed on the figure. The intersection of the deaerated E_{corr} curve with the E_{prot} curve indicates that the specimen will suffer no pitting corrosion only in deaerated solutions with chloride concentrations lower than 2 X 10^{-4} M.

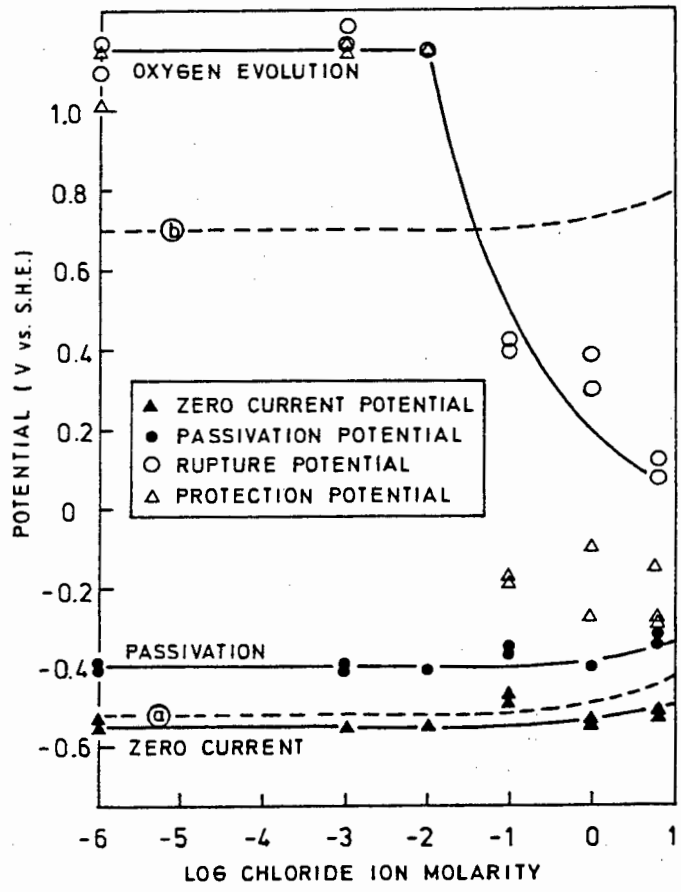

Figure 2.10 : Potential vs log chloride ion molarity at pH = 8.8 (after Verink and Pourbaix, (1971))

Palumbo, King and Aust (1987) showed that the overpotentials for pit nucleation in neutral chloride solutions at 30°C for Alloy 800 varied linearly with the log of the chloride concentration. Below 0.01 M concentrations of chloride, they found no evidence of stable pitting nucleation. They did not find a systematic relationship between E_{prot} and the chloride concentration, which they attributed to the dependence of the protection potential on factors such as pit depth, pit occlusivity and resistivity of the internal pit solution.

Azzerri, Mancia and Tamba (1982) constructed stability diagrams for AISI 316, 304, 430 and 410 by plotting E_p and E_{prot} against the chloride concentration at a range of pH values. A logarithmic dependence between chloride content and E_p was found in agreement with the results obtained by Leckie and Uhlig (1966). E_p was pH dependent while E_{prot} showed no dependence on pH since the aggressive environment at the bottom of the pit was the same regardless of the pH of the bulk solution. This lead Azzerri et al. to propose the existence of two protection mechanisms : (i) by repassivation and (ii) by deactivation. By polarizing the metal to potentials more negative than the working potential, it can be cath-anodically protected i.e. the passive regions remain passive while the pits and crevices are deactivated.

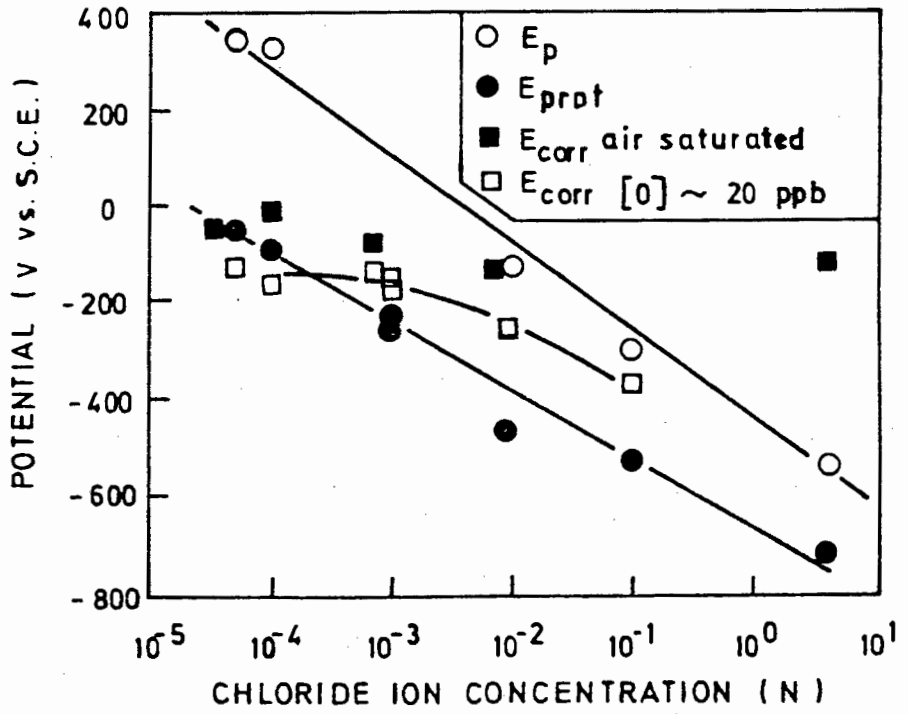

Figure 2.11 : Potential versus log chloride ion molarity at 80°C for a 12% Cr martensitic stainless steel (after Atrens, (1983)).

2.5.2 Effect of Nitrate Ions

Uhlig and Gilman (1964) used immersion testing to show that chloride induced pitting of an 18-8 stainless steel was inhibited by sufficiently high nitrate ion concentrations. A specimen exposed to a 10% $FeCl_3$ + 3% $NaNO_3$ solution showed no pitting over a period of 25 years whereas a specimen exposed to a 10% $FeCl_3$ solution was severely pitted within hours. Man and Gabe (1981) also reported the inhibition of pitting corrosion by nitrate ions.

Leckie and Uhlig (1966) using a potentiostatic step-by-step polarization technique found that nitrate ions at sufficiently high concentrations inhibited pitting corrosion of 18-8 stainless steel in chloride solutions. Complete inhibition was determined by the concentration of nitrate ions required to increase E_p to the point

where breakdown occurred due to transpassive dissolution rather than pitting corrosion. Leckie and Uhlig found that the logarithm of the minimum amount of nitrate for inhibition expressed in terms of anion activity was linear with the logarithm of the corresponding chloride activity. The relationship is shown in equation 2.2 and the plot of the relationship is shown in figure 2.12.

$$\log [Cl^-] = 1.88 \log [NO_3^-] + 1.18 \qquad \text{Equation 2.2}$$

Potentiodynamic polarization curves were used by Capendale (1985) to show that nitrate ions inhibited pitting corrosion of AISI 431 in chloride solutions. The same inhibition criterion was used as by Leckie and Uhlig, and a linear relationship between critical chloride concentration and nitrate concentration was found as shown by the following equation:

$$[Cl^-]_{crit} = 1.18 [NO_3^-] + 95 \qquad \text{Equation 2.3}$$

The relationships that Leckie & Uhlig and Capendale found are shown in figure 2.12 below.

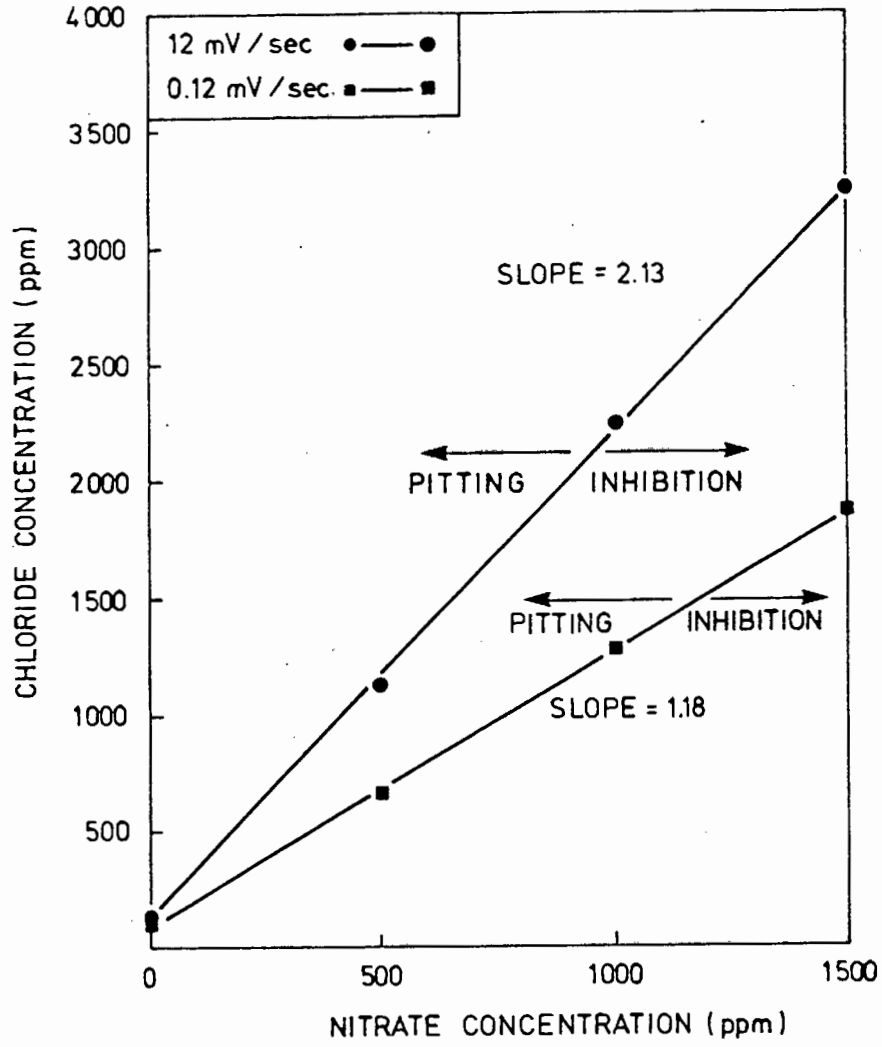

Figure 2.12 : $[Cl^-]_{crit}$ plotted as a function of nitrate concentration for AISI 431 ((Capendale, (1985)) and results obtained by Leckie & Uhlig for 18-8 stainless steel (after Capendale).

Newman and Ajjawi (1986) found that nitrate showed no inhibiting effect on active (film free) dissolution of AISI 304. At potentials above a critical value the nitrate inhibition involved the abrupt passivation under the chloride film. A model which involves the consumption of H^+ and nucleation of stable passivity by electroreduction and/or redox reactions of nitrate within the salt film was proposed.

2.5.3 Effect of Sulphate Ions

Leckie and Uhlig (1966) found that sulphate ions had a similar but less pronounced effect than nitrate ions on the inhibition of pitting corrosion in 18-8 stainless steel. The following relationship was found:

$$\log[Cl^-] = 0.85 \log[SO_4^{2-}] - 0.05 \qquad \text{Equation 2.4}$$

Using a fast scan rate of 12 mV/sec in potentiodynamic polarization scans Capendale (1985) found a linear relationship between the critical chloride concentration and the sulphate concentration. This relationship is shown in equation 2.5 and in figure 2.13.

$$[Cl^-]_{crit} = 0.27\ [SO_4^{2-}] + 120 \qquad \text{Equation 2.5}$$

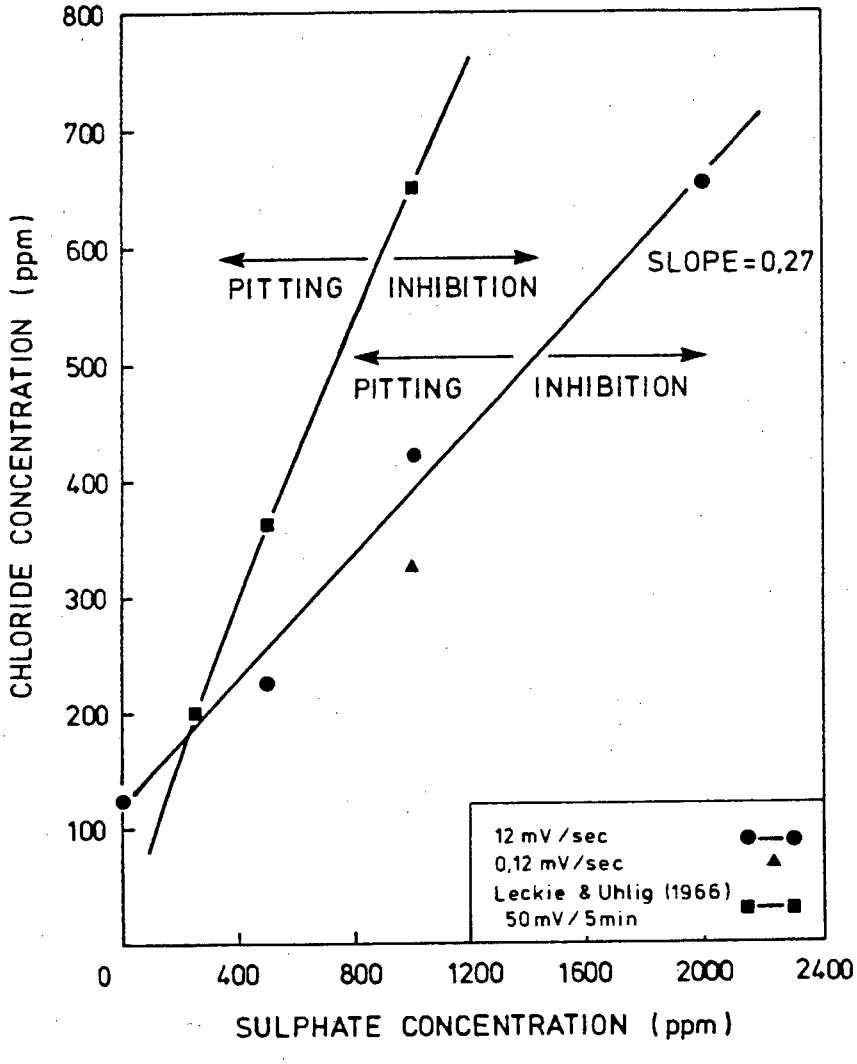

Figure 2.13 : $[Cl^-]_{crit}$ plotted as a function of sulphate concentration (after Capendale).

Bogaerts et al. (1980) found that sulphate ions inhibited chloride induced pitting corrosion of AISI 304 and 316 at temperatures less than 100°C and at temperatures greater than 100°C at elevated pressures. Sulphates were found to have a deteriorative effect on the passivation behaviour of nickel based alloys. Man and Gabe (1981) found that sulphates inhibited pitting corrosion of 18-8 stainless steel.

Contrary to the general beneficial effects of sulphate ions reported in the literature, Mitrovic-Scepanovic and Brigham (1987) found that AISI 410 stainless steel suffered pitting and crevicing in high purity sulphate solutions as a result of attack by sulphate ions. The localized corrosion was difficult to initiate and slow to propagate, but it was proposed that the same mechanism as for chloride ion attack was taking place, but at a slower rate.

2.5.4 Effect of Other Ions

Leckie and Uhlig (1966) found that OH^-, ClO_4^- and $acetate^-$ also inhibited pitting corrosion of 18-8 stainless steel in chloride solutions. Inhibition efficiencies were in the following order :

$$OH^- > NO_3^- > acetate^- > SO_4^{2-} > ClO_4^-$$

The relationships obtained were as follows :

$$\log[Cl^-] = 1.62 \log[O_H^-] + 1.84 \qquad \text{Equation 2.6}$$

$$\log[Cl^-] = 1.13 \log[acetate^-] + 0.06 \qquad \text{Equation 2.7}$$

$$\log[Cl^-] = 0.83 \log[ClO_4^-] - 0.44 \qquad \text{Equation 2.8}$$

Bogaerts et al. (1980) found that HCO_3^- and OH^- inhibited chloride induced pitting of AISI 304 and 316. Hospadaruk and Petrocelli (1966) found that calcium ions caused E_p to shift to more noble values for AISI 201, 301, 316, and 434 in near neutral chloride solutions. Strehblow and Titze (1977) found that nitrate and perchlorate inhibited pitting corrosion of iron in chloride solutions, but that perchlorate induces pitting at sufficiently noble potentials.

CHAPTER 3

EXPERIMENTAL TECHNIQUES

The experimental techniques chapter begins by describing the rationale behind selecting the potentiodynamic polarization technique for the test programme. Thereafter, the preparation of the specimens and test solutions and the equipment used in the testing is described, and finally the test technique and the materials used are dealt with.

3.1 SELECTION OF A TEST METHOD

After comparing current test methods available for determining the pitting corrosion resistance of stainless steels, Oldfield (1987) concluded that :

(1) none of the tests examined relate directly to service experience and therefore they simply provide a ranking order
(2) correlation between techniques, when studying alloys of similar corrosion resistance, is poor and therefore the ranking order obtained depends to a large extent on the test selected
(3) of the widely used tests, the potentiostatic methods, carried out in environments relating to service, are probably the best while ferric chloride tests are the worst.

Degerbeck (1973) used ten different tests to test twenty different steels and drew similar conclusions to Oldfield, finding that it was difficult to relate the tests to one another because of the poor correlation between tests.

Three variations of obtaining anodic polarization curves by potentiostatic means are listed below :

(1) Stationary - holding the specimen at each potential until a constant current is attained.
(2) Potentiodynamic - changing potential at a constant rate.
(3) Quasi-stationary - step-wise change of potential at a certain rate.

After finding little agreement in the literature on which method was most suitable, Capendale (1985) selected the potentiodynamic method using a scan rate of 0.12 mV/sec which was sufficiently slow to allow the near equilibrium conditions to develop during polarization scans. France and Greene (1970) found the slow scan rate potentiodynamic

polarization technique to be a conservative estimate of AISI 430 stainless steel's resistance to pitting because of the migration and surface accumulation of chloride ions during the electrochemical polarization of the specimen. Manning (1983) found a reasonably good correlation between the slow scan rate pitting tests and immersion pitting temperature tests for AISI 317L.

The scratch technique was first used by Pessal and Liu (1971) and involves scratching the passive surface of the metal with a diamond stylus and monitoring the current transient at a range of potentials. E_p is established since the scratch should repassivate at potentials below E_p and dissolve above E_p. Barbosa and Scully (1982) examined the rate of repassivation of AISI 304 at pH 2 as a function of the potential and concluded that the scratch technique was not a suitable method of determining E_p for the following reasons : (i) the scratched areas were not preferentially pitted and (ii) pitting was found to occur at potentials at which the repassivation rate was high. Lizlovs and Bond (1975) reported that the slow potential scan, fast potential scan and the scratch technique gave pitting potentials of comparable magnitude for a number of ferritic grade stainless steels. However, for 18Cr-5Mo, E-Brite 26-1 and 21Cr-3Mo-Ti steels the scratch technique gave consistently less noble pitting potentials. Burstein and Davies (1981) examined the anodic behaviour of iron using a rapid scratch technique and concluded that the scratching of metals under potentiostatic control has the power to reveal the presence of intermediates in electrode reactions and elucidate the kinetics of fast electron transfer processes. Obviously the scratch technique is very powerful for the study of repassivation kinetics, but for the purpose of determining the pitting corrosion behaviour of an alloy it was disregarded.

The findings of France & Greene, Manning and Oldfield confirmed that the slow scan potentiodynamic polarization technique was well suited to the test programme, and the scratch technique was rejected on the findings of Barbosa and Scully for AISI 304. Additionally, by selecting the slow scan potentiodynamic polarization technique a direct comparison of the results obtained could be made with the work completed by Capendale. For the above reasons, the slow scan rate potentiodynamic polarization technique was selected.

3.2 PREPARATION OF SPECIMENS AND SOLUTIONS

3.2.1 Specimen Mounting

Capendale (1985) tried three techniques of specimen mounting for potentiodynamic testing. These were:

(1) Hot mounting resin
(2) Heat shrunk polytetrafluoroethylene (P.T.F.E.)
(3) Compression gasket specimen holder

Capendale (1985) concluded that the compression gasket specimen holder was the most practical since crevice corrosion was least serious in this configuration, since the grinding, polishing and ultrasonic cleaning processes undermined the integrity of the seal in cases 1 and 2. The Stern-Makrides gasket recommended by the ASTM Standard G5-78 (ASTM, (1980) was regarded as being impractical to use due to the difficulties associated with specimen manufacture, polishing, and the achievement of a constant surface area for the determination of current density.

The compression gasket specimen holder was selected for specimen mounting, since this allowed results obtained in Capendale's work and this work to be directly compared, without introducing unnecessary variables. New specimen holders were manufactured, and these proved satisfactory in both test systems when the ASTM standard G5-78 (ASTM, (1980)) test was performed on AISI 430 in 1N H_2SO_4. During the testing program other mounting techniques were experimented with, however none of them were as practical and efficient as the compression gasket specimen holder.

Figure 3.1 shows the specimen holder that was used. Capendale (1985) notes that similar holders were described by France (1967) and Chance, Schreiber and France (1975). The holder was manufactured from crystalline polyester, which provided the necessary rigidity, while the bolt and circular gasket were made from P.T.F.E.. The seal between the specimen and the teflon gasket is created when the gasket is tightened.

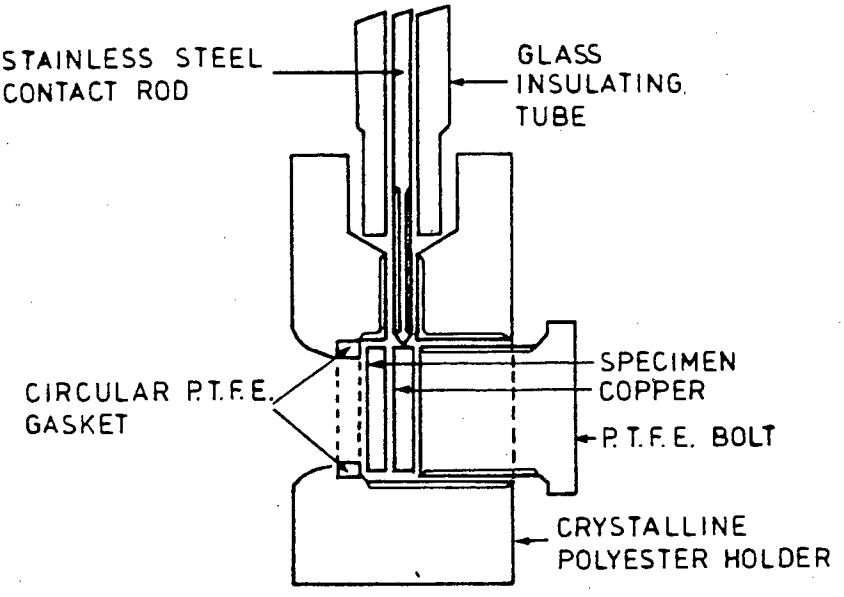

Figure 3.1 : The compression gasket specimen holder

The specimen holder has the following features :

(1) It exposes 1 cm^2 of specimen which facilitates easy determination of current density.

(2) The surfaces exposed other than the specimen are inert in the test solutions used.

(3) The specimen can be reused by grinding and polishing the exposed surface.

3.2.2 Specimen Preparation

Compositional variation was avoided between tests by using a single source of material for all four alloys. The materials were tested as received. Prior to testing a 15.7 mm diameter bar was machined. This was sectioned into 4 mm thick disc-shaped specimens. Three specimens at a time were mounted onto a brass backing plate in the shape of a triangle and ground on silicon carbide pads, which ensured that they were ground parallel to the backing plate. They were washed and cleaned in an alcohol solution placed in an ultrasonic bath prior to being polished to a 3 μm diamond finish. The diamond polish allowed easier microscopic examination of the corroded surface. This surface finish was also used by Capendale (1985) and thus allowed comparative interpretation of his results with the present work. Specimens were cleaned in alcohol, in an ultrasonic

bath and wiped with a cotton wool swab saturated with alcohol before being dried with a hair drier and then mounted in the specimen holder.

3.2.3 Solution Preparation

Accuracy and consistency were achieved by using analytical reagent grade chemicals. Caution was taken to avoid contamination of solutions at all times, and cleaning procedures were thorough. After all cleaning procedures the equipment was rinsed with distilled water. To avoid small variations in solution concentration, batch solutions of twenty litres were made prior to starting a series of tests, and the pH of the decanted solution was adjusted just prior to the test. The batch solution was always well shaken prior to the decanting of solution, although this was only a precaution since all the salts that were used were readily dissolved into their ionic form, and were well below saturation levels.

The pH was adjusted just prior to a test with the addition of NaOH, and the pH was recorded to an accuracy of 0.1 pH units. The quantity of chemicals used was dependent on the composition required for the particular batch solution.

3.2.3.1 Experimental E-pH Diagrams

500 ppm of sulphate was added as H_2SO_4. The pH was varied by the addition of NaOH. NaOH was selected rather than $Ca(OH)_2$ since the resulting solution did not suffer from precipitation or pH variations during the test. It was found that $Ca(OH)_2$ solutions were not stable for the duration of the test. The recommendation by the C.O.M.R.O. that sodium salts were to be used whenever possible, also prompted the decision to use NaOH.

3.2.3.2 Nitrate plus Chloride Solutions

Nitrate was added as $Mg(NO_3)_2.6H_2O$ and chloride was added as NaCl. The pH of the solution was adjusted using NaOH, since the solutions were below the required pH of 6.2 when the nitrate and chloride had been added.

3.2.3.3 Sulphate plus Chloride Solutions

Sulphate was added as H_2SO_4 and chloride was added as NaCl. The pH was adjusted using NaOH.

3.2.3.4 Nitrate plus Sulphate plus Chloride Solutions

Nitrate was added as $Mg(NO_3)_2.6H_2O$, sulphate was added as H_2SO_4 and chloride was added as NaCl. The pH of the solution was adjusted using NaOH.

3.3 INSTRUMENTATION

The potentiodynamic polarization technique was used to obtain polarization curves for the different metal/environment conditions. Two self-contained potentiostat testing systems were utilized.

3.3.1 E & G Princeton Applied Research Potentiostat

The existing equipment was an E & G Princeton Applied Research Model 173 potentiostat/galvanostat. Conversion of the current density to the logarithm of current density was done directly using Model 376 logarithmic current converter. A Saturated Calomel reference Electrode (S.C.E.) was used and was monitored by a Model 178 electrometer probe. A Model 178/41 noise filter was used to reduce the pick-up of noise from power lines at the cell. Potentiodynamic scanning was done using an Eliscint Model ABA-26 external baseline advance. The potential and logarithm of the current were plotted using a Houston Omnigraphic S-200 X-Y plotter. A limit switch was made and fitted to the system to enable the potentiostat to be switched off at any selected current density. Figure 3.2 shows a photograph of Princeton instrumentation.

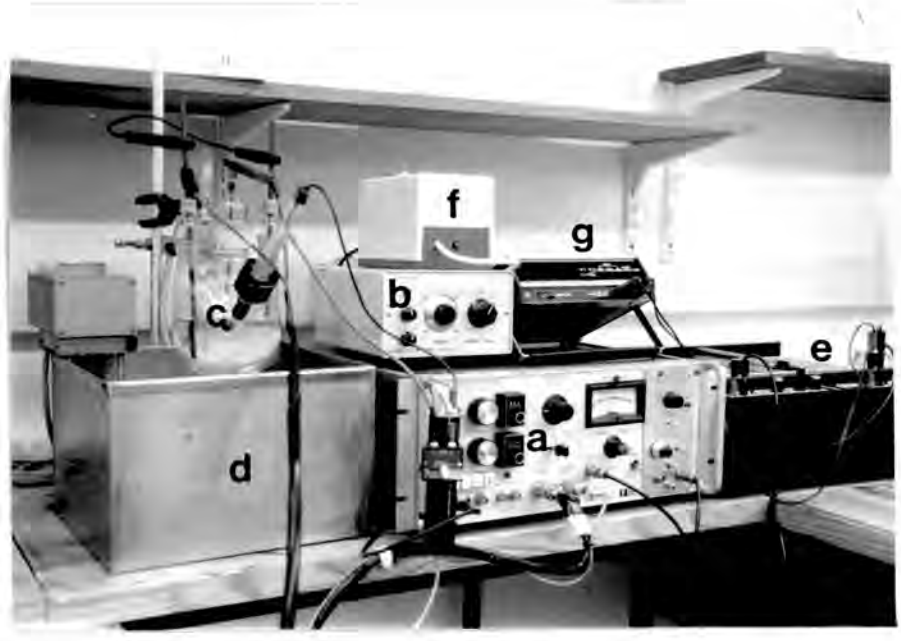

Figure 3.2 : A photograph of the Princeton potentiodynamic testing instrumentation showing : (a) - potentiostat and logarithmic current converter, (b) - scan generator, (c) - corrosion flask, (d) - thermoregulated water bath, (e) - X-Y recorder, (f) - automatic switch off trigger and (g) - the voltmeter.

3.3.2 Wenking Model LT-78 Potentiostat

A Wenking Model LT-78 potentiostat was acquired during the testing program. The current output from the potentiostat is a voltage which is proportional to the current scale selected, and ranges from -200mV to +200mV. This voltage is amplified using a 20 dB gain and the logarithm of the amplified signal is obtained using a Philips Model PM5171 amplifier/logarithmic converter. The resulting output is to a Bryans Southern Equipment A3 XY recorder. The XY recorder was calibrated using an accurate range of input voltages (which correspond to current densities, depending on the scale selected on the potentiostat output) applied to the input of the amplifier/logarithmic converter. The X scale of the XY recorder is thus calibrated for the current scale that is selected at the potentiostat current output. A 50 Hz filter was used on the current input to the XY recorder to reduce the noise which is picked up in the instrumentation from the mains.

A S.C.E. was used as a reference electrode. Potentiodynamic scanning was achieved using a Wenking Model VSG 83 voltage Scan Generator. During potentiodynamic polarization scans, the input switch to the logarithmic converter had to be changed manually from negative to positive at the point where the output voltage from the current output of the potentiostat changed from negative to positive, which

corresponds to the free corrosion potential. This shortcoming is being addressed at present by the design and manufacture of combined logarithmic converter/polarity change over apparatus. A limit switch was also fitted to the Wenking potentiostat system. Figure 3.3 shows a photograph of the Wenking equipment.

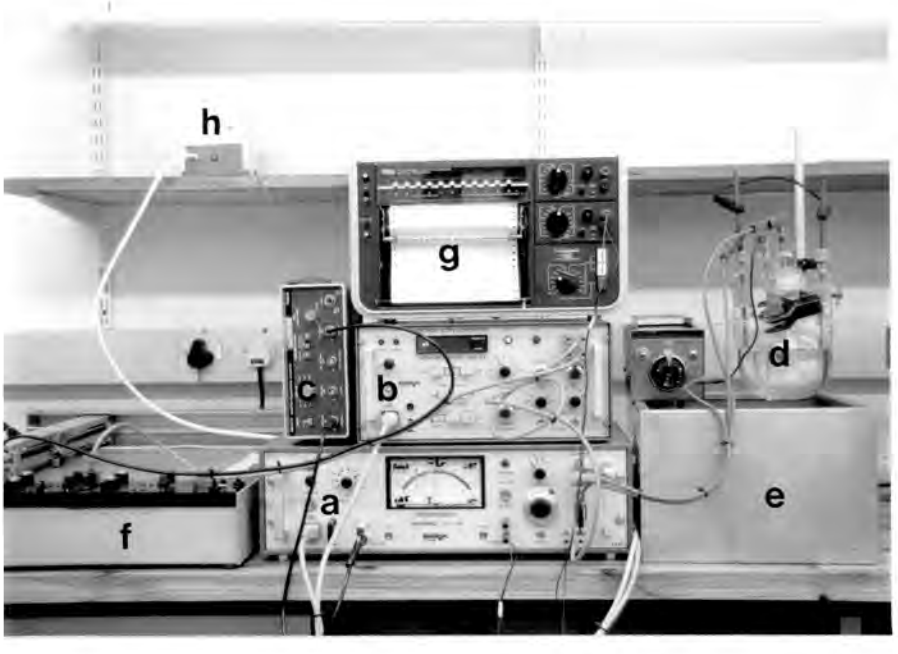

Figure 3.3 : A photograph of the Wenking potentiodynamic polarization testing equipment showing : (a) - potentiostat, (b) - scan generator, (c) - logarithmic current converter, (d) - corrosion flask, (e) - thermoregulated water bath, (f) - X-Y recorder, (g) - two pen recorder and (h) - the automatic switch off trigger.

3.3.3 Corrosion Cell

The same type of corrosion cell was used for both the Princeton and the Wenking systems. All the glass components were copied from the original Princeton Applied Research design, and the work was done by the UCT resident glass blower. A Saturated Calomel Electrode was used as a reference electrode, and has a potential of 0.241 V with reference to the standard hydrogen electrode. The electrolyte in the S.C.E. was changed regularly at the same time that the tip of the electrode was replaced.

Figure 3.4 : A photograph showing the components making up the corrosion cell showing : (a) - P.T.F.E. specimen holder, (b) - saturated calomel electrode and (c) - the graphite electrode.

3.4 TESTING PROCEDURE

3.4.1 Standard Test

Prior to testing with both systems, the ASTM standard G5-78 (ASTM, (1980)) test on AISI 430 in 1N H_2SO_4 was performed to ensure that the systems were operating correctly. Both systems returned results which were very close to the ASTM standard curve. The systems were presumed to be functioning correctly after this test was completed, and the standard tests were run again midway in the testing program to re-check the systems. Again, the resulting curves corresponded well with the ASTM curve.

3.4.2 Construction of an Experimental E-pH Diagram

Alloy 1210, Alloy 825 and 3CR12 had experimental E-pH diagrams constructed for them. The test conditions were the same for each material, and correspond to the method that Capendale used to construct an experimental E-pH diagram for AISI 431. This allows Capendale's work to be included in the evaluation of these materials. The test solution was maintained at a constant 30°C by immersing the corrosion cell in a thermoregulated water bath. Ultra-high purity nitrogen was purged through the system for two hours prior to the test beginning, thereby de-aerating the solution. The specimens were polarized to a cathodic potential of -1.4V vs S.C.E. half an hour before the commencement of the test. Potentiodynamic scanning was performed at a rate of 0.12 mV/second in the noble direction until the breakdown potential, E_{br}, had been achieved. The test was then terminated.

The experimental pH diagram was constructed by plotting the corrosion potential, E_{corr}, the breakdown potential, E_{br}, and when present the Flade potential ,E_f, against the pH. Figure 3.5 shows how this was done.

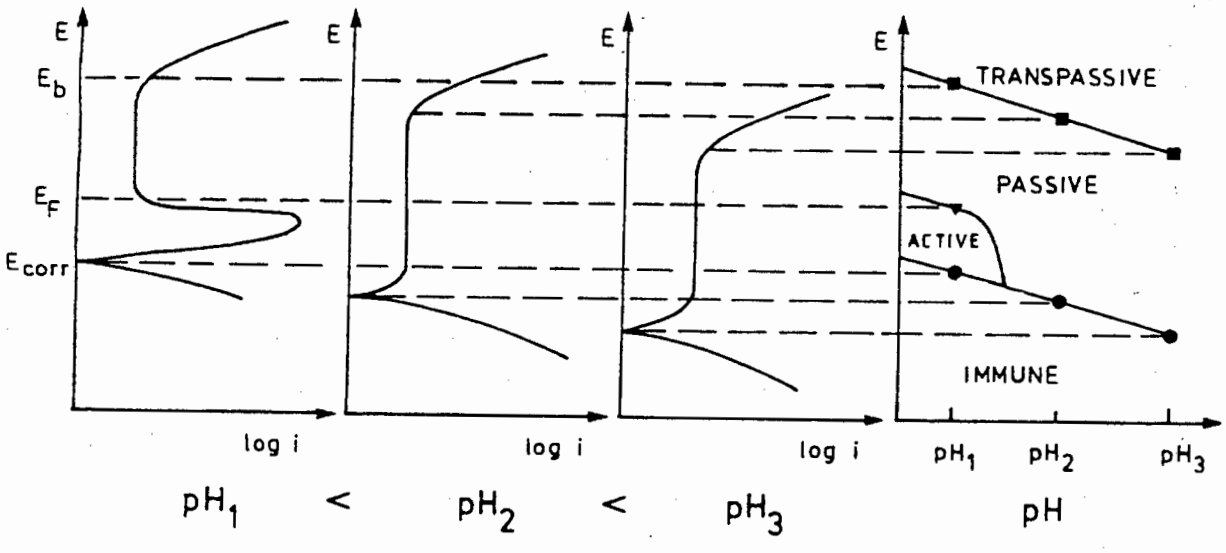

Figure 3.5 : The construction of an experimental E-pH diagram. (after Capendale (1985)).

3.4.3 Determination of Critical Chloride Concentrations

The tests were performed in oxygen saturated solutions. This was done by bubbling of oxygen through the test solution for thirty minutes prior to the test beginning. The solution temperature was maintained at 30°C by placing the corrosion cell in a thermoregulated

water bath. Twenty minutes prior to the potentiodynamic test beginning, the specimen was polarized to 100 mV cathodic to its free corrosion potential.

The potentiodynamic scan was carried out at a rate of 0.12 mV/second in the anodic direction. The test was continued until the potential exceeded the breakdown or pitting potential and reached a current density of approximately 1 mA/cm^2. At this point the scanning direction was reversed.

Two distinct types of return scan were evident. (i) When the passive film had broken down transpassively, then the return scan followed the prior scan line. (ii) However, when the passive film had broken down locally, the return scan resulted in a hysteresis loop. The point at which this hysteresis loop returned to the passive region of the scan, was regarded as the protection potential, E_{prot}.

The chloride concentration above which localized breakdown of passivity occurred due to pitting and below which uniform corrosion occurred due to transpassivity was defined to be the critical chloride concentration, $[Cl^-]_{crit}$. Figure 3.6 shows how $[Cl^-]_{crit}$ is determined experimentally. The diagram on the left shows a schematic polarization scan for a solution where the chloride concentration is below $[Cl^-]_{crit}$. The values of E_{corr} and E_{br} are plotted on the centre diagram at the corresponding chloride concentration. The schematic polarization curve on the right shows the condition where the chloride concentration is above $[Cl^-]_{crit}$ and therefore the passive film has broken down locally by pitting corrosion. This results in a pitting potential, E_p, and a protection potential E_{prot}, as well as a corrosion potential, E_{corr}. These are plotted on the central diagram at their corresponding chloride concentration. Experimentally, E_{corr}, E_{br} / E_p and E_{prot} are determined at increasing chloride concentrations in a solution containing the same pH, and other ionic concentrations.

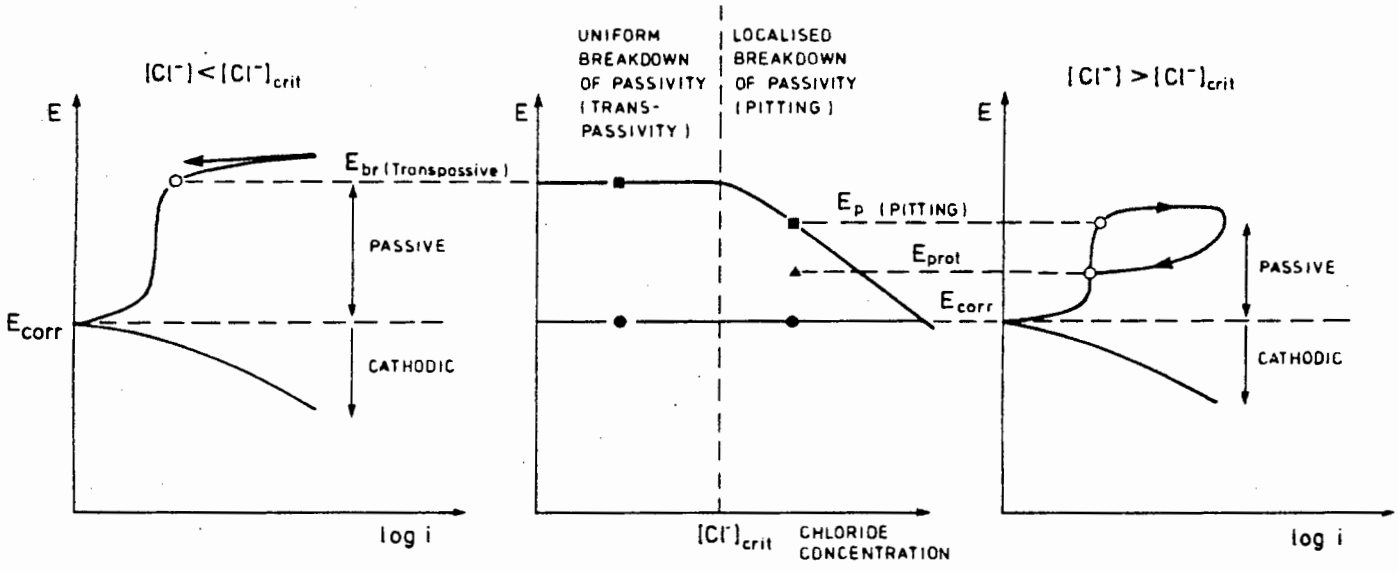

Figure 3.6 : The determination of $[Cl^-]_{crit}$ (after Capendale (1985))

It can be seen in the central diagram that $[Cl^-]_{crit}$ for the material is between the chloride concentrations of the two tests.

3.4.4 Free Corrosion Potential vs Time Tests

An E_{corr} vs time test was done over a twelve hour period for each of the four steels. The solution contained 500 ppm nitrate, 1000 ppm sulphate, 1000 ppm chloride at a pH of 6.2. The solution was maintained saturated with oxygen throughout the test, and the temperature was maintained at 30°C. The corrosion potential was monitored on a pen recorder at a scan rate of 2 cm/hour.

3.4.5 Microscopic Examination

After testing specimens were cleaned and examined using optical microscopy. This examination was used to determine whether the passive layer broke down by transpassive or pitting corrosion. Figure 3.7 shows a pitted surface while figure 3.8 shows a surface that has been transpassively corroded.

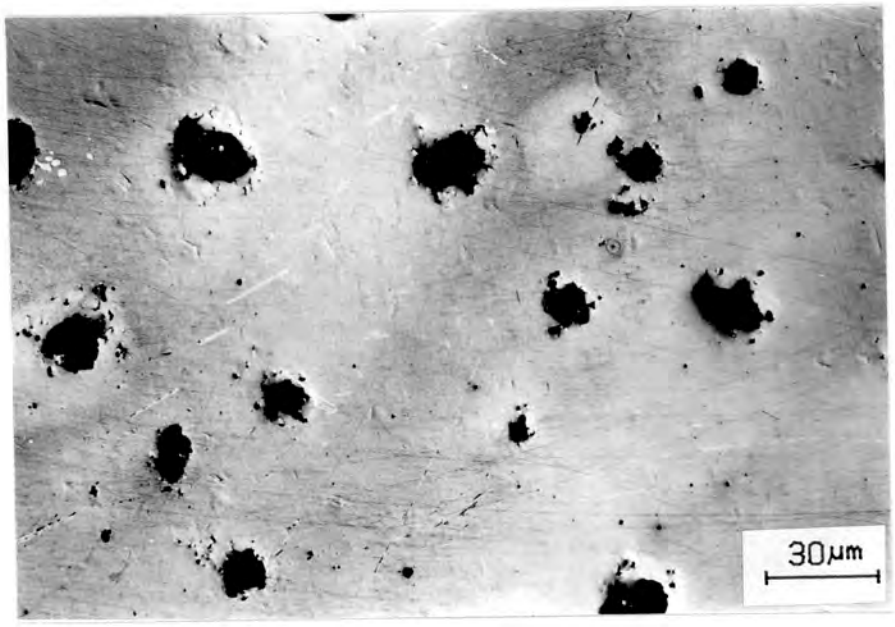

Figure 3.7 : Pitted surface of Alloy 1210

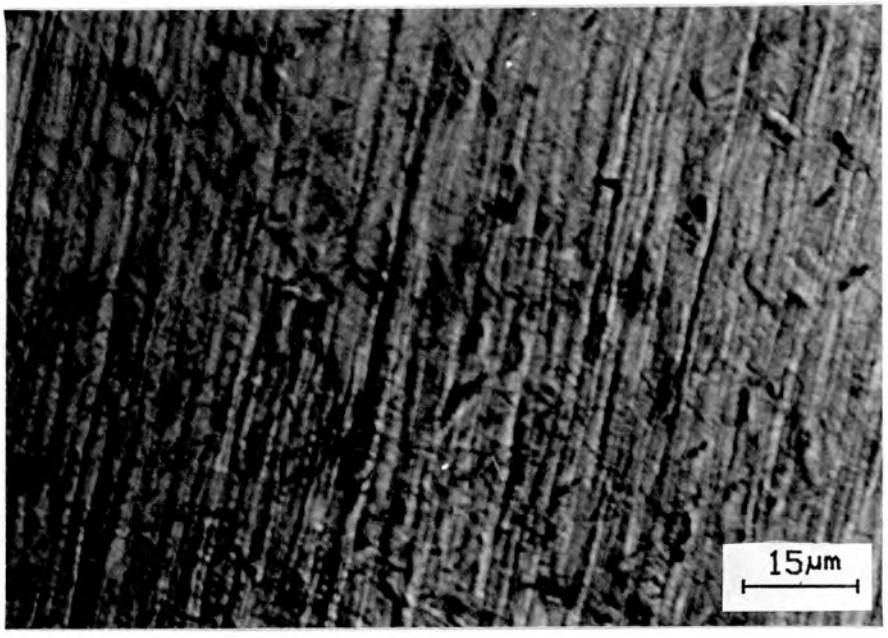

Figure 3.8 : Transpassive surface of Alloy 1210

Optical microscopy was complemented by the use of scanning electron microscopy (SEM).

3.5 THE MATERIALS

Four materials were considered, namely AISI 431, ALLOY 1210, 3CR12 and ALLOY 825. All of the alloys were tested in the as received condition which was characterised by microstructural work.

AISI 431 was selected as a standard, for the following reasons :

(i) Capendale (1985) selected AISI 431 as a standard material, since no final selection of the development alloys had been made at the time. AISI 431 was chosen because it had been selected as an initial choice by the Chamber of Mines for many of the moving components in mining machinery operating in water. By selecting AISI 431 as a standard material the results that Capendale obtained can be utilised in an ongoing research program.

(ii) AISI 431 has a martensitic microstructure, and contains more chromium than the development alloys. This allows the effect of reduced chromium content on the corrosion resistance of the development alloys to be evaluated.

The compositions of these alloys is shown in table 3.1 below.

% COMPOSITION	AISI 431	ALLOY 1210	3CR12	ALLOY 825
Carbon	0.15	0.046	0.022	0.27
Chromium	16.34	12.07	11.52	7.97
Nickel	2.33	0.09	0.61	2.96
Nitrogen	0.045	0.180	0.019	0.006
Sulphur	0.009	0.005	0.006	0.006
Manganese	0.54	9.31	1.24	0.01
Molybdenum	0.079	0.001	0.016	0.000
Cobalt	0.056	0.012	0.012	0.006
Aluminium	0.010	0.020	0.016	0.016
Phosphorus	0.025	0.016	0.026	0.000
Titanium	0.002	0.000	0.334	0.003
Niobium	2.33	0.005	0.004	0.003
Silicon	0.38	0.43	0.42	0.01
Copper	0.111	0.022	0.088	0.010

Table 3.1 : Compositions of AISI 431, ALLOY 1210, 3CR12 and ALLOY 825 (Middelburg Steel and Alloys, (1987))

3.5.1 AISI 431

AISI 431 is a martensitic alloy which has a recommended 16.5% chromium, 1.8% nickel and 0.18% carbon composition. It is easily

quench hardened to high strength levels, and has been recommended by the Chamber of Mines as an initial choice for many of the moving components in mining machinery operating in mine water. Examination of the microstructure revealed islands of austenite in a matrix of martensite. The material was tested in the as received condition (275 HV), and a photograph of the microstructure is shown in figure 3.9.

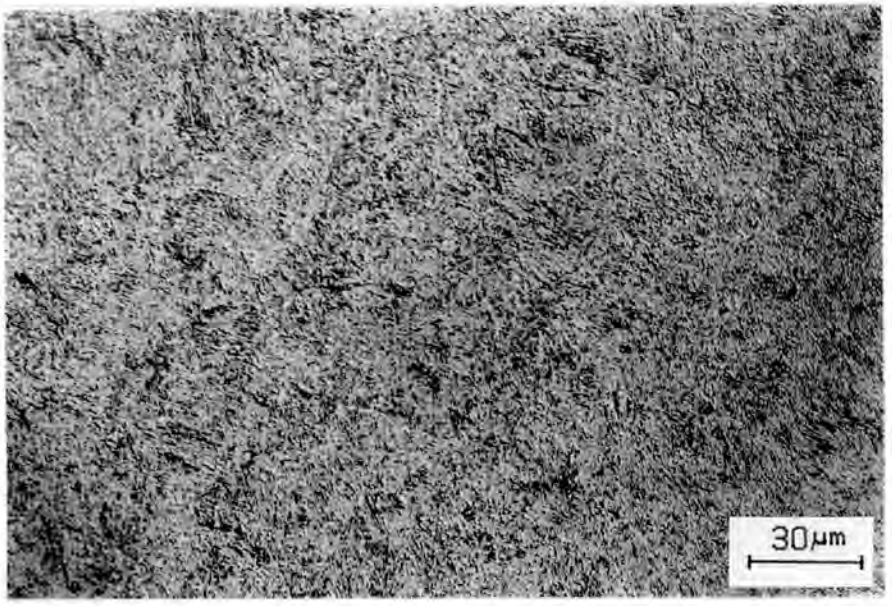

Figure 3.9 : Microstructure of AISI 431 in the as received condition. Specimen etched in 5g $FeCl_3$ + 15 ml conc. HCl + 15 ml EtOH + 20 ml water + 5 drops HNO_3 for 10 seconds at room temperature.

The AISI 431 that was used had a clean martensitic structure that was free of other precipitates (Barker (1988)). There was no evidence of coarse manganese sulphide inclusions.

3.5.2 Alloy 1210

1210 is an unstable austenitic nitrogen bearing steel that has a composition of 12% chromium, 10% manganese, 0.05% carbon and 0.2% nitrogen. The unstable austenite transforms to hard martensite under deformation, conferring very high work hardening and potentially good wear resistance. 1210 has proof strength, ductility, toughness and hardness similar to austenitic stainless steels (such as 304) with fracture strength similar to martensitic stainless steels (such as 410) (Lenel and Knott, (1986)). Alloy 1210 was tested in the as received condition (232 HV), and the specimen was etched to examine the microstructure after it had been mechanically polished. Electrolytic etching was not used because the surface of the test

specimens was mechanically polished and by using electrolytic etching the effect of the mechanical polishing on the surface layer microstructure would not have been seen. Figure 4.10 shows the austenitic microstructure of Alloy 1210 with strain induced martensite on the surface.

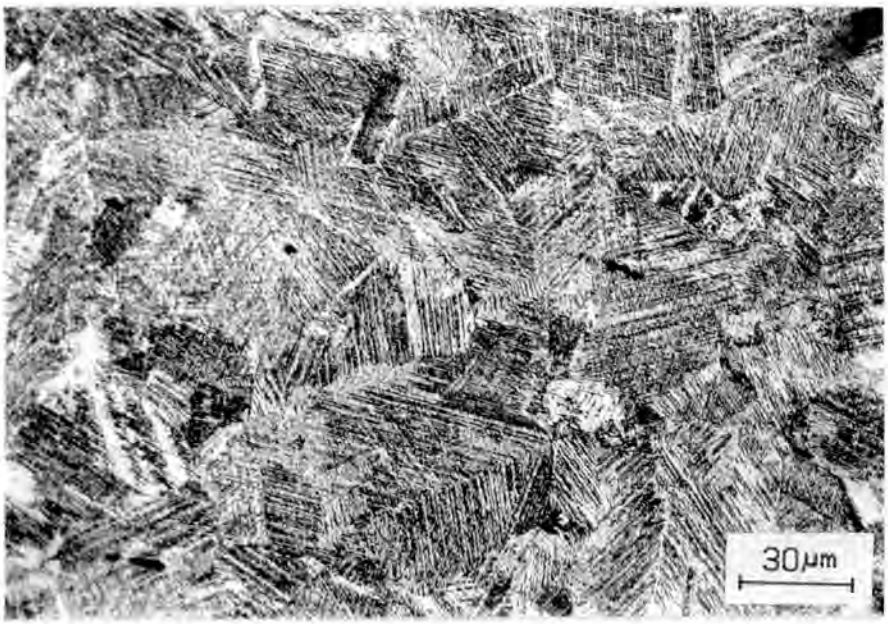

Figure 3.10 : Microstructure of Alloy 1210 in the as received condition. Specimen etched in 5g $FeCl_3$ + 15 ml conc. HCl + 15 ml EtOH + 20 ml water + 5 drops HNO_3 for 20 seconds at room temperature.

The microstructure shows twinning which is typical of FCC matrices. The fine parallel lines are due to selective etching along slip lines. There is a low incidence of carbides and other precipitates in the matrix (Barker, (1988)). X-ray diffraction revealed that there was 85% austenite on the surface of the specimens being used.

3.5.3 3CR12

3CR12 is a microduplex 12% chrome steel, which has a very fine grained dual phase microstructure of ferrite and low carbon lath martensite. It has a composition of 12% chromium (max.), 0.03% carbon (max.), and 0.4% Ti (min.). 3CR12's attractive strength, toughness and forming properties have been associated with the stable, fine grained structure that results from annealing at temperatures between 675°C and 750°C (Ball and Hoffman, (1981)). 3CR12 is regarded as a corrosion resisting steel that has very promising corrosion-abrasion resistance (Allen, Ball and Protheroe, (1981)). 3CR12 was tested in the as received condition (162 HV), and the microstructure is shown in figure 3.11.

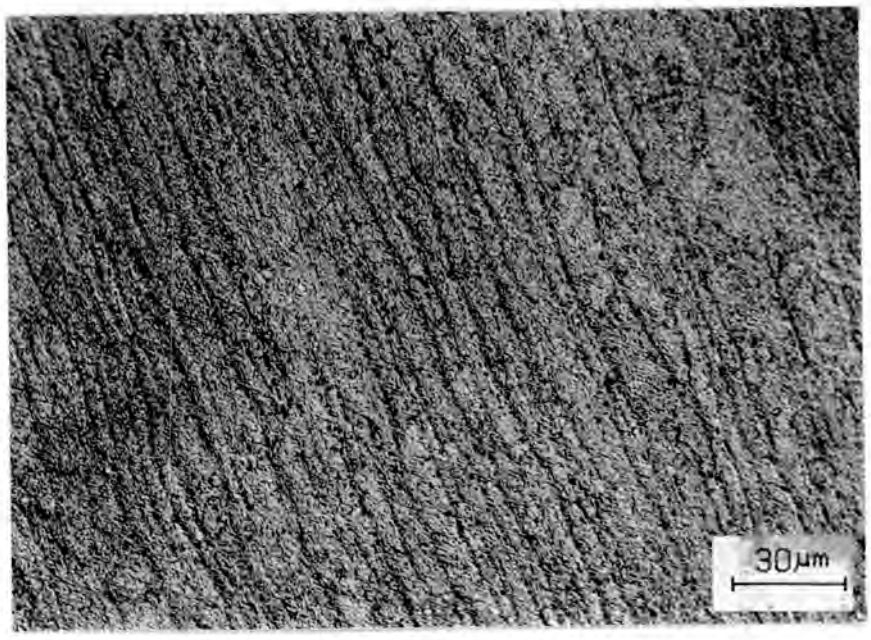

Figure 3.11 : Microstructure of 3CR12 in the as received condition. Specimen initially etched in 20 ml conc. HCl + 10 ml HNO_3 + 30 ml water for 180 seconds at room temperature and then etched in 1g potassium meta bisulphite + 2g ammonium biflouride + 100 ml 20 volume % HCl for 10 seconds at room temperature.

There is 25 - 35% ferrite in the form of elongated islands following the rolling direction of the steel and equiaxed grains of martensite. Impurities in the matrix consist mainly of fine titanium carbonitrides and manganese sulphides. The microstructure displays more fine impurities than Alloy 1210, but the equivalent number of coarser precipitates.

3.5.4 Alloy 825

Alloy 825 has a martensitic microstructure and contains 8% chromium, 0.25% carbon and 3% nickel. Alloy 825 was tested in the as received condition (245 HV). The photograph in figure 4.12 shows a homogenous lath martensite microstructure which results from the prior austenite which had a grain size of approximately 30 micro metres. There is no evidence of coarse precipitates along the grain boundaries or within the matrix. There are fine Fe_3C, Cr_6C_{23} and MnS precipitates within the lath martensite.

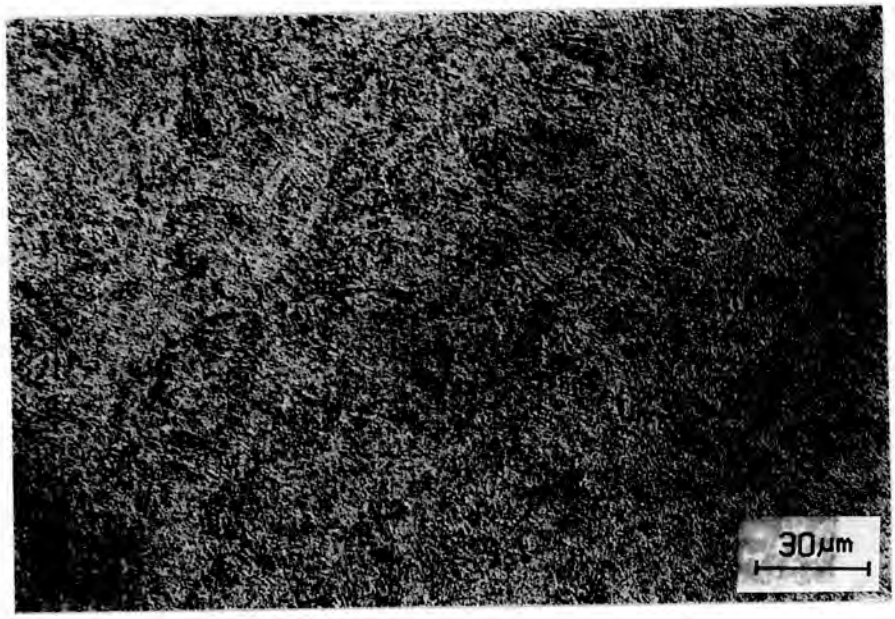

Figure 3.12 : Microstructure of Alloy 825 in the as received condition. Specimen etched in 5g $FeCl_3$ + 15 ml conc. HCl + 15 ml EtOH + 20 ml water + 5 drops HNO_3 for 8 seconds at room temperature.

CHAPTER 4

RESULTS AND DISCUSSION

4.1 CONSTRUCTION OF EXPERIMENTAL E-pH DIAGRAMS FOR THE ALLOYS

Capendale (1985) constructed an experimental E-pH diagram for the martensitic stainless steel AISI 431 (figure 4.1) by recording potentiodynamic polarization curves in a series of solutions containing 500 ppm of sulphate ions (added as H_2SO_4), and increasing amounts of $Ca(OH)_2$ to vary the pH. The curves were measured in solutions deaerated by ultra high purity nitrogen, at 30°C using a scan rate of 0.12 mV/second. He then compared his diagram with a simplified theoretically constructed E-pH diagram for chromium. The similar nature of the two E-pH diagrams lead him to conclude that the corrosion resistance of AISI 431 could be ascribed to the chromium enriched oxide layer present on the surface of AISI 431. He proposed that the experimentally determined E-pH diagram for AISI 431 be regarded as a standard for other stainless steels which were likely to be developed for the mining industry.

The composition and microstructure of the new development alloys Alloy 1210, 3CR12 and Alloy 825 are different from that of AISI 431. This necessitated the establishment of experimental E-pH diagrams for these alloys which were determined under similar experimental conditions as for AISI 431.

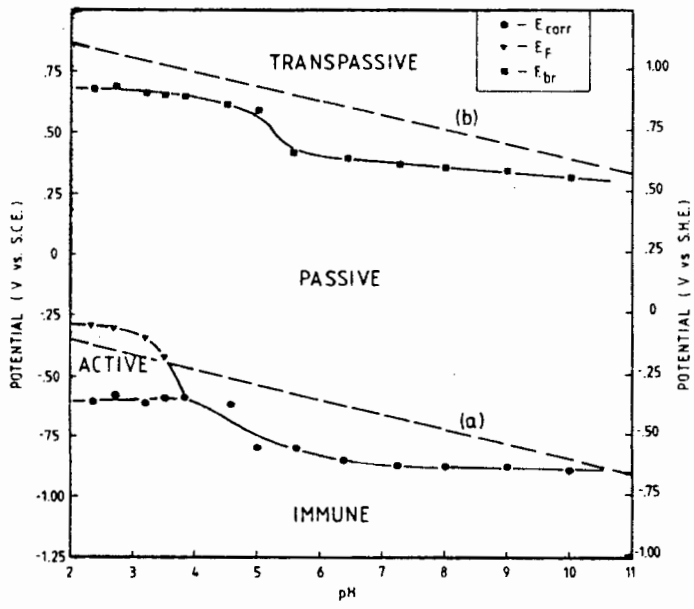

Figure 4.1 : Experimental E-pH diagram for AISI 431 in 500 ppm SO_4^{2-} + xmg $Ca(OH)_2$ solutions (after Capendale, (1985))

4.1.1 Alloy 1210

Below a pH of 9.2 active to passive polarization behaviour was observed, resulting in the specimen being generally corroded on the exposed surface. Figure 4.2 shows the polarization curve obtained for a solution with a pH of 2.2. The potentials recorded for the corrosion potential (E_{corr}), the Flade potential (E_F) and the breakdown potential (E_{br}) are shown in the figure.

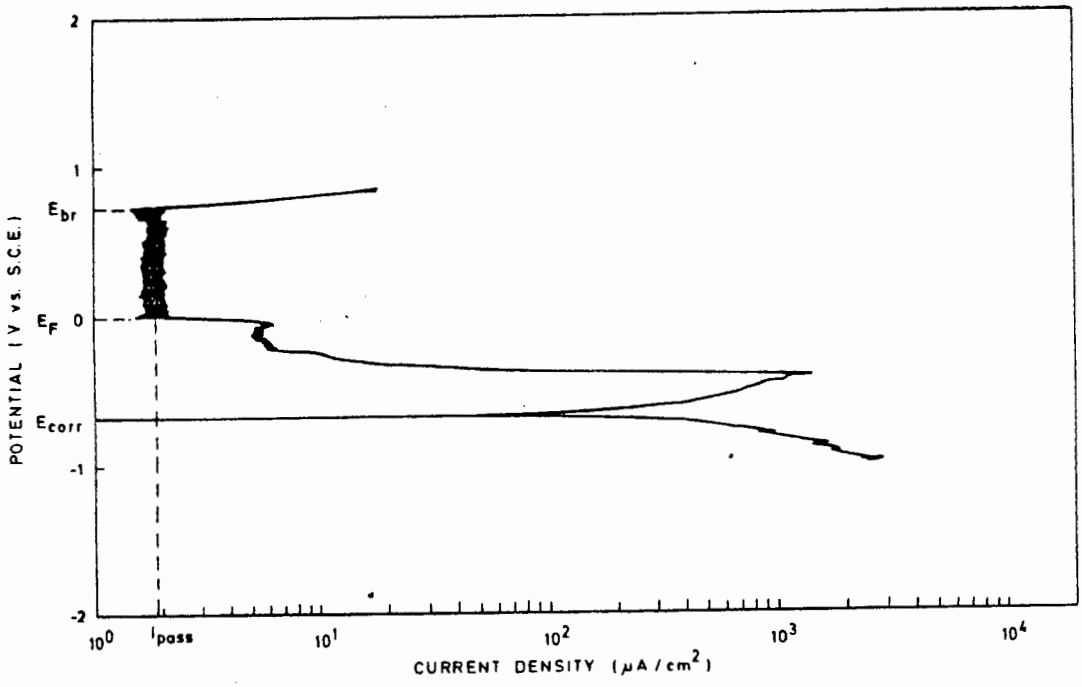

Figure 4.2 : Potentiodynamic curve for Alloy 1210 in a solution of pH 2.2. The positions of E_{corr}, E_F and E_{br} are shown on the curve.

Above a pH of 10.2 the corrosion potential of the specimen lies in the passive region. Figure 4.3 shows the potentiodynamic polarization curve for a solution of pH 10.2. No active to passive transition is observed which indicates that the cathodic and anodic curves intersect in the passive range of the anodic curve. Transpassive breakdown occurs at 0.18 V (S.C.E.) and results in the exposed surface of the specimen being transpassively corroded.

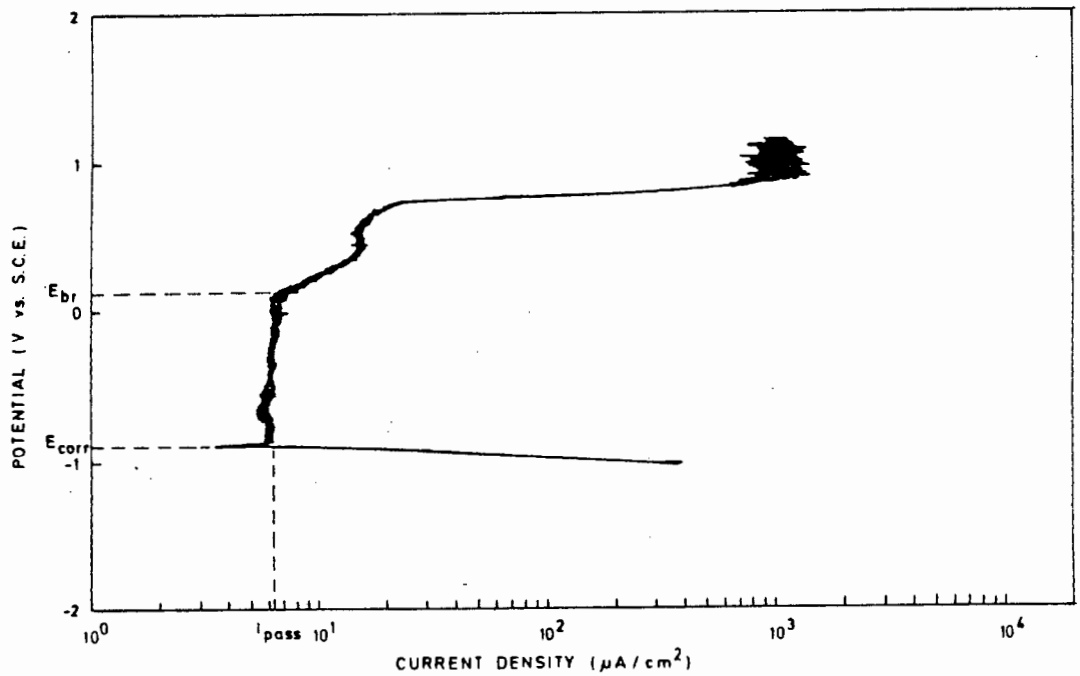

Figure 4.3 : Potentiodynamic curve for Alloy 1210 in a solution of pH 10.2. The positions of E_{corr} and E_{br} are shown on the curve.

An experimental E-pH diagram was constructed from the values of E_{corr}, E_F and E_{br} between pH 2.2 and 9.2 and from the values of E_{corr} and E_{br} above pH 10.2. Figure 4.4 shows the resulting experimental E-pH diagram indicating the potential with reference to both the saturated calomel electrode (S.C.E.) and the standard hydrogen electrode (S.H.E.).

Line 'a' represents the hydrogen evolution reaction (HER) whereas line 'b' represents the oxygen reduction (ORR) reaction. Between pH 2.2 and 9.2, active to passive behaviour is predicted where the HER is the cathodic reaction. However, the ORR could raise the corrosion potential above the potential of the active to passive transition resulting in the passivation of the surface of the steel in this pH range. Above a pH of 9.2 both cathodic reactions could raise the corrosion potential above the active to passive transition thereby resulting in the passivation of the surface.

The pH of mine water is expected to be between 3.8 and 9.4, while near neutral solutions are most common. Therefore for mine waters that contain sulphate ions in concentrations of 500 ppm or greater, Alloy 1210 could be in the active state if the redox potential of the solution caused the corrosion potential to fall in the active range as indicated by the experimental E-pH diagram. By comparison AISI 431 showed active to passive behaviour only in mildly acidic solutions at pH's below 3.8. Mine water is generally saturated with

oxygen, and therefore the corrosion potential of Alloy 1210 would be expected to be in the passive range for solutions containing sulphate ions at this level. However, in stagnant water which is oxygen depleted, there is a possibility that the steel will be in an active state, depending on the level of other oxidising species in solution.

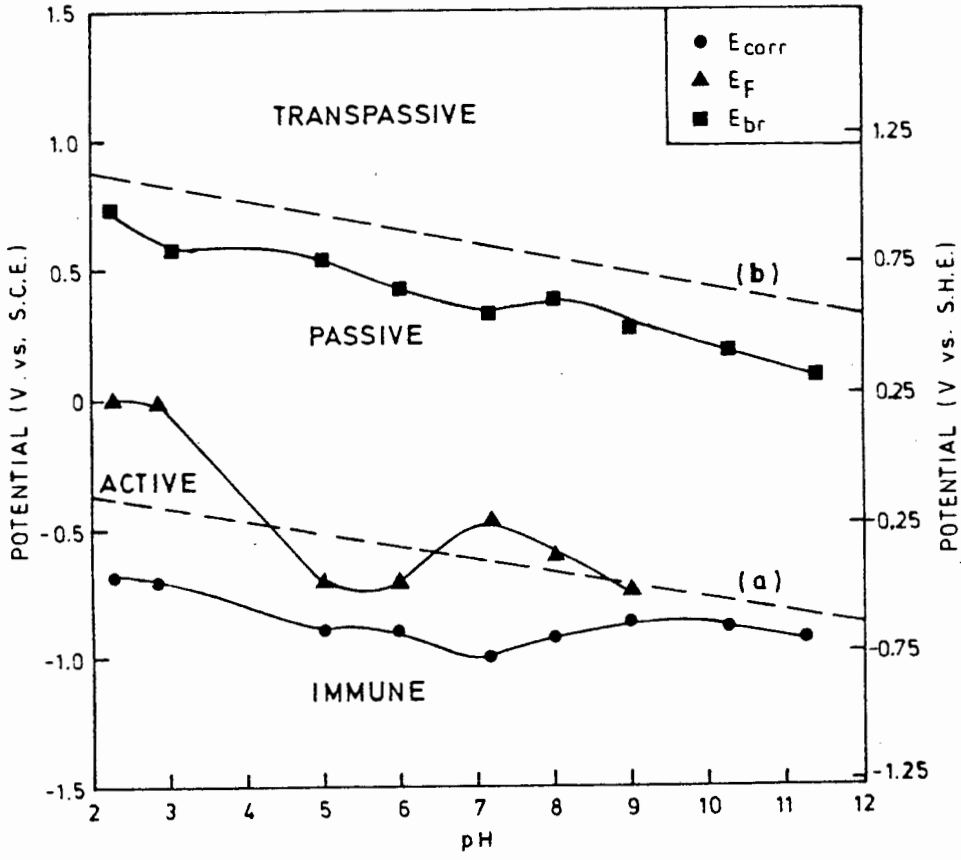

Figure 4.4 : Experimental E-pH diagram for Alloy 1210 in 500 ppm SO_4^{2-} + xml NaOH solutions.

For all pH values, polarization of the specimen to sufficiently high potentials resulted in transpassive breakdown of the passive layer. A general trend of decreasing breakdown potentials with increasing pH was observed. There was trebling of the passive corrosion current density from 2 $\mu A/cm^2$ (pH range = 2.2 - 6.0) to 6$\mu A/cm^2$ (pH range = 9.18 - 11.25), and a high average current density of 30$\mu A/cm^2$ for the pH range of 8 to 9.18. The exceptionally high current densities at this pH range could not be explained.

The increased active range of Alloy 1210 compared to AISI 431 is evident from the experimental E-pH diagrams and can be attributed to the lower chromium content present in Alloy 1210 (12%) compared to AISI 431 (16%).

4.1.2 3CR12

An experimental E-pH diagram was constructed from the values of E_{corr}, E_F and E_{br} as described in the previous section. Figure 4.5 shows the resulting E-pH diagram indicating the potentials with reference to the S.C.E. and the S.H.E.. Active to passive behaviour was observed over the whole range of pH values tested (2.0 - 10.0).

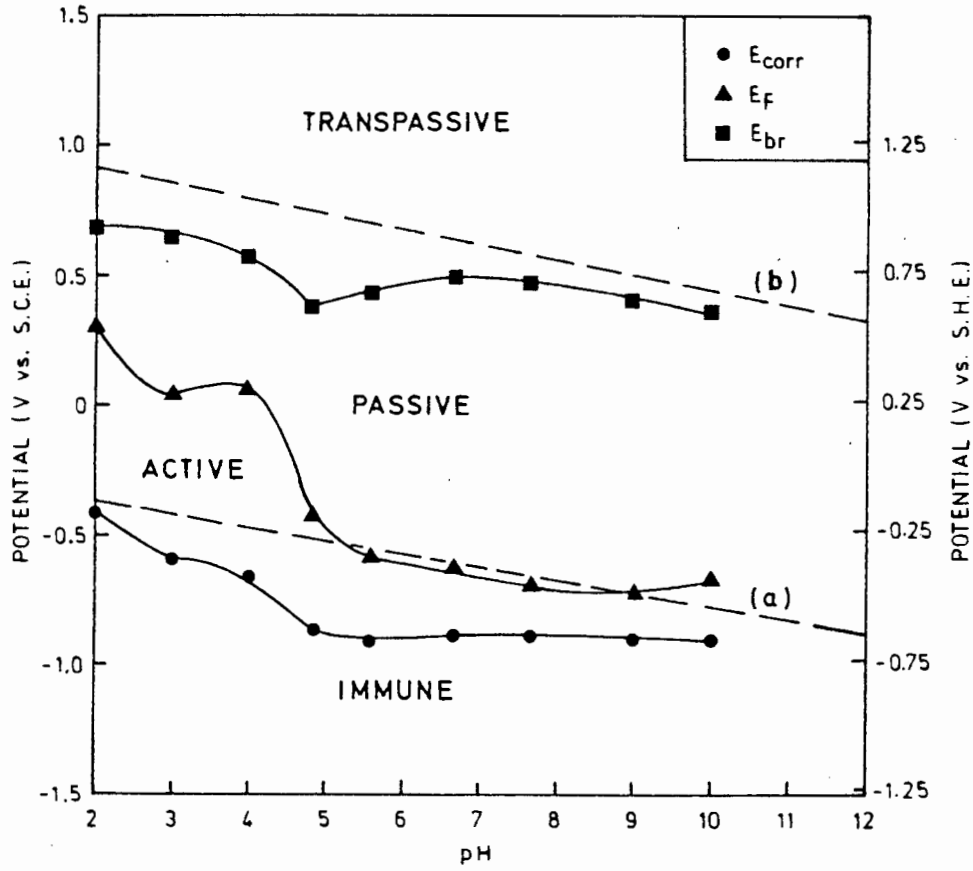

Figure 4.5 : Experimental E-pH diagram for 3CR12 in 500 ppm SO_4^{2-} + xml NaOH solutions.

At pH values less than 5, the passive region is constricted by the large active region as shown in the experimental E-pH diagram above. It is significant that the active to passive behaviour extends throughout the range of pH values tested. The large potential range of the active region indicates that in mildly acidic to acidic sulphate containing mine waters, there is a strong possibility that 3CR12 will be in the active state. As in the case of Alloy 1210, 3CR12 could be in the active state in sulphate containing mine waters that have a suitable redox potential to cause the corrosion potential to fall into the active region. The redox potential is dependent on the oxidizer concentration in solution, and oxygen and metallic ions are the most common oxidizers present in mine water. The passive corrosion current density centred around 6 $\mu A/cm^2$ throughout the pH

range tested. For all pH values, polarization of the specimen to sufficiently high potentials resulted in transpassive breakdown of the passive layer. As was the case for AISI 431 and Alloy 1210, a general trend of decreasing breakdown potentials with increasing pH was observed.

3CR12 and Alloy 1210 have similar chromium contents in the region of 12%. Regardless of the effects of microstructure and other alloying elements, it can be seen that the experimental E-pH diagrams are similar as a result of the comparative chromium contents. Although this is a simplification, it is an indication that the ability of an alloy to passivate in sulphate solutions of varying pH, is strongly dependent on the chromium alloying content at these levels.

4.1.3 Alloy 825

Below a pH of 6.0 the the potentiodynamic polarization curves for Alloy 825 exhibited a direct transition from the corrosion potential to transpassive behaviour. No passive region was evident in this range. The polarization curve for a solution of pH 2.10 shows this transition in figure 4.6.

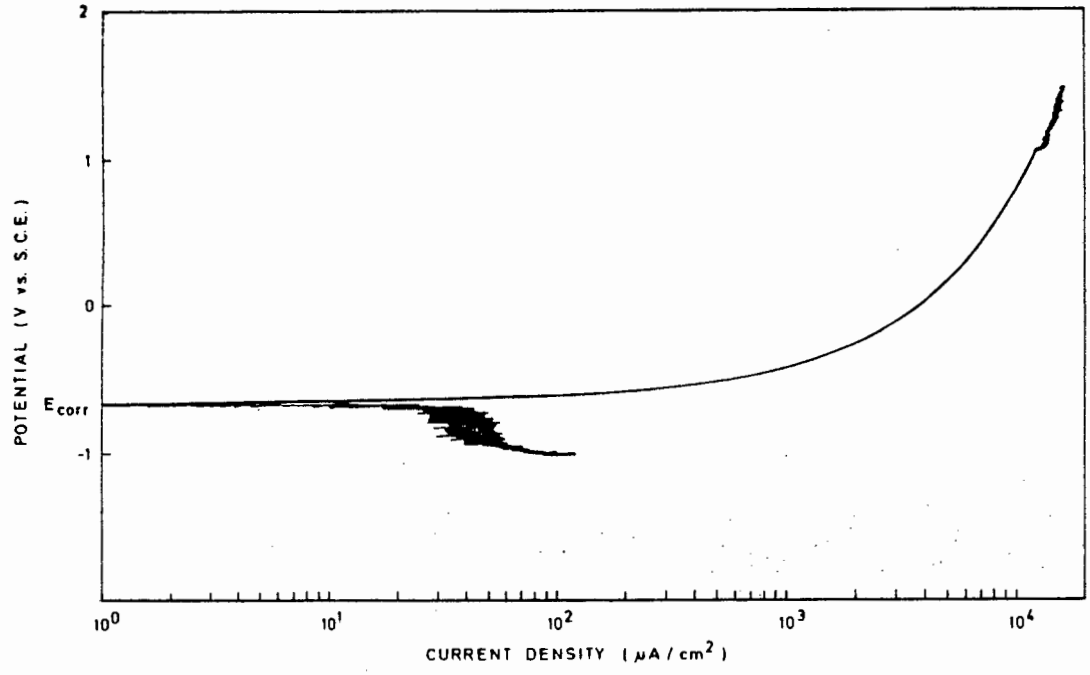

Figure 4.6 : The potentiodynamic polarization curve for Alloy 825 in a 500 ppm SO_4^{2-} solution at pH 2.10.

Between pH 6.0 and 9.3 active to passive behaviour was present. The passive region between pH 6.0 and 8.0 was smaller than 50 mV, and only increased in magnitude at pH values greater than pH 8.0. The

active to passive transition was no longer present at pH 10. The resulting values of E_{corr}, E_F (when present) and E_{br} were plotted against their corresponding pH values to obtain an experimental E-pH diagram, shown in figure 4.7 below.

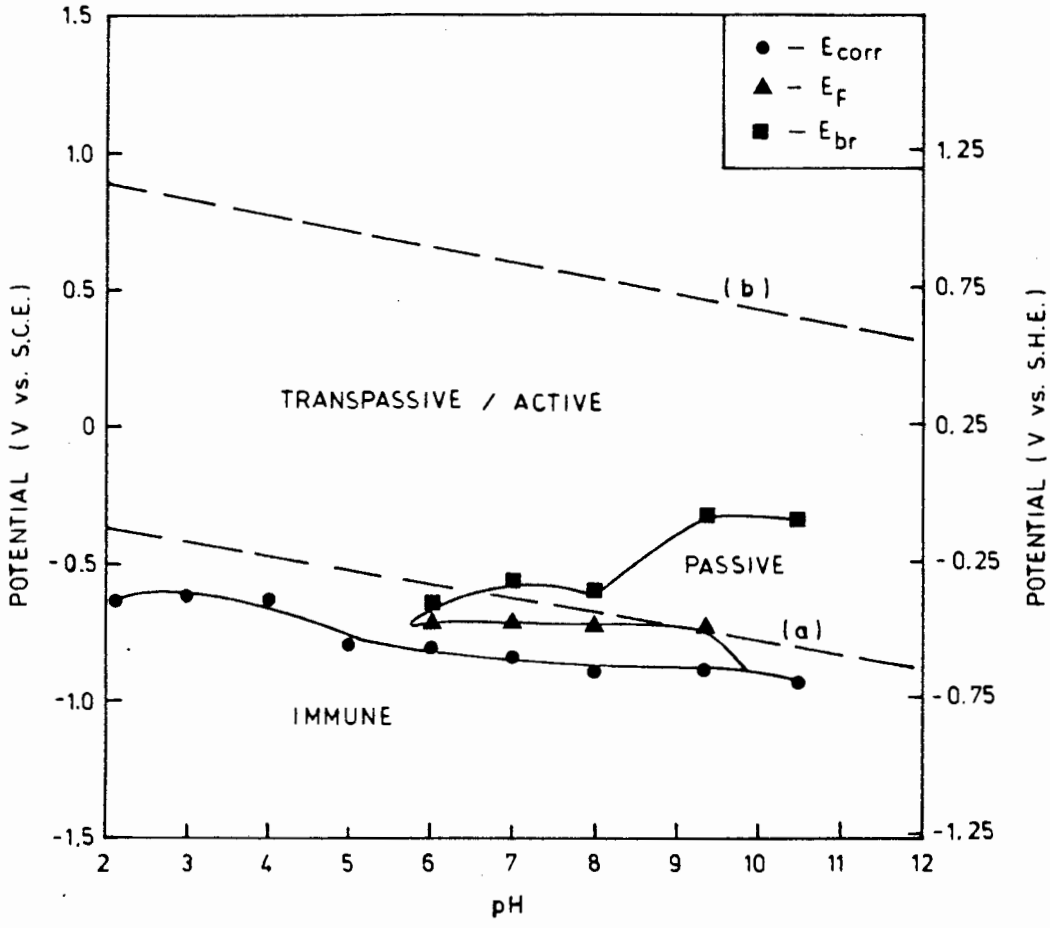

Figure 4.7 : Experimental E-pH diagram for Alloy 825 in 500 ppm SO_4^{2-} + xml NaOH solutions.

Below pH 6.0 there is no active or passive region and both the HER and the ORR will result in Alloy 825 corroding transpassively. Alloy 825 has a low chromium content of approximately 8%, which is below the 11% chromium level that is regarded as being essential for a stainless steel (Sedriks, (1979)). For this reason it is expected that the passive layer that is formed on Alloy 825 will not be of the Cr_xO_x type found on stainless steels and therefore it will not show passive characteristics like a stainless steel (Proctor, (1988). In a solution of 500 ppm SO_4^{2-} below a pH of 6.0, Alloy 825 does not have a stable passive layer. Between pH 6.0 and 9.3 active to passive behaviour is shown and the passive layer is only stable over a small potential range as is shown in the E-pH diagram. Above pH 9.3 the cathodic and anodic curves intersect in the passive range of the anodic curve, and there is a direct transition from an immune condition to a passive state.

It is expected that sulphate ions will decrease the stability of the passive layer on Alloy 825 by increasing the conductivity in solution. A similar detrimental effect of sulphate ions on corrosion rates of mild steel has been shown by Rawat (1976) and Mursalo et al (1988). The E-pH behaviour of Alloy 825 suggests that it's corrosion behaviour is similar to that of low alloy steels and mild steel.

4.2 THE PITTING CORROSION BEHAVIOUR OF THE ALLOYS IN CHLORIDE SOLUTIONS

The pitting corrosion behaviour of the development alloys was determined in distilled water and in distilled water plus chlorides to enable a comparison to be made with the pitting behaviour in solutions which had sulphate and nitrate ions added to inhibit pitting attack by chloride ions. Polarization scans were performed for the four alloys in fully aerated distilled water in the absence of chloride, and with the addition of 100 ppm of chloride ions. The resulting polarization scans are shown in the figures below.

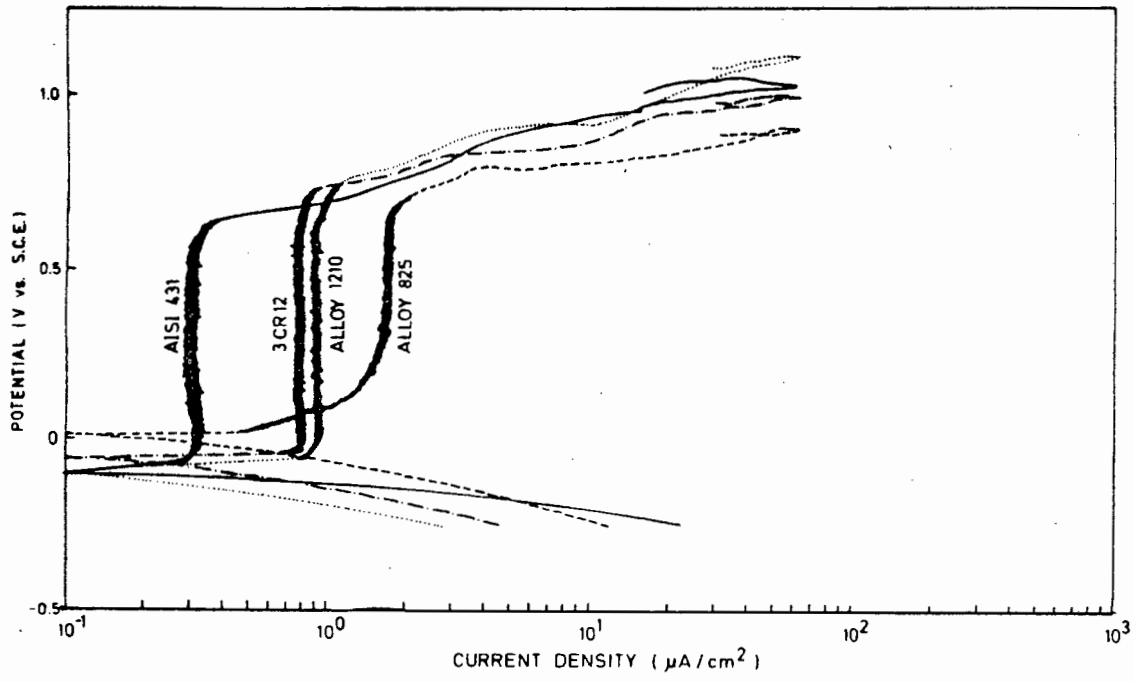

Figure 4.8 : The polarization curves for AISI 431, Alloy 1210, 3CR12 and Alloy 825 in aerated distilled water.

Figure 4.8 shows the polarization curves for the alloys in distilled water. All of the alloys show a well defined passive region which extends until breakdown by transpassive corrosion above 0.5 V (S.C.E.).

All the alloys show the reverse scan following the forward scan closely with no evidence of a hysteresis loop. Examination by optical microscopy revealed transpassively corroded specimen surfaces with no pitting corrosion present. The passive corrosion current density is highest for Alloy 825 and lowest for AISI 431, which corresponds with the chromium level in each of the alloys i.e. AISI 431 (16%) > Alloy 1210 and 3CR12 (12%) > Alloy 825. The higher chromium content allows the formation of a more stable passive layer and therefore reduces the passive corrosion current density.

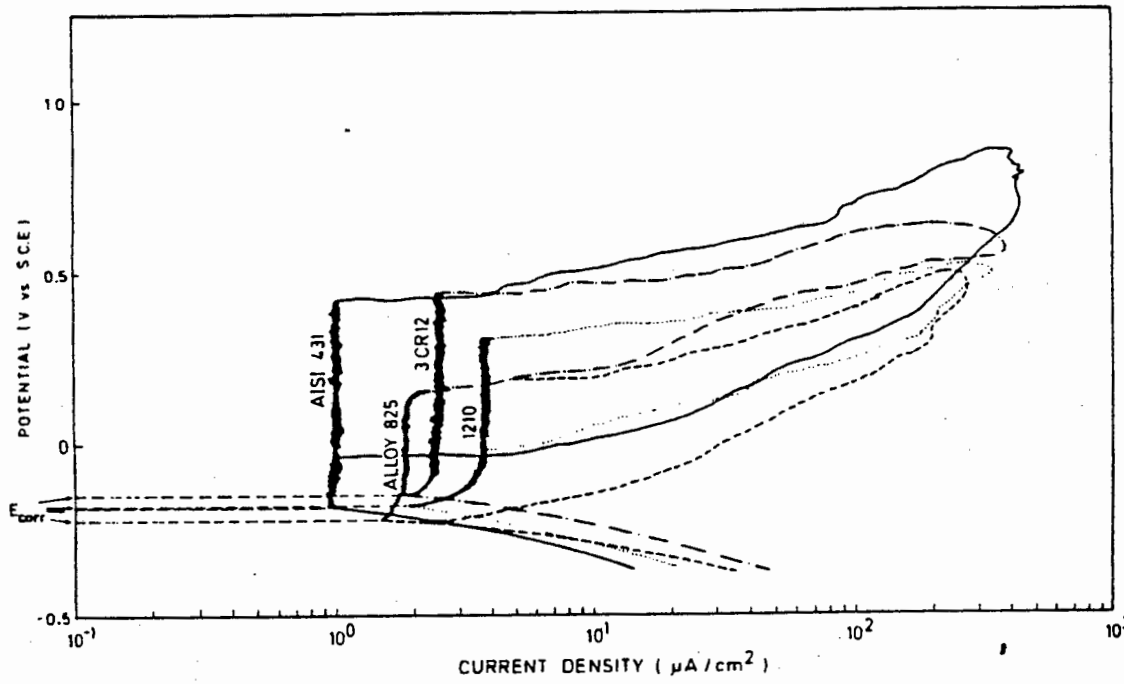

Figure 4.8 : The polarization curves for AISI 431, Alloy 1210, 3CR12 and Alloy 825 in aerated distilled water plus 100 ppm chloride.

Figure 4.9 shows the polarization curves for the alloys in distilled water plus 100 ppm chloride. All of the alloys showed a reduced passive range, and localised breakdown of the passive layer by pitting corrosion. All four curves show a hysteresis loop as a result of the reverse scan. In the case of AISI 431, Alloy 1210 and 3CR12 the hysteresis loop intersects the passive range, whereas the hysteresis loop for Alloy 825 meets the start of the passive range at the corrosion potential. Microscopic examination of the specimens showed that all of the alloys were pitted as a result of the pitting corrosion. AISI 431 showed the highest pit density, while Alloy 1210, 3CR12 showed similar pitting densities and Alloy 825 showed the lowest pitting density. This could be attributed to the propagation of pits occurring at a higher rate for the low chromium alloys due to their reduced chromium content and therefore cathodically protecting the specimen surface and preventing additional pits from initiating. Additionally, the propagating pits of the lower chromium alloys are less likely to repassivate and

therefore continue to cathodically protect the specimen surface and reduce the likelihood of further pits initiating. A similar effect is caused by the addition of inhibitors to solution.

In the absence of inhibiting anions, all four of the alloys showed poor resistance to pitting corrosion in chloride solutions. As discussed in section 2.5, nitrates, sulphates, hydroxyl ions and chlorates inhibit the pitting corrosion effect of chlorides by increasing the concentration at which chlorides have to be present to cause pitting corrosion. Capendale (1985) confirmed that nitrate ions inhibited pitting corrosion in AISI 431 and established a linear relationship between the nitrate concentration and the critical chloride concentration (The critical chloride concentration was the maximum concentration of chloride below which pitting corrosion was not found). Using a fast scan rate he showed that sulphates also inhibited the pitting corrosion of AISI 431.

4.3 THE PITTING CORROSION BEHAVIOUR OF THE ALLOYS IN SYNTHETIC MINE WATER

4.3.1 AISI 431

4.3.1.1 The Effect of Sulphates on the Pitting Corrosion of AISI 431 in Chloride Solutions

A series of tests were conducted to establish the concentration of chloride required to cause pitting corrosion of AISI 431 in solutions containing 100, 500, 1000 and 2000 ppm of sulphate at a pH of 6.2. The polarization scans were run in fully aerated solutions at a scan rate of 0.12 mV/sec. The method used to establish the chloride concentration required to cause pitting of AISI 431 is illustrated below for a 2000 ppm sulphate solution.

Potentiodynamic polarization curves were recorded for a range of chloride additions. In solutions with a chloride concentration of less than 500 ppm chloride, a constant breakdown potential of 0.54 V vs S.C.E. was measured due to transpassive breakdown of the passive film. Reversing the direction of the scan indicated no hysterisis loop and microscopic examination of the specimen showed a transpassive surface. Figure 4.10 shows the polarization curve for 2000 ppm sulphate plus 300 ppm chloride solution. The breakdown potential of 0.55 V vs S.C.E. and the absence of a hysterisis loop is shown.

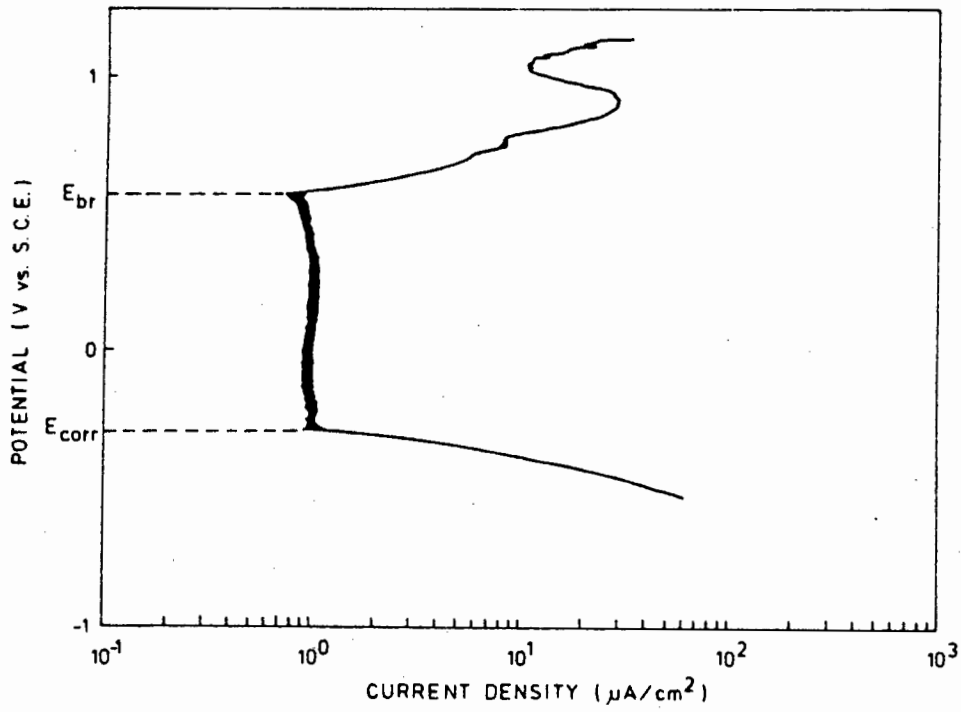

Figure 4.10 : Potentiodynamic polarization curve for AISI 431 in a 300 ppm chloride + 2000 ppm sulphate solution at pH 6.2.

In solutions with chloride concentrations equal to or greater than 600 ppm, breakdown of passivity was as a result of pitting corrosion occurring at specific pitting potentials. Pitting corrosion was identified by the following factors :

(i) Breakdown of the passivity at a value lower than the constant breakdown potential recorded during transpassive breakdown of the passive film.

(ii) The hysterisis effect and determination of a protection potential, E_{prot}, during reverse scanning.

(iii) Pitting of the exposed surface of the specimen, seen during microscopic examination. Figure 4.11 shows a SEM photograph of a pit on the surface of AISI 431.

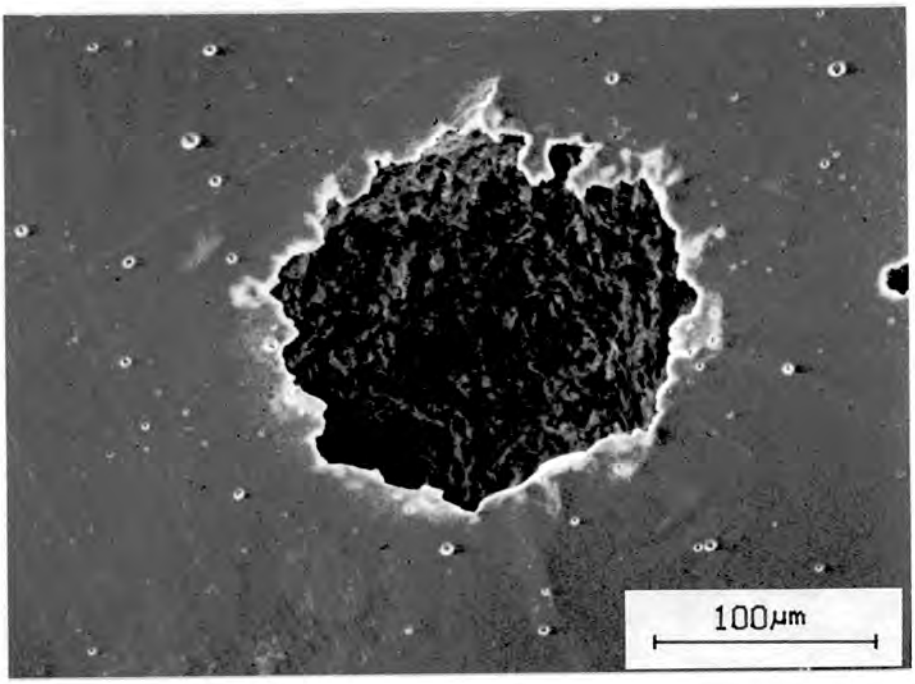

Figure 4.11 : A SEM photograph of a pit and surrounding smaller pits on the passive surface of AISI 431. The photograph is typical of pits that developed in all of the pitting corrosion tests that were done on AISI 431.

Figure 4.12 shows the potentiodynamic polarization curve of AISI 431 in 700 ppm chloride plus 2000 ppm sulphate, and illustrates the hysterisis effect and the determination of E_p and E_{prot}.

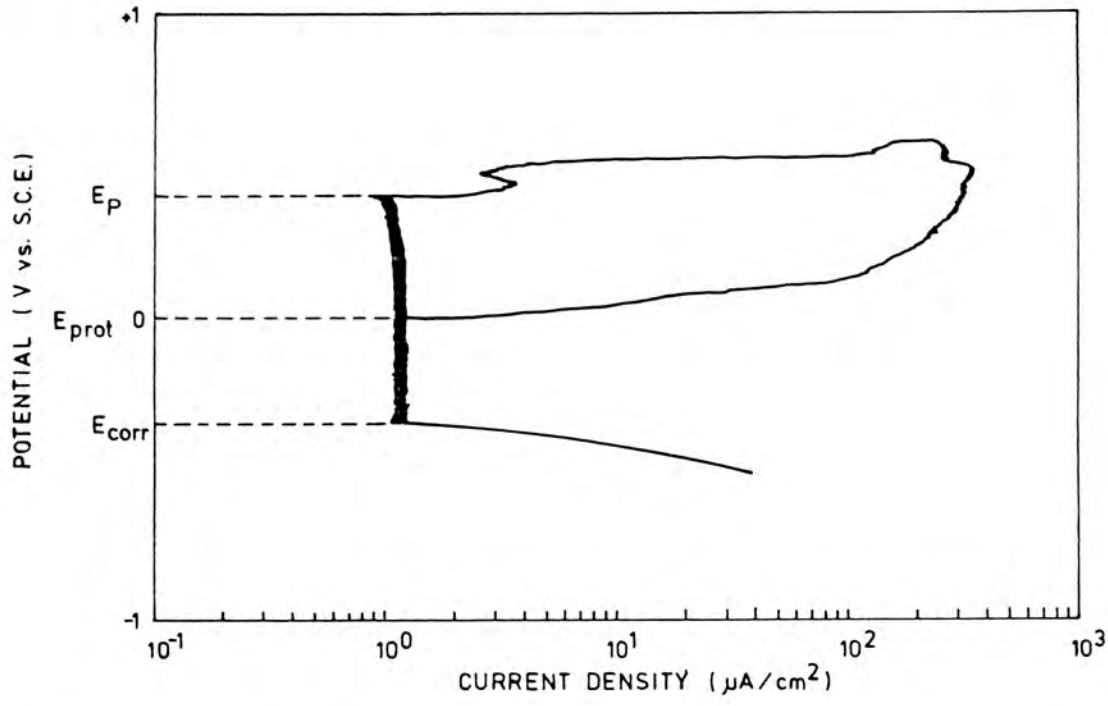

Figure 4.12 : Potentiodynamic polarization curve for AISI 431 in a 700 ppm chloride + 2000 ppm sulphate solution at pH 6.2.

The establishment of the chloride concentration above which AISI 431 suffers pitting corrosion in this solution is illustrated in figure 4.13 below. The values of E_{corr}, E_{br}, E_p and E_{prot} are plotted against the chloride concentration. The chloride concentration at which E_{br} falls sharply in magnitude as a result of the change from transpassive to pitting corrosion, is defined as the critical chloride concentration. $[Cl^-]_{crit}$ was confirmed by optical examination.

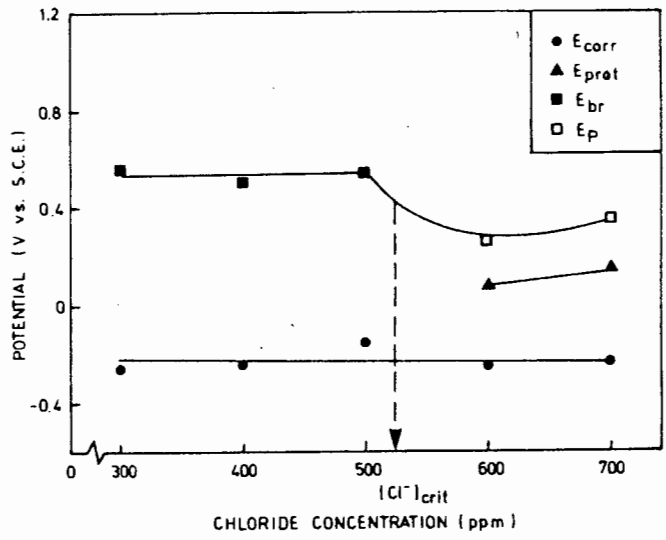

Figure 4.13 : E_{corr}, E_{br}, E_p and E_{prot} of AISI 431 (in a 2000 ppm sulphate solution at pH 6.2) versus chloride concentration.

Potentiodynamic polarization scans were recorded for 100, 500 and 1000 ppm sulphate solutions at pH 6.2, each sulphate concentration having a series of curves recorded for a range of chloride concentrations. E_{corr}, E_{br}, E_p and E_{prot} were plotted against the chloride concentration to obtain critical chloride concentrations for each series of tests. The resulting figures can be seen in appendix C. The passive corrosion current densities associated with each of the tests are recorded in appendix B. The expected trend of E_{corr} becoming more active at higher chloride concentrations is not seen on the plots of E_{corr}, E_{br}, E_p and E_{prot} vs chloride concentration because the range of chloride concentration which was tested was close to the critical chloride concentration. For the trend to be seen a wide range of chloride concentrations have to be used.

The critical chloride concentrations for 100, 500, 1000 and 2000 ppm sulphate solutions were plotted in figure 4.14. On the left side of the curve the conditions allow pitting to occur if the potential is raised above the pitting potential. On the left side

of the curve the sulphates offer complete inhibition and raising the potential results in transpassive breakdown of the passive layer of AISI 431. Critical chloride concentrations obtained by Capendale (1985) at a fast scan rate of 12 mV/sec for AISI 431 in the same solution are shown on the plot. A curve from work by Leckie and Uhlig (1966) on an 18-8 stainless steel has been calculated from equation 2.3 and shown in the figure.

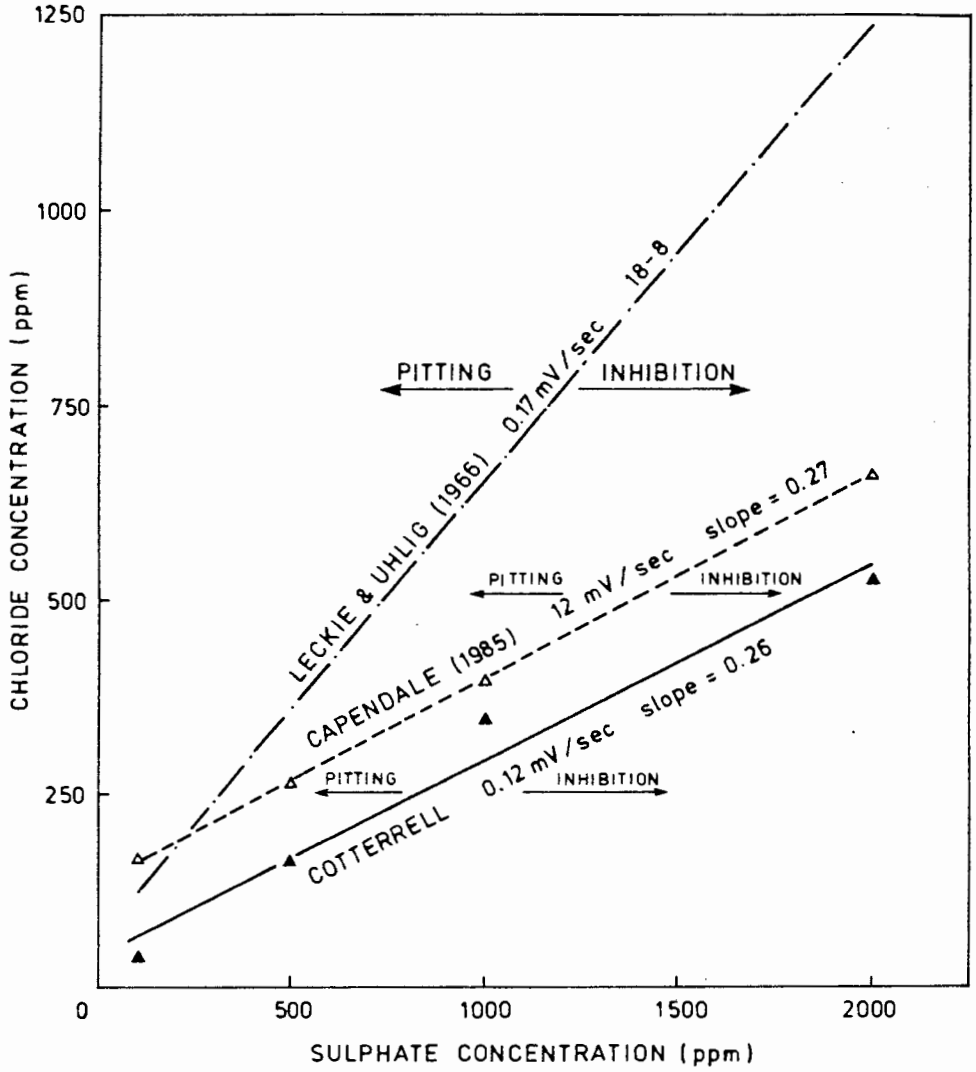

Figure 4.14 : $[Cl^-]_{crit}$ plotted as a function of sulphate concentration

A least squares analysis of the points yields a line with a slope of 0.26 and an intercept of 32 on the chloride concentration axis. This results in the following relationship :

$$[Cl^-]_{crit} = 0.26[SO_4^{2-}] + 32 \qquad \text{Equation 4.1}$$

Using the a fast scan rate of 12 mV/sec Capendale (1985) found the following relationship for AISI 431 :

$[Cl^-]_{crit} = 0.27[SO_4^{2-}] + 120$ Equation 4.2

Leckie and Uhlig (1966) found the following relationship for an 18-8 type AISI 304 stainless steel :

$\log[Cl^-] = 0.85 \log[SO_4^{2-}] - 0.05$ Equation 4.3

Comparing the results obtained to Capendale's fast scan rate results confirms that the slow scan rate gives a more conservative estimate of the critical chloride concentration. The slow scan rate is preferred since it permits conditions nearer to a steady state than the fast scan rate. Leckie and Uhlig's curve for an 18-8 stainless steel shows a non linear dependence of critical chloride concentration on sulphate concentration and the steel shows a higher resistance to pitting corrosion in the presence of chlorides in sulphate solutions than AISI 431.

The increased critical chloride concentration for higher sulphate concentrations is best explained by the competitive adsorption theory proposed by Leckie and Uhlig (1966). This theory proposes that adsorbed oxygen on the metal surface rather than the oxide layer makes up the passive layer. Chloride and sulphate compete with oxygen for sites on the surface double layer. Usually oxygen has a higher affinity for adsorption sites than chloride, but as the potential of the metal is shifted in the noble direction more chloride ions move into the double layer. At sufficient concentration corresponding to the critical potential (E_p), chloride ions succeed at favoured sites in displacing the adsorbed oxygen ions. Sulphate ions are adsorbed onto the passive layer and exclude chloride ions thereby not allowing oxygen to be displaced by the chloride ions.

Leckie and Uhlig(1966) assumed that the amount of anion adsorbed depended on its activity in solution in accordance with the Freundlich adsorption isotherm and that pitting was inhibited when a critical ratio of anion to chloride activity was reached. This resulted the following equation:

$\log[Cl^-] = \text{constant} + n1/n2 \log[\text{anion}]$ Equation 4.4

where n1 corresponds to the exponent in the Freundlich adsorption isotherm : amount adsorbed = k1 $[Cl^-]^{1/n1}$ and n2 is the corresponding exponent for the inhibitor ion.

This work and the results obtained by Capendale (1985) show a linear relationship between sulphate concentration and the critical chloride concentration as shown by equations 4.1 and 4.2. Although this is not in agreement with the logarithmic dependence proposed by Leckie and Uhlig, this could be due to the difficulty associated with determining trends from testing done over such a narrow range of sulphate concentrations.

4.3.1.2 The Effect of Sulphates plus Nitrates on the Pitting Corrosion of AISI 431 in Chloride Solutions

A series of tests were conducted to establish the effect of nitrate additions to the critical chloride concentrations determined for AISI 431 in sulphate solutions at pH 6.2. Potentiodynamic polarization curves were run for a range of chloride concentrations to determine the critical chloride concentration for each of the following solutions :

500 ppm NO_3^- at pH 6.2
500 ppm NO_3^- + 100 ppm SO_4^{2-} at pH 6.2
500 ppm NO_3^- + 500 ppm SO_4^{2-} at pH 6.2
500 ppm NO_3^- + 1000 ppm SO_4^{2-} at pH 6.2
500 ppm NO_3^- + 1500 ppm SO_4^{2-} at pH 6.2

1000 ppm NO_3^- + 200 ppm SO_4^{2-} at pH 6.2
1000 ppm NO_3^- + 500 ppm SO_4^{2-} at pH 6.2
1000 ppm NO_3^- + 1000 ppm SO_4^{2-} at pH 6.2
1000 ppm NO_3^- + 1500 ppm SO_4^{2-} at pH 6.2

The polarization scans were run in fully aerated solutions at a scan rate of 0.12 mV/sec. The method used to establish the critical chloride concentration is the same as was used to determine the critical chloride concentrations of AISI 431 in sulphate solutions.

Figures of chloride concentration vs potential used to determine the critical chloride concentration for the above series of tests are shown in appendix C. The values for the critical chloride concentrations are plotted against sulphate concentration as shown in figure 4.15.

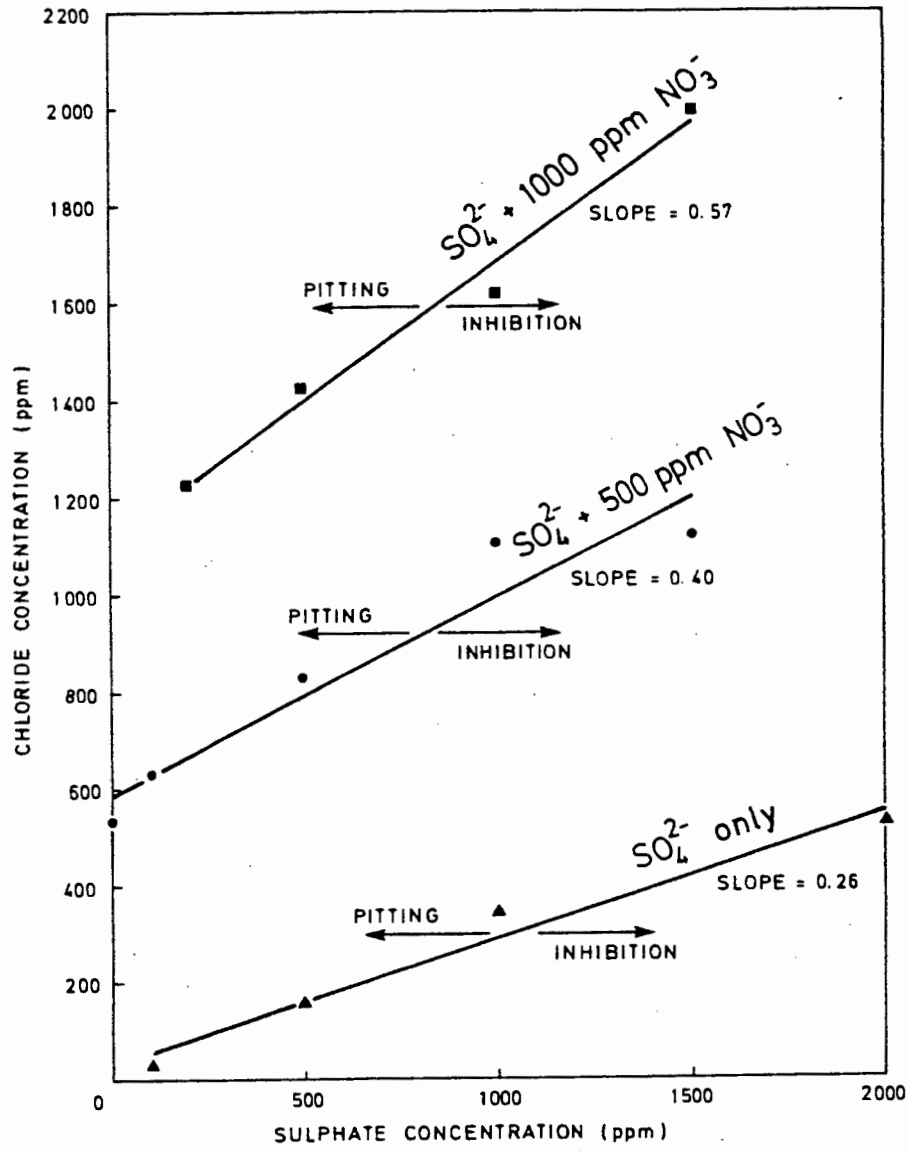

Figure 4.15 : $[Cl^-]_{crit}$ plotted as a function of sulphate concentration for AISI 431 at pH 6.2. The three curves are marked and show the effect of 0 ppm, 500 ppm and 1000 ppm of nitrate additions.

The 500 and 1000 ppm nitrate additions shift the critical chloride concentrations to higher values as shown in the above figure. The inhibitive effect of nitrate is shown to be larger than that of sulphate, which is as predicted by work done by Leckie and Uhlig (1966) and Capendale (1985). The following relationships were found from the curves :

For sulphates:

$$[Cl^-]_{crit} = 0.26[SO_4^{2-}] + 32 \qquad \text{Equation 4.1}$$

For sulphates + 500 ppm nitrates :

$$[Cl^-]_{crit} = 0.40[SO_4^{2-}] + 593 \qquad \text{Equation 4.5}$$

For sulphates plus 1000 ppm nitrates:

$$[Cl^-]_{crit} = 0.57[SO_4^{2-}] + 1112 \qquad \text{Equation 4.6}$$

The critical chloride concentrations predicted by the above equations in the absence of sulphate ions are 32, 593 and 1112 ppm chloride respectively. The slope of the curve for sulphate in the absence of nitrate is 0.26. In the case of 500 ppm and 1000 ppm additions of nitrate, the slope becomes steeper at values of 0.40 and 0.57 respectively. This indicates that there is a synergistic effect between sulphate and nitrate which causes more effective inhibition of pitting initiation when they are present together. The slope is steeper for the case when the nitrate concentration is 1000 ppm, and the combined inhibition by sulphate and nitrate is thus more effective at high nitrate concentrations. The improved inhibition of pitting initiation at high concentrations of nitrate in the presence of sulphate could be explained by the following hypothesis.

Nitrate ions are more readily adsorbed onto the passive layer and have a higher affinity for the metal surface than sulphate ions. The nitrate ions are competitively adsorbed onto the passive surface displacing chloride ions. If sulphate ions are adsorbed onto sites where nitrates have already displaced chloride ions and at sites between adsorbed nitrate ions, then fewer favoured sites may be present for chloride ions to reach concentrations able to destroy the passive layer. Therefore it may be possible that in the presence of nitrate ions, sulphate ions will take up positions on the adsorbed layer which will effectively increase the concentration of nitrate ions available at the interface to displace chloride ions from the passive layer.

4.3.1.3 The Interactive Effect of pH, Sulphates and Nitrates on the Pitting Corrosion of AISI 431 in Chloride Solutions

A series of tests were conducted to establish the effect of varying the pH in a solution containing 1000 ppm sulphate plus 1000 ppm nitrate on the critical chloride concentration of AISI 431. Three pH values, 3.8, 6.2 and 9.4 were selected to correspond with the pH range present in mine waters. The potentiodynamic polarization scans were run at 0.12 mV/sec in fully aerated solutions. The potential vs. chloride concentration curves for the three pH values are shown in figures 4.16 (a), (b) and (c).

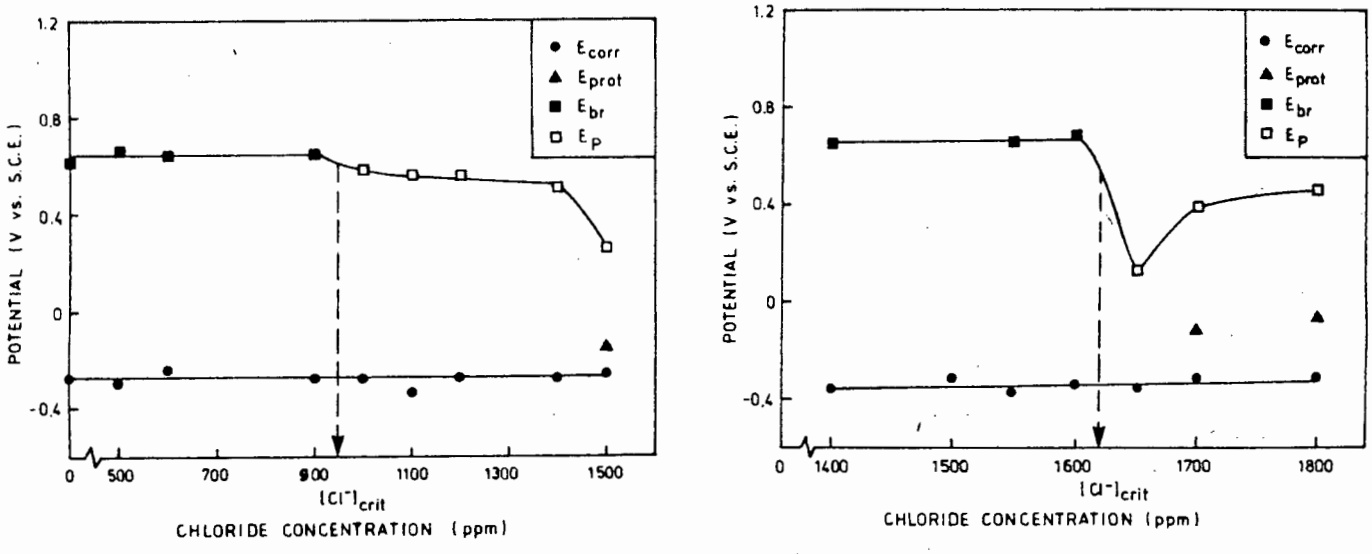

Figure 4.16 (a) : E_{corr}, E_{br}, E_p and E_{prot} of AISI 431 in 1000 ppm SO_4^{2-} + 1000 ppm NO_3^- versus chloride concentration at pH 3.8 and (b) : at pH 6.2.

Figure 4.16 (a) shows that the critical chloride concentration of AISI 431 in 1000 ppm sulphate plus 1000 ppm nitrate at pH 3.8 is approximately 950 ppm. Upon reversal of the scan direction, the polarization curves showed hysterisis behaviour but fell below the passive region of the curve. Figure 4.16 (b) shows the critical chloride concentration of AISI 431 at pH 6.2 as approximately 1600 ppm. The hysterisis loop intersects the passive range of the polarization curve.

Figure 4.16 (c) shows the critical chloride concentration of AISI 431 at pH 9.4 as approximately 1950 ppm. Again the hysterisis loop intersects the polarization curve in the passive range.

The critical chloride concentrations for the above diagrams are plotted as a function of pH in figure 4.17 below. Pitting is possible on the left side of the curve, while inhibition is indicated on the right side of the line. The critical chloride concentration increases in magnitude with increased pH. This can be explained by the local acidification mechanism which requires a low critical pH at the initiation site for pitting to occur (Galvele, (1976)). Low pH values of the bulk solution will help to maintain the low pH of the pitting site.

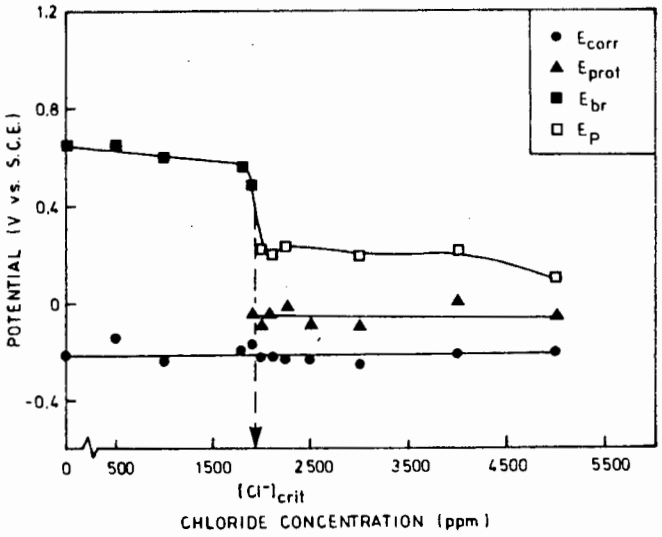

Figure 4.16 (c) : E_{corr}, E_{br}, E_p and E_{prot} of AISI 431 in 1000 ppm SO_4^{2-} + 1000 ppm NO_3^- versus chloride concentration, pH 9.4

Leckie and Uhlig (1966) showed that hydroxyl ions inhibited pitting at pH values above 10 according to the follow equation :

$$\log[Cl^-] = 1.62 \log[OH^-] + 1.84 \qquad \text{Equation 4.7}$$

The mechanism for the pitting inhibition was regarded to be competitive adsorption as discussed in the previous sections.

The results that Capendale obtained for AISI 431 in 1000 ppm nitrate are shown on the figure. At pH 3.8 the effect of the added sulphate is to reduce the effectiveness of the inhibition below that of the pure nitrate. This is contrary to the expected behaviour since both sulphates and nitrates are inhibitory anions. The added sulphate shows the expected effect by pushing the critical chloride concentration above that for pure nitrate at pH 6.2. At pH 9.4 the effect of the sulphate is again to reduce the critical chloride concentration below that for pure nitrate.

The effect at pH 6.2 corresponds with the findings shown in figure 4.15 at pH 6.2 where a synergistic interaction between sulphate and nitrate was seen found. At pH 3.8 and 9.4 there is an interaction between the solution and the passive layer that reduces the effective inhibition of the sulphate and nitrate.

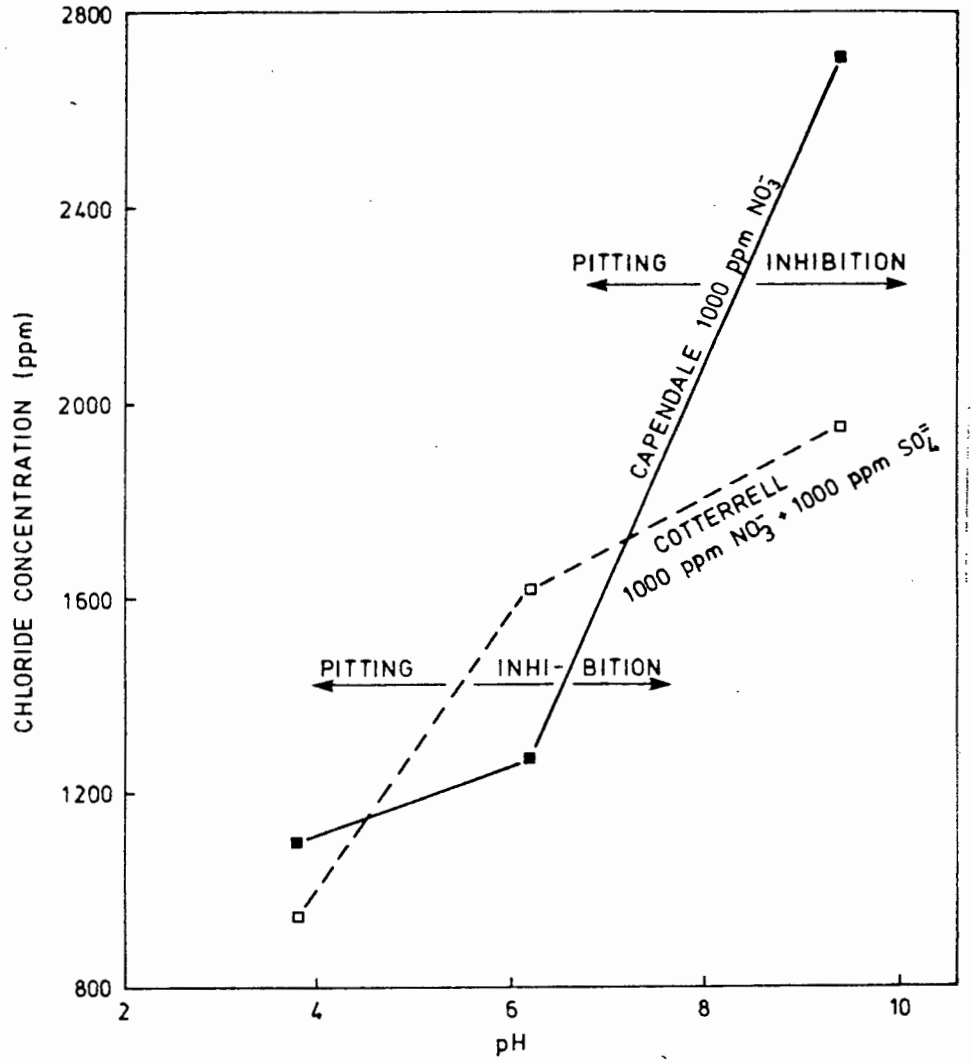

Figure 4.17 : $[Cl^-]_{crit}$ plotted as a function of the pH for AISI 431 in a 1000 ppm sulphate + 1000 ppm nitrate solution.

4.3.2 Alloy 1210

4.3.2.1 The Effect of Sulphates plus Nitrates on the Pitting Corrosion of Alloy 1210 in Chloride Solutions

The following three solutions were selected to establish the interactive effects of sulphate and nitrate on the pitting corrosion behaviour of Alloy 1210 in chloride solutions. Subsequently 3CR12 and Alloy 825 were tested in the same range of solutions.

500 ppm NO_3^- + 200 ppm SO_4^{2-} at pH 6.2
500 ppm NO_3^- + 1000 ppm SO_4^{2-} at pH 6.2
500 ppm NO_3^- + 2000 ppm SO_4^{2-} at pH 6.2

The solutions were selected to highlight the effect of variable sulphate concentrations with constant nitrate concentrations on the critical chloride concentration for the alloys. The compositions were chosen as a result of the extensive testing program that had been completed on AISI 431 to enable comparisons between the pitting corrosion resistance of the alloys to be made and to gain data on the pitting corrosion behaviour of the alloys. The polarization scans were run at 0.12 mV/sec and the solution was fully aerated.

Figures 4.18 (a), (b) and (c) show the chloride concentration plotted against the E_{corr}, E_{br}, E_p and E_{prot} for the above solutions.

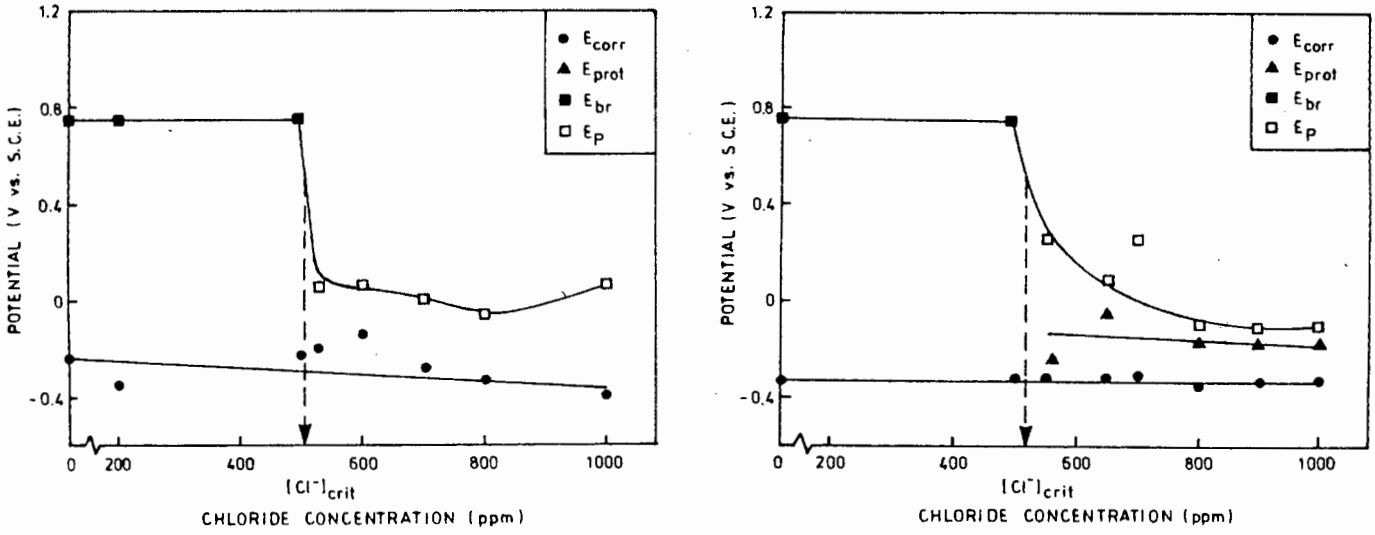

Figure 4.18 (a) : E_{corr}, E_{br} and E_p of Alloy 1210 in 200 ppm SO_4^{2-} + 500 ppm NO_3^- versus chloride concentration at pH 6.2 and (b) : E_{corr}, E_{br}, E_p and E_{prot} of Alloy 1210 in 1000 ppm SO_4^{2-} + 500 ppm NO_3^- versus chloride concentration at pH 6.2.

In figure 4.18 (a) the critical chloride concentration can be seen to be 500 ppm since E_{br} drops suddenly at this concentration. This was confirmed by optical examination of the specimens. The hysterisis loop fell below the corrosion potential and therefore any pits that initiate in this environment/metal combination would readily propagate at potentials above and including the corrosion potential. The corrosion current density averaged below 2 micro amps per square centimetre for all of the chloride concentrations that were tested. Figure 4.18 (b) shows the critical chloride concentration to be 525 ppm. This value for $[Cl^-]_{crit}$ was estimated since optical examination showed that the 550 ppm chloride solution pitted the specimen while the 500 ppm chloride solution caused transpassive breakdown. The hysterisis loop intersected the passive range at an average potential of -0.20 V (S.C.E.) and the

passive corrosion current density was below 1 micro amp per square centimetre for all the tests. The additional 800 ppm of sulphate only shifted the critical chloride concentration up by 25 ppm.

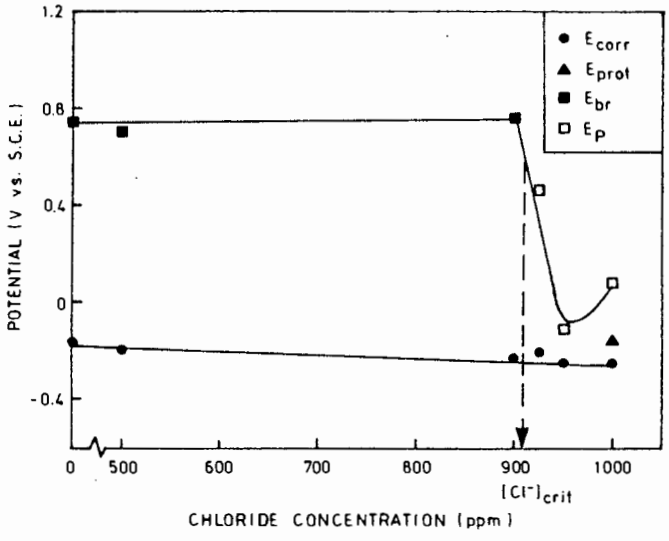

Figure 4.18 (c) : E_{corr}, E_{br}, E_p and E_{prot} of Alloy 1210 in 2000 ppm SO_4^{2-} + 500 ppm NO_3^- versus chloride concentration at pH 6.2.

Figure 4.18 (c) shows the effect of 2000 ppm sulphate on the $[Cl^-]_{crit}$ for Alloy 1210. The $[Cl^-]_{crit}$ shifts to 910 ppm showing the added inhibition by the additional sulphate ions. The shift in $[Cl^-]_{crit}$ is comparable with the effect that sulphate additions had on the $[Cl^-]_{crit}$ of AISI 431. The reported effect of increasing E_p was not found to be the case with the additional sulphate that was added. This is probably due to the narrow range of chloride concentrations that were tested once the $[Cl^-]_{crit}$ had been passed.

A SEM photograph of a typical pit on the surface is shown in figure 4.19 and the transpassively corroded surface in a specimen where no pitting corrosion occurred is shown in figure 4.20. Probable reasons for the shape of the pit are discussed in section 1.2.3.

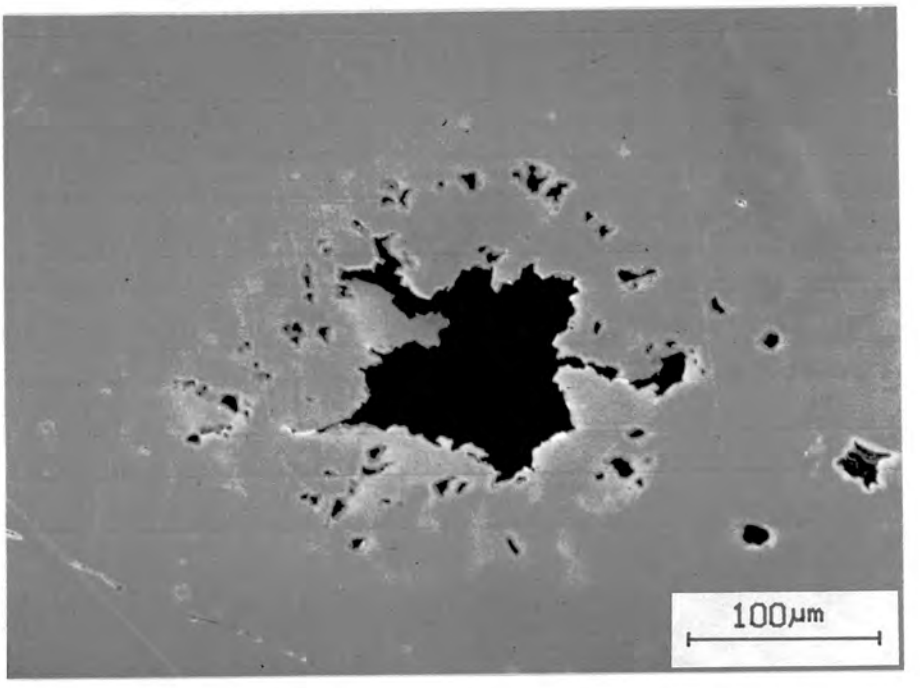

Figure 4.19 : A SEM photograph of a single pit on the surface of Alloy 1210 indicating the multiple pits in the thin layer of material on top of the pit opening.

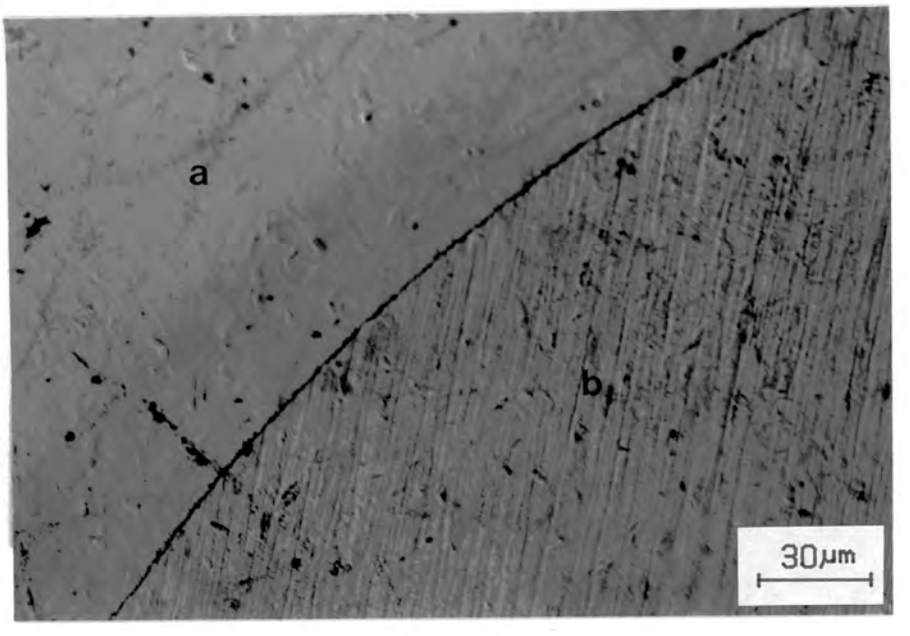

Figure 4.20 : An optical microscope photograph illustrating the transpassive breakdown of the passive layer (a) and the polished area below the gasket (b) of Alloy 1210 in a solution with a chloride concentration below $[Cl^-]_{crit}$.

4.3.3 3CR12

4.3.3.1 The Effect of Sulphates plus Nitrates on the Pitting Corrosion of 3CR12 in Chloride Solutions

Critical chloride concentrations were established for the same solutions as for Alloy 1210. The resulting potential vs. chloride concentration plots are shown in figures 4.21 (a), (b) and (c).

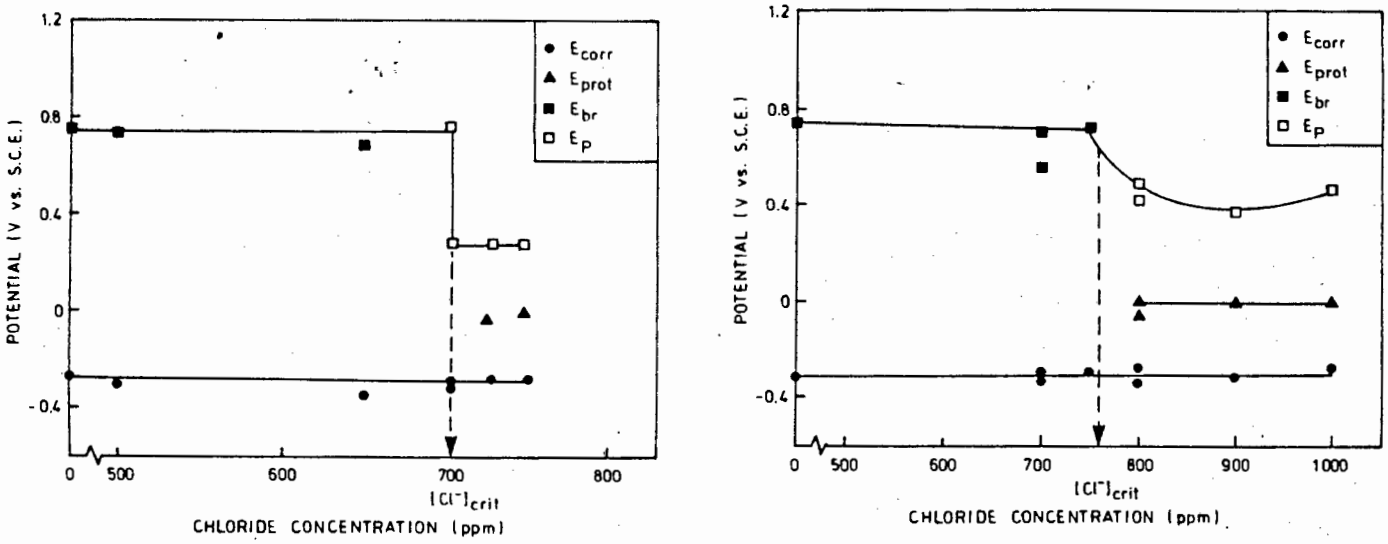

Figure 4.21 (a) : E_{corr}, E_{br}, E_p and E_{prot} of 3CR12 in 200 ppm SO_4^{2-} + 500 ppm NO_3^- versus chloride concentration at pH 6.2 and (b) : E_{corr}, E_{br}, E_p and E_{prot} of 3CR12 in 1000 ppm SO_4^{2-} + 500 ppm NO_3^- versus chloride concentration at pH 6.2.

In figure 4.21 (a) the critical chloride concentration is shown to be 700 ppm. Pitting corrosion occurred when the pitting potential was exceeded at chloride concentrations above 700 ppm. The pitting density on the surface of the specimen was similar to Alloy 1210 but significantly lower than for AISI 431, in spite of the scan being reversed at the same current density. The reduction in the pitting density can be attributed to the lower chromium content of Alloy 1210 and 3CR12 which allows propagation of pits to occur at a higher rate than for AISI 431, thereby cathodically protecting the surface of the specimen and reducing the number of pits that can initiate. The passive corrosion current density was stable at 2 micro amps per square centimetre over the whole range of chloride concentrations. The hysterisis loop intersected the passive range of the polarization curve at a positive value (S.C.E.).

Figure 4.21 (b) illustrates the effect of an additional 800 ppm of sulphate on the pitting corrosion behaviour of 3CR12 by shifting the critical chloride concentration to 760 ppm. The passive corrosion current density remains the same and the protection potential is reduced to an average of 0 V (S.C.E.). The improvement of the pitting corrosion resistance of 3CR12 by the addition of sulphate ions was confirmed by Mursalo et al (1988) who found that increased sulphate levels lowered the passive current density and caused E_{br} to shift to more noble values. Whereas Mursalo et al established the beneficial effect of sulphate, they did not present any quantitative data which would allow sulphate to chloride ratios to be maintained at levels which would ensure no pitting corrosion of 3CR12 in mine waters. The beneficial effect of sulphate on the passive corrosion current density was established when the sulphate concentration was increased to 2000 ppm.

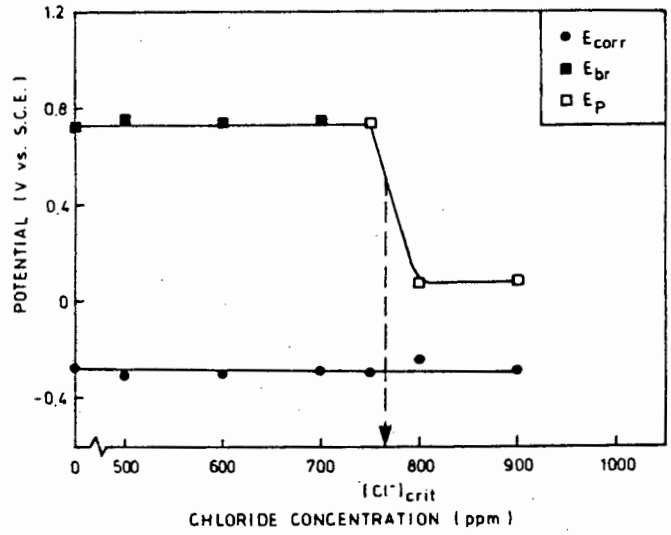

Figure 4.21 (c) : E_{corr}, E_{br}, E_p and E_{prot} of 3CR12 in 2000 ppm SO_4^{2-} + 500 ppm NO_3^- versus chloride concentration at pH 6.2.

The effect of 2000 ppm of sulphate is to increase the critical chloride concentration to 765 ppm as shown in figure 4.21 (c). The protection potential has been shifted to below the corrosion potential therefore affording no protection against pit propagation even at the free corrosion potential measured in the non steady state of the test. The addition of sulphate has increased the $[Cl^-]_{crit}$ at low concentrations but it has made E_{prot} more active at higher concentrations thereby reducing the ability of propagating pits to repassivate. This effect also causes the pitting density to be reduced since existing pits are less likely to repassivate and therefore reduce the probability that new pits will initiate

due to cathodic protection of the specimen surface by the propagating pits. The passive corrosion current density was reduced to 1 micro amp per square centimetre. From the three potential vs. chloride concentration diagrams it can be seen that the beneficial inhibitive effect of sulphate at 2000 ppm which was evident for AISI 431 and Alloy 1210 is not found for 3CR12.

Pits on the surface of the specimen were characterised by being covered by a thin layer of corroded metal as is shown in figure 4.22.

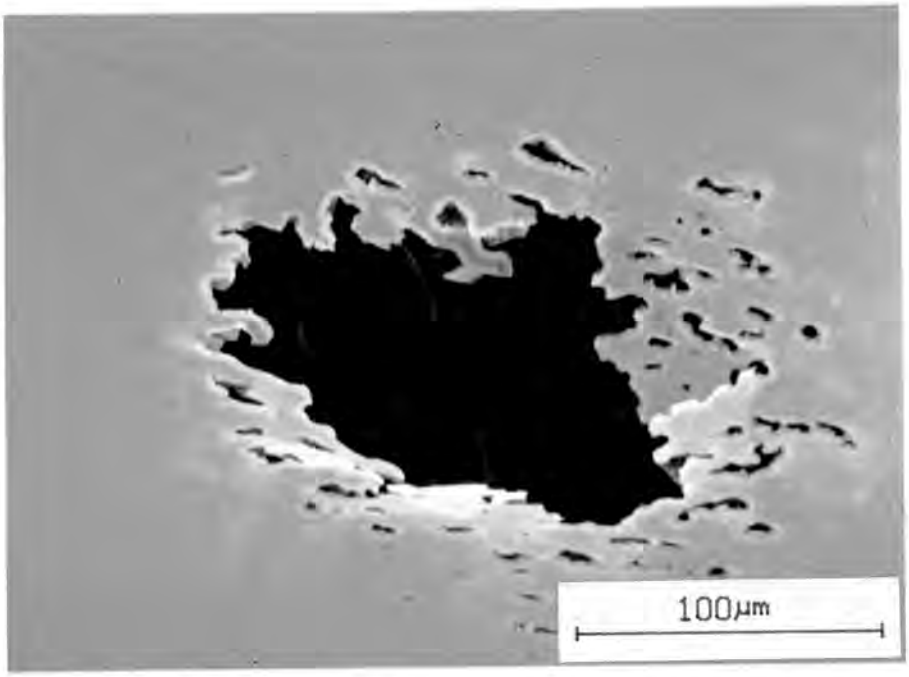

Figure 4.22 : A SEM photograph of a single pit on the surface of 3CR12 showing a thin corroded layer of material around the pit opening

The pit closely resembled that for Alloy 1210, and both were markedly different from the clean cut away pit shape for AISI 431. 3CR12 and Alloy 1210 have different microstructures and it is likely that the similar chromium contents of their compositions lead to the shape of the pits being the same. Both 3CR12 and Alloy 1210 have chromium contents at the bottom end of the stainless steel range of approximately 12%, and the probability of repassivation of the inside surface of the pit during propagation would therefore be reduced. This could lead to the initiated pit growing rapidly during the propagation stage and result in it propagating towards the surface and puncturing the surface around the pit. Additionally, if the propagation is rapid, other pits in the initiation stage would be cathodically protected and therefore the pit density on the specimen would be reduced as was found to be the case for the two alloys when compared to AISI 431.

4.3.4 Alloy 825

4.3.4.1 The Effect of Sulphates plus Nitrates on the Pitting Corrosion of Alloy 825 in Chloride Solutions

In a 200 ppm SO_4^{2-} + 500 ppm NO_3^- solution at pH 6.2 Alloy 825 was found to have a critical chloride concentration of 115 ppm as shown in figure 4.23 (a). For chloride concentrations above 125 ppm the passive corrosion current density was shifted from 2 up to 8 micro amps per square centimetre, and the hysterisis loop fell below the corrosion potential.

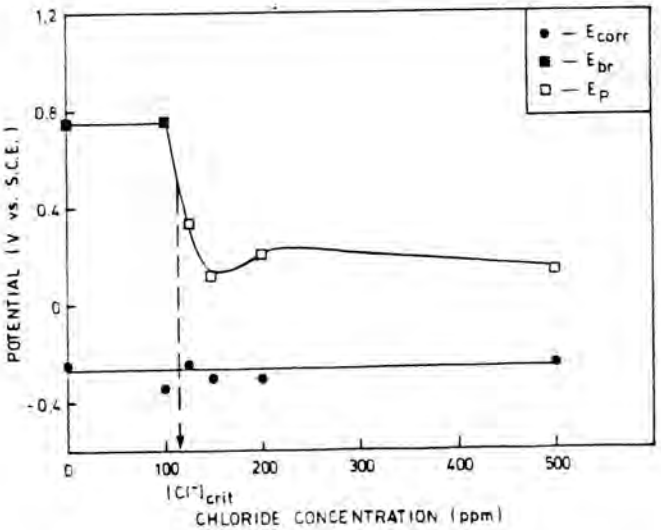

Figure 4.23 (a) : E_{corr}, E_{br}, E_p and E_{prot} of Alloy 825 in 200 ppm SO_4^{2-} + 500 ppm NO_3^- versus chloride concentration at pH 6.2.

Increasing the sulphate concentration from 200 to 1000 ppm results in the passive region of the polarization scan being reduced to 90 mV in the absence of any chloride addition. The transpassive corrosion was very rapid and the current density reached 100 micro amps per square centimetre within 250 mV of the breakdown. The corrosion behaviour could be compared with that of Alloy 825 in 500 ppm sulphate solutions as tested in the E-pH experimental work presented in section 4.1.3. Figure 4.23 (b) shows the potential vs. chloride concentration plot for Alloy 825 in 1000 ppm SO_4^{2-} + 500 ppm NO_3^- at pH 6.1.

Figure 4.23 (b) shows that the passive layer is stabilised by the addition of 50 and 200 ppm of chloride, but is unstable at 100 ppm of chloride. The specimen surface was transpassively corroded in the case of the 50 and 200 ppm chloride addition, but higher

current densities for the 100 ppm chloride addition resulted in a heavier general corrosion of the specimen with no evidence of localized corrosion at any point. For chloride concentrations of 300 ppm and above general corrosion and pitting occurred. The critical chloride concentration was taken to be between 200 and 300 ppm. The additional sulphate lowered the passive corrosion current density to approximately 1 micro amp per square centimetre and lowered the stability of the passive layer. The hysterisis loop fell below the corrosion potential for polarization scans at chloride concentrations above the critical level.

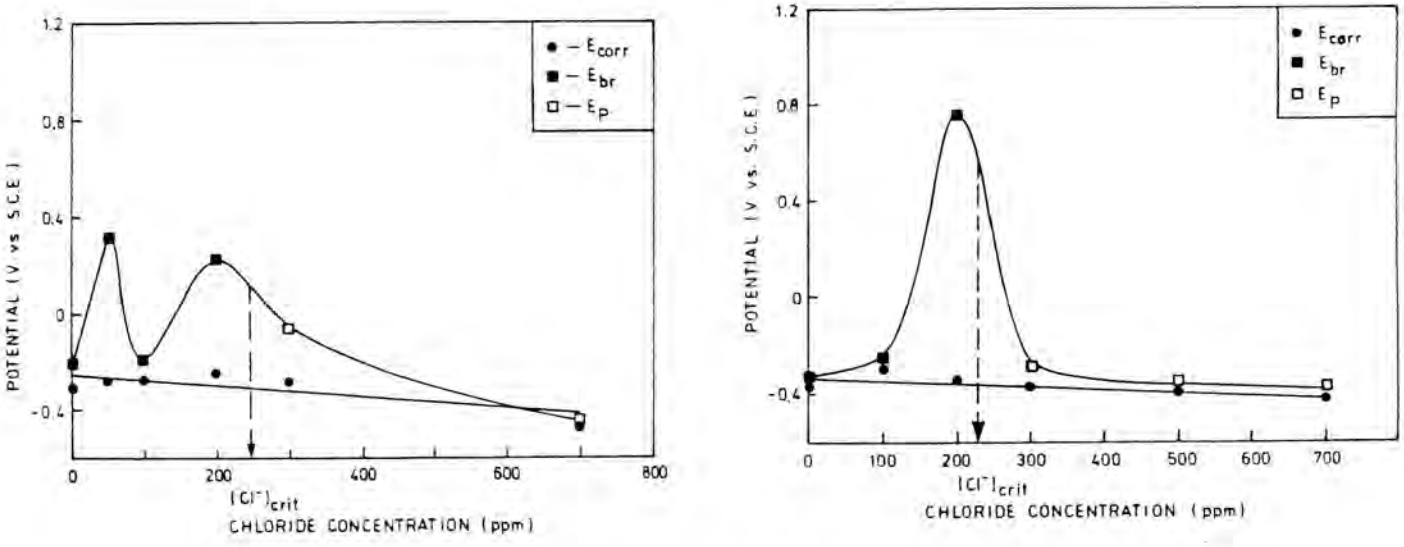

Figure 4.23 (b) : E_{corr}, E_{br}, E_p and E_{prot} of Alloy 825 in 1000 ppm SO_4^{2-} + 500 ppm NO_3^- versus chloride concentration at pH 6.2 and (c) : E_{corr}, E_{br}, E_p and E_{prot} of Alloy 825 in 2000 ppm SO_4^{2-} + 500 ppm NO_3^- versus chloride concentration at pH 6.2.

By increasing the sulphate concentration to 2000 ppm the effect of the sulphate on the stability of the passive layer was worsened. No stable passive layer was present prior to the addition of 200 ppm chloride, and pitting was found present at chloride concentrations equal and higher than 300 ppm. Chloride unexpectedly stabilises the passive film of Alloy 825 in the presence of high sulphate concentrations, which is shown in figure 4.23 (c). No evidence for this effect was found in the literature and private communications did not reveal any mechanisms which may explain this effect. Possibly the chloride ions are part of a ligand complex that forms on the surface of Alloy 825. The ability of the chloride stabilised passive layer to protect Alloy 825 from pitting corrosion could be determined by time vs current density plots. If the passive layer remains stable then the passive current density would not increase for the duration of the test.

The pits on the specimen surface were surrounded by an area where general corrosion had removed the passive layer and this is shown in figure 4.24. The general corrosion can be attributed to the low chromium content (8%) and the high carbon content (0.25%) which ties up additional chromium in the form of chromium carbides. The general corrosion has the same appearance as the corrosion that occurred on the surface of the specimens that did not passivate. Below 100 ppm sulphate the passive layer was stable and showed no signs of breaking down by the general corrosion mechanism that corroded the areas around the pits in solutions with chloride concentrations above 125 ppm.

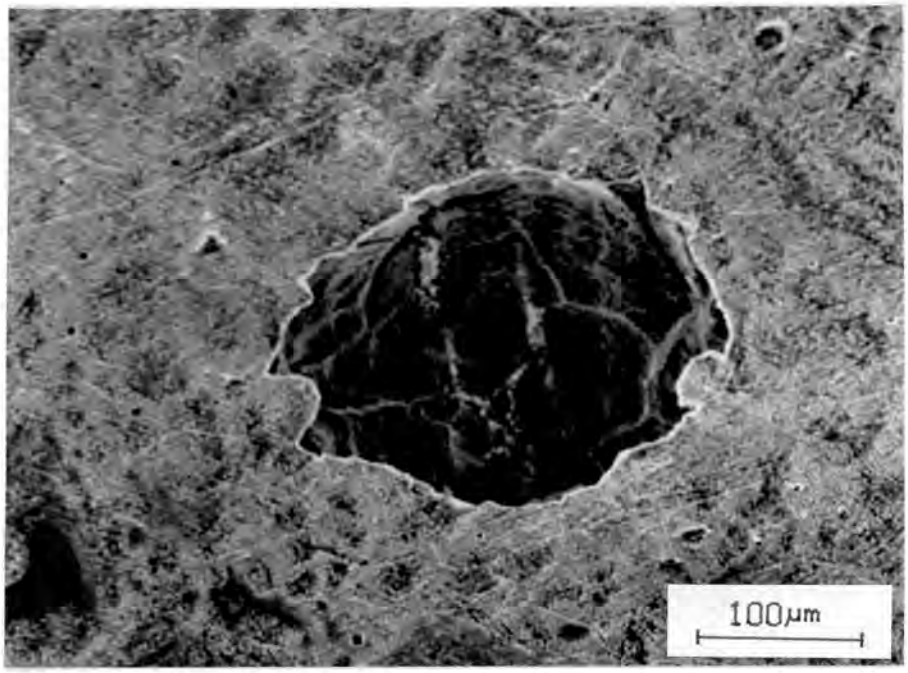

Figure 4.24 : A SEM photograph of a single pit on the surface of Alloy 825 showing the general corrosion surrounding the pit.

Crevicing below the gasket caused problems in a high percentage of the tests that were performed on Alloy 825. Similar crevicing problems have been experienced by Barker (1988), Bechet (1988) and Joubert (1988). The specimens that showed crevicing were redone a number of times and the results were used from the specimens that showed the least crevicing. The results clearly demonstrated that crevicing corrosion occurs at more active potentials than pitting corrosion and that crevicing corrosion is possible at chloride concentrations below the critical chloride concentration required for pitting corrosion. A typical crevice is shown in figure 4.25, which demonstrates the crevices position at the gasket/specimen interface.

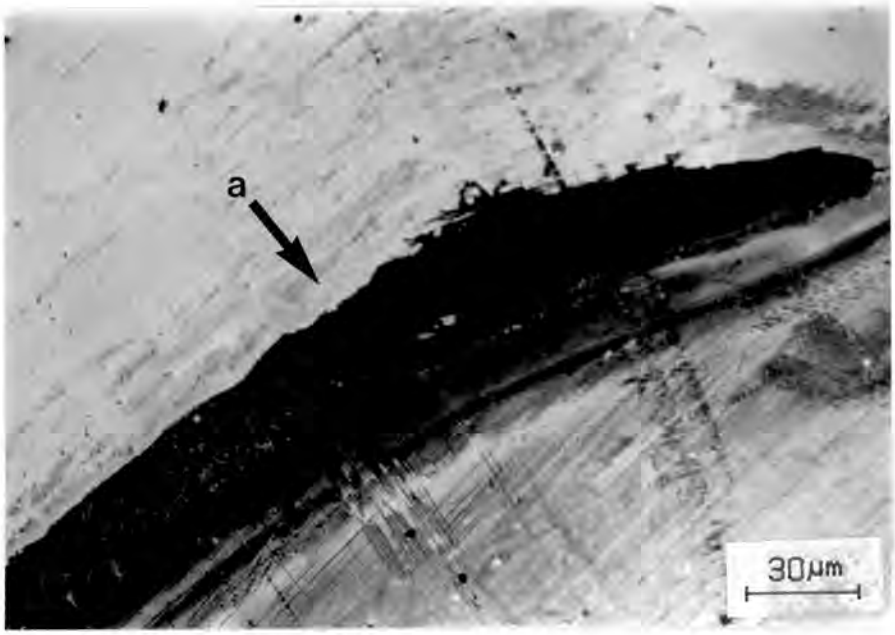

Figure 4.25 : An optical microscope photograph of a large crevice (a) at the gasket/specimen interface on the surface of Alloy 825.

4.4 COMPARISON OF THE ALLOYS PITTING CORROSION RESISTANCE

Figure 4.26 shows the critical chloride concentration of the alloys plotted against the sulphate concentration in a 500 ppm nitrate solution at pH 6.2. AISI 431 has the highest pitting corrosion resistance of the four alloys, Alloy 825 has the lowest pitting corrosion resistance, and Alloy 1210 and 3CR12 have a similar pitting corrosion resistance midway between that of AISI 431 and Alloy 825.

Both AISI 431 and Alloy 1210 show an increased resistance to chloride pitting attack as the sulphate concentration is increased. The beneficial effect of increased sulphate concentrations is shown by the slope of the critical chloride line. The pitting corrosion resistance of 3CR12 and Alloy 825 benefits by the addition of up to 500 ppm sulphate, but between 500 and 2000 ppm sulphate the pitting corrosion resistance remains constant. This is shown by the critical chloride concentration lines for 3CR12 and Alloy 825 which have a minimal slope at sulphate concentrations above 500 ppm.

The pitting corrosion resistance of AISI 431 was better than the other alloys due to it's higher chromium content (16%) and very clean microstructure. Alloy 1210 and 3CR12 showed similar pitting corrosion resistance due to their similar chromium contents (12% and 11.5%

respectively). A similar decrease in the resistance to pitting corrosion was found by Chen and Stephens (1979) when they reduced the chromium content of AISI 304 stainless steel from 18% to 12%. Alloy 825 showed the worst pitting corrosion resistance due to it's very low chromium level (8%) and high carbon content (0.25%) (tying up some chromium as chromium carbides), which was insufficient to allow the formation of a stable passive layer. Alloy 825 cannot be regarded as a stainless steel, and future studies should compare it's corrosion resistance with that of low alloy steels and mild steel (Proctor, (1988)).

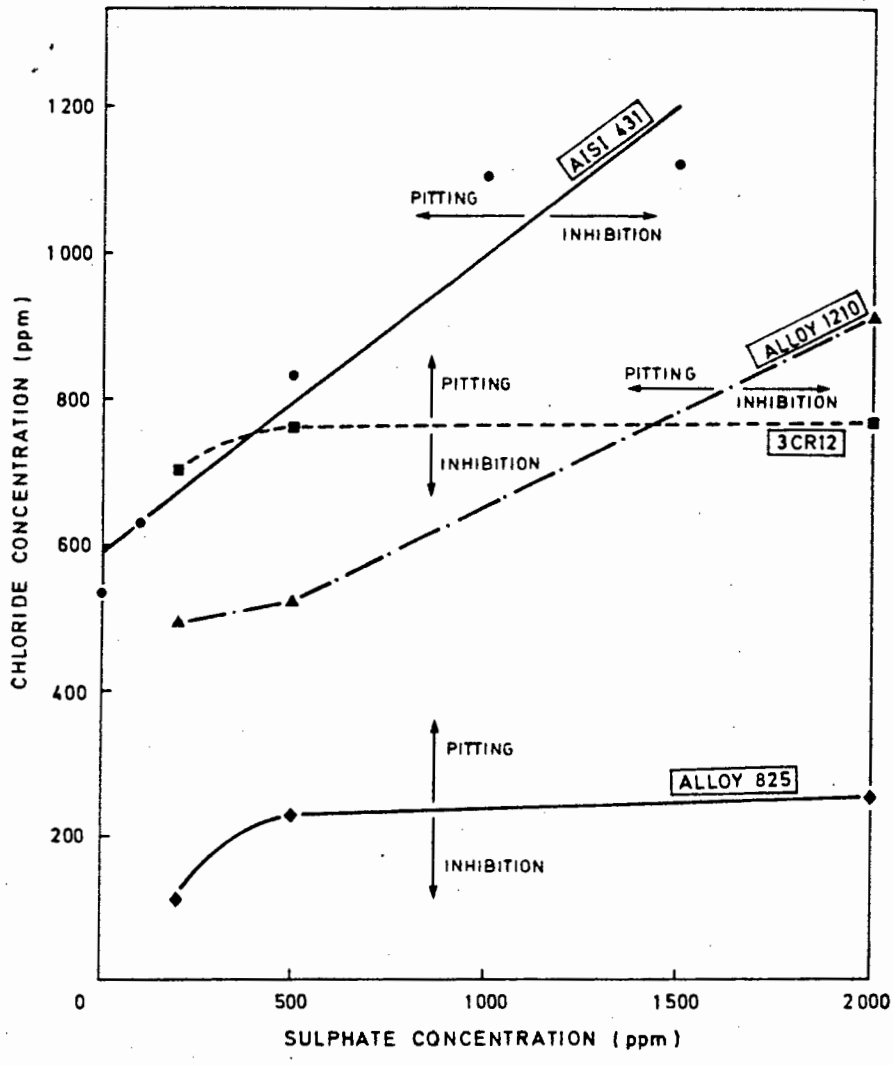

Figure 4.26 : $[Cl^-]_{crit}$ as a function of the sulphate concentration in a 500 ppm nitrate solution at pH 6.2 for AISI 431, Alloy 1210, 3CR12 and Alloy 825

4.5 THE PRACTICAL SIGNIFICANCE OF THE EXPERIMENTAL RESULTS

The use of stainless type steels in the mining environment requires that they remain in the passive state during service thereby corroding at very low rates during their service life. This requires the careful matching of materials selection and water treatment of the mine water. The four steels that have been tested present valuable information about the interactive effects of ions present in mine waters. The following discussion highlights the practical implications of the experimental results obtained.

The experimental E-pH diagrams determined for Alloy 1210, 3CR12 and Alloy 825 in 500 ppm sulphate have an active region extending over the whole range of pH values commonly encountered in mine water (pH 3.8 - 9.4). The active region of AISI 431 in 500 ppm sulphate (as determined by Capendale (1985)) extends to pH 4, which allows neutralization of the mine water by the addition of $Ca(OH)_2$ to keep it in the passive state. Regardless of the pH, Alloy 1210, 3CR12 and Alloy 825 can be in the active state if the corrosion potential falls within the active portion of the E-pH diagrams determined for them. The active region is between 200 to 300 mV for Alloy 1210 and 3CR12 in near neutral solutions, which allows them to passivate in oxidising environments. For Alloy 825 active/transpassive corrosion is likely to occur throughout the pH range because the passive layer that forms is not stable (as discussed earlier). The experimental E-pH diagrams show that the stability of the passive layer on the alloys varies and depends mainly on the chromium content of the alloy. A mine water that is adjusted to maintain AISI 431 in the passive state may not passivate Alloy 1210 and 3CR12, and will be very unlikely to passivate Alloy 825.

Localized corrosion in the form of pitting and crevice corrosion contributes very little to the total volume of material lost by corrosion. However, the significance of pitting corrosion is that it is insidious and can be a precursor to environmental sensitive fracture and to catastrophic failure. Pitting corrosion is particularly serious in pipes and pressure vessels that are at high pressures since perforation could lead to a loss of pressure and downtime while the component is being replaced. It is therefore important to maintain the chloride concentration below $[Cl^-]_{crit}$ for a particular water/material combination. When the chloride concentration is above $[Cl^-]_{crit}$ then E_{corr} should be kept below E_p to avoid pitting corrosion initiating and below E_{prot} to avoid pit propagation or crevice corrosion occurring. Even when pitting corrosion does not occur, crevice corrosion may occur at potentials significantly active to E_p (Frankenthal and Pickering, (1972)).

The corrosion potential of an alloy can be increased to more noble values by microbial activity, strongly oxidising ions such as Cu^{2+} and Fe^{3+}, and temperature and flow velocity. E_{corr} measured in potentiodynamic polarization scans is more active than E_{corr} which is measured in solution after it has allowed to reach equilibrium. Figure 4.27 shows the E_{corr} vs. time plots for each of the four alloys in a 500 ppm nitrate + 1000 ppm sulphate solution at pH 6.2. It can be seen that all of the alloys show E_{corr} becoming more noble with increasing time from initial immersion. 3CR12 was the quickest to reach equilibrium, and after 12 hours the free corrosion potential had stabilised at 30 mV (S.C.E.). AISI 431 stabilised after 15 hours at 20 mV (S.C.E.) and Alloy 1210 stabilised after 16 hours at -4 mV. Alloy 825 had not stabilised by 18 hours, and the test was stopped after 36 hours when the corrosion potential had reached 35 mV (S.C.E.) and still showed signs of fluctuating between active and noble directions. The implications of the equilibrium E_{corr} values are described for each alloy below.

For AISI 431, E_p ranged between 90 mV and 680 mV (S.C.E.). In practice the presence of microbial activity, oxidising ions, bimetallic contact, high temperatures or increased fluid velocities may increase the corrosion potential above the low end values of E_p and cause pitting corrosion. It is well established that as the chloride concentration is increased, E_p is reduced. Although AISI 431 may not suffer pitting corrosion in solutions which have chloride concentrations higher than $[Cl^-]_{crit}$ there is a possibility that it will occur as a result of E_{corr} being increased to more noble values.

Alloy 1210 has pitting potentials in the range -120 to 460 mV (S.C.E.) and 3CR12 has pitting potentials in the range 70 to 490 mV (S.C.E.) for tests performed in chloride concentrations exceeding $[Cl_-]_{crit}$. Both alloys display pitting potentials established near to the $[Cl^-]_{crit}$ more active than those established for AISI 431, showing lower resistance to pitting corrosion both by lower values for the $[Cl^-]_{crit}$ and by having a narrower potential range between the equilibrium E_{corr} and E_p than AISI 431. The equilibrium E_{corr} of Alloy 1210 is more noble than E_p in a number of cases which would result in pitting corrosion in the solution tested in freely corroding conditions. The reason that E_p was found to be lower for Alloy 1210 than that of 3CR12 may be due to the 10% manganese content. Lunarska et al. (1975) found that for an 18Cr-5Ni stainless steel, the addition of 5.7 to 15 % Mn diminished their ability to be passivated and their resistance to pitting. In mine waters Alloy 1210 and 3CR12 are more likely to suffer pitting corrosion than AISI 431, and this is attributed to the higher chromium content of AISI 431 forming a passive layer which is more resistant to chloride attack.

Alloy 825 has an equilibrium E_{corr} which is often higher than E_p which could result in pitting corrosion. It should be emphasized that alloy 825 is not a stainless steel and that general corrosion would probably cathodically protect the steel from pitting corrosion. In stagnant water where oxygen becomes deficient and the acidity of the surrounding solution is decreased by the anodic dissolution of material by general corrosion, crevice corrosion is likely to be a problem. This was demonstrated by Capendale (1985) in crevice corrosion tests, and the polarization behaviour indicated a poor resistance to crevice corrosion.

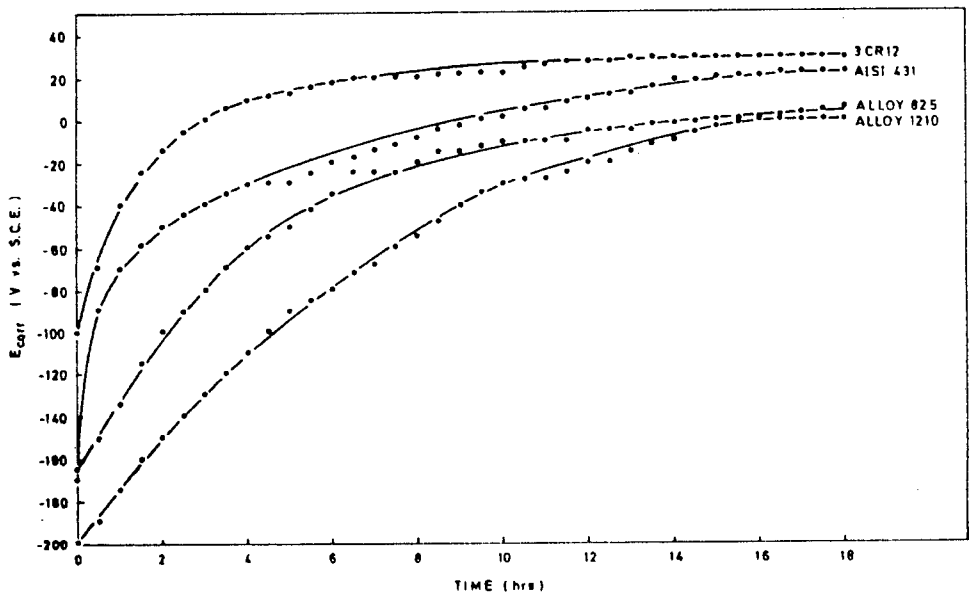

Figure 4.27 : The corrosion potential vs. time in a 500 ppm NO_3^- + 1000 ppm SO_4^{2-} for each of the alloys

Capendale (1985) proposed that the localized accumulation of ions that takes place due to evaporation and at crevices would not cause pitting corrosion if the chloride concentration was below $[Cl^-]_{crit}$ if the following assumptions are met :

i) The build-up of ions occurs in the same proportion as they are present in bulk solution.

ii) No significant change in pH is caused by the buildup of ions.

iii) The linear relationship which was derived between $[Cl^-]_{crit}$ and the inhibitor concentrations may be extrapolated to higher inhibitor concentrator.

Capendale found a linear relationship existed between $[Cl^-]_{crit}$ and nitrate concentration for AISI 431, and a linear relationship was shown to exist for AISI 431 between the $[Cl^-]_{crit}$ and a combination of sulphate and nitrate ions. Based on Capendale's assumptions AISI 431 and Alloy 1210 are not likely to suffer pitting corrosion as a result of local concentration of solution if the chloride concentration is below

$[Cl^-]_{crit}$. However, in the case of 3CR12 and Alloy 825, local concentration of mine water could cause pitting corrosion even if the chloride concentration is below the $[Cl^-]_{crit}$, which is shown by the slope of the $[Cl^-]_{crit}$ line reducing to low values after a concentration of 500 ppm sulphate (see figure 4.26). This finding again emphasizes the importance of being cautious of judging an alloys' pitting corrosion resistance upon that of a similar alloy.

Figure 4.28 is a schematic showing the factors that affect the pitting corrosion behaviour of an alloy. It can be seen that the best region for E_{corr} to be kept to avoid pitting corrosion is in the complete inhibition region. By increasing the chloride concentration above $[Cl^-]_{crit}$ the corrosion behaviour of the alloy depends upon the E_{corr} of the alloy. At potentials below E_{prot} the allow will be in the passive state. If E_{corr} becomes more noble and falls between E_{prot} and E_p then existing pits may propagate but new pit may not initiate. E_{corr} may become more active as a result of oxidizers, microbes, temperature, bimetallic-contact and fluid-velocity. If E_{corr} becomes more noble than E_p then pitting will initiate after an incubation period. The diagram shows that the increasing $[NO3^-]$, $[SO_4^{2-}]$ and the pH will increase the value of $[Cl^-]_{crit}$. Increasing the sulphate concentration above 500 ppm has no positive effect on the $[Cl^-]_{crit}$ for 3CR12 and Alloy 825.

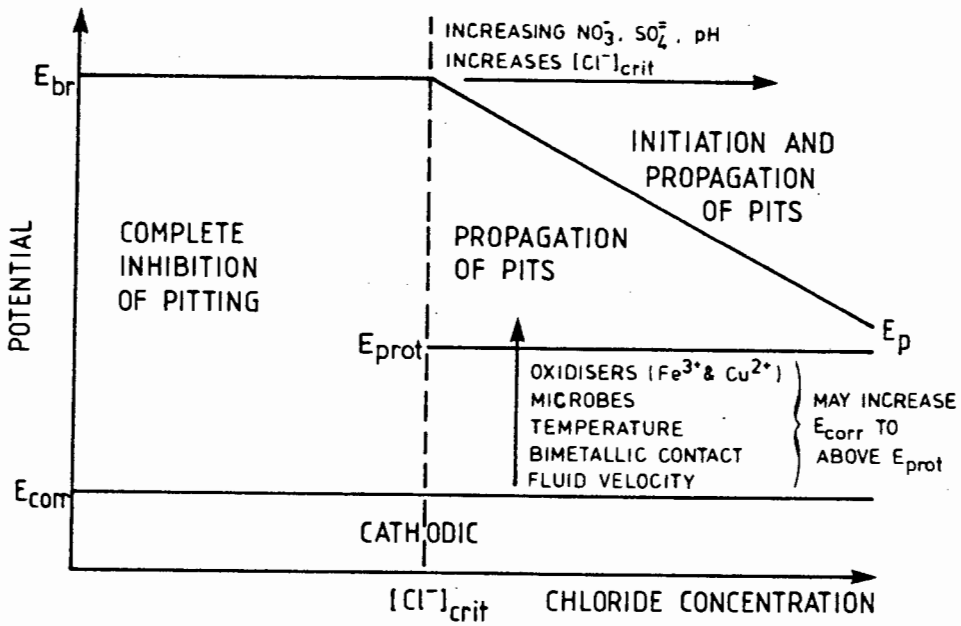

Figure 4.28 : A diagram summarising the factors which affect the possibility of pitting corrosion of a material in mine water solutions (after Capendale, (1985)).

Although sulphate ions seem to improve the pitting corrosion resistance of stainless steels, there is a danger that the action of sulphate reducing bacteria could reduce sulphate ions to highly corrosive species

such as sulphides. In addition sulphate has been found to increase the rate of corrosion of mild steel, and it could therefore increase the rate of corrosion of low alloy alloys. The beneficial effects that sulphate offers in inhibiting the pitting corrosion of stainless steels would have to be carefully evaluated by corrosion engineers due to the detrimental effects that could be suffered as a result of it. The complexity of corrosion phenomena require caution to be exercised prior to any major change in the water treatment system of a mine.

The relationships established between $[Cl^-]_{crit}$ and inhibiting ions for the alloys tested need to be checked in real mine water solutions which have chloride concentrations above and below $[Cl^-]_{crit}$. This will allow corrosion engineers to use the quantitative relationships that have been derived for AISI 431, and to qualitatively use the relationships that have been established for Alloy 1210 and 3CR12. As has been discussed, Alloy 825 is not a stainless type steel, and it is unlikely that pitting corrosion will be a problem for it in service.

CHAPTER 5

FINDINGS AND CONCLUSIONS

The potentiodynamic polarization technique was used at a scan rate of 0.12 mV/second in fully aerated solutions, and the following findings and conclusions were made from the experimental results :

1. Increasing the sulphate concentration resulted in an increase of the $[Cl^-]_{crit}$ of AISI 431 in solutions at pH 6.2. The inhibitive effect of sulphates was less than that of nitrates (Capendale, (1985)) and the $[Cl^-]_{crit}$ values were lower than those established by Capendale (1985) using a fast scan rate. A linear relationship between the $[Cl^-]_{crit}$ and the $[SO_4^{2-}]$ was found.

2. Increasing the sulphate concentration in solutions containing 500 and 1000 ppm nitrate at pH 6.2 resulted in an increase of the $[Cl^-]_{crit}$ of AISI 431. The $[Cl^-]_{crit}$ increased linearly with increased sulphate concentration and the slope of the resulting relationship increased with increasing nitrate concentration, indicating a synergistic interaction by sulphate and nitrate in inhibiting pitting corrosion.

3. Reducing the pH to 3.8 in a solution containing 1000 ppm sulphate plus 1000 ppm nitrate resulted in the $[Cl^-]_{crit}$ of AISI 431 being reduced from $[Cl^-]_{crit}$ obtained at pH 6.2. Increasing the pH to 9.4 for the same solution resulted in an increase of $[Cl^-]_{crit}$ to a value greater than for pH 6.2. The resulting $[Cl^-]_{crit}$ values were lower than those established by Capendale the same solution minus the 1000 ppm sulphate. The addition of sulphate was found to reduce the efficiency of nitrate as an inhibitor at low and high pH values, and increase the efficiency of nitrate as an inhibitor at neutral pH's.

4. An experimental E-pH diagram was constructed for Alloy 1210 in a deaerated 500 ppm sulphate solution. It was found that at a pH less than 9, Alloy 1210 could corrode in the active state. At a pH greater than 9 it was found to be in the passive state. The active state extended over a greater range than that of AISI 431 (Capendale, (1985)) which extended from low pH values to pH 3.8.

5. Increasing the sulphate concentration in solutions containing 500 ppm nitrate at pH 6.2 resulted in the increase of $[Cl^-]_{crit}$ for Alloy 1210. The $[Cl^-]_{crit}$ values established for Alloy 1210 were lower than those established for the same solutions for AISI 431. A linear relationship was established between $[Cl^-]_{crit}$ and the sulphate concentration.

6. An experimental E-pH diagram was established for 3CR12 in a deaerated 500 ppm sulphate solution. The active range extended over the whole pH range from 2 to 10. The active range was extended over a larger range than for AISI 431 or Alloy 1210.

7. Increasing the sulphate concentration up to 500 ppm in solutions containing 500 ppm nitrate at pH 6.2 resulted in the $[Cl^-]_{crit}$ being increased for 3CR12. Increasing the sulphate concentration above 500 ppm had little effect on the $[Cl^-]_{crit}$. The $[Cl^-]_{crit}$ at 200 ppm sulphate was higher than for AISI 431 and Alloy 1210. At 500 ppm sulphate the $[Cl^-]_{crit}$ was below that of AISI 431 but above that for Alloy 1210. At 200 ppm sulphate the $[Cl^-]_{crit}$ was lower than both AISI 431 and Alloy 1210.

8. An experimental E-pH diagram was constructed for Alloy 825 in a deaerated 500 ppm sulphate solution. Active corrosion occurred without the development of a passive layer up to pH 6. The passive layer that developed was unstable and was not expected to be a chromium oxide layer such as expected for AISI 431, Alloy 1210 and 3CR12. Alloy 825 showed similar corrosion behaviour to low alloy steels and mild steel.

9. Increasing the sulphate concentration reduced the stability of the passive layer on Alloy 825 in a 500 ppm nitrate solution at pH 6.2. The addition of low concentrations of chloride ions stabilised the layer, but the addition of further chlorides quickly resulted in a combination of general and pitting corrosion of Alloy 825.

10. The results obtained show that the interactive effect of different ions on the pitting corrosion behaviour varies for different alloys. For this reason results obtained for a particular alloy should not be used to predict the pitting corrosion behaviour of another alloy without doing some experimental test work first.

CHAPTER 6

FUTURE WORK

The results obtained for this work should form part of the ongoing research programme being carried out by the Chamber of Mines Research Organisation. The shortened test programme should be used to determine the pitting corrosion resistance of further development alloys that COMRO needs evaluating. This will enable the results obtained to be directly compared with those of AISI 431, Alloy 1210, 3CR12 and Alloy 825. This will allow a database of pitting corrosion information to be collected for materials selection and water treatment purposes.

Future alloys that have chromium levels of less than or equal to 10% should not have their pitting corrosion resistance evaluated using the shortened pitting corrosion test programme. Techniques should be employed which evaluate the general corrosion rates of the materials since the passive layer that develops on their surface is not stable, and therefore general corrosion is likely to be the predominant corrosion mechanism and not pitting corrosion.

CHAPTER 7

REFERENCES

ALKIRE R., CANGELLARI A. (1983) *Formation of Salt Films during Anodic Metal Dissolution in the Presence of Fluid Flow*, J. Electrochem. Soc., **130**, p. 1252.

ALKIRE R., ERNSBERGER D., DAMON D. (1976) *The Role of Conductivity Variations Within Artificial Pits During Anodic Dissolution*, J. Electrochem. Soc., **123**, p. 458.

ALKIRE R., SIITARI D. (1979) *The Location of Cathodic Reaction during Localized Corrosion*, J. Electrochem. Soc., **126**, p. 15.

ALLEN C., PROTHEROE B.E., BALL A. (1981) *The Selection of Abrasion-corrosion-resistant Materials for Gold-mining Equipment*, J. of S. A. I. of Mining and Metallurgy, p. 289.

ALLEN C., BALL A., PROTHEROE B.E. (1981) *The Abrasive-corrosive Wear of Stainless Steel*, Wear, **74**, p. 287.

ASTM STANDARDS (1980) *Standard Reference Method for Making Potentiostatic and Potentiodynamic Anodic Polarization Measurements*, ASTM Standards **G5-78**, p. 816.

ASTM STANDARDS (1980) *Conducting Cyclic Potentiodynamic Polarization Measurements for Localized Corrosion*, ASTM Standards **G5-78**, p. 1033.

ASTM STANDARDS (1980) *Conventions Applicable to Electrochemical Measurements in Corrosion Testing*, ASTM Standards **G3-74**, p. 794.

ATRENS A. (1983) *Environmental Conditions Leading to Pitting/Crevice Corrosion of a Typical 12% Chromium Stainless Steel at 80°C*, Corrosion-NACE, **39**, p. 483.

AZZERRI N., MANCIA F., TAMBA A. (1982) *Electrochemical Prediction of Corrosion Behaviour of Stainless Steels in Chloride Containing Waters*, Corrosion Science, **22**, p. 675 .

BABOIAN R., HAYNES G.S. (1981) *Cyclic Polarization Measurements - Experimental Procedure and Evaluation of Test Data*, Electrochemical Corrosion Testing, ASTM STP 727, Florian Mansfeld and Ugo Bertocci, Eds., ASTM, p. 274.

BARBOSA M., SCULLY J.C (1982) *The Role of Repassivation Kinetics in the Measurement of the Pitting Potential of AISI 304 Stainless Steel by the Scratch Method*, Corrosion Science, 22, p. 1025.

BARKER K.C. (1988) *Private Communication*, PHd student, Materials Engineering Department, University of Cape Town.

BECHET M.J.R. (1988) *Private Communication*, MSc student, Materials Engineering Department, University of Cape Town.

BECK T.R. (1973) *Pitting of Titanium. II. One Dimensional Pit Experiments*, J. Electrochem. Soc., **120**, p. 1317.

BECK T.R. (1977) *Effect of Hydrodynamics on Pitting*, Corrosion-NACE, **33**, p. 9.

BEE J.V., PETERS J.A., ATKINSON M.W., GARRETT G.G. (1987) *Improved Wear and Corrosion Resistant Steels*, J. S. African Inst. Min. Metall., **87**, p. 1.

BOGAERTS W., VAN HAUTE A. et al (1980) *Influence of Cl-, HCO3-, SO42- on the Corrosion of Fe-Cr-Ni Alloys in Hot Water Systems*, Proc. 8th Int. Congress on Metallic Corrosion, Dechema, Fed. Rep. of Germany, 2, p.1887.

BROWN C.J., WYMER D.G. (1986) *The Engineering of Water Powered Equipment for Mine Hydro Power Systems*, Proc. of Minemech 86, The S. Afr. Inst. of Mechanical Engineers.

BURSTEIN G.T., DAVIES D.H. (1981) *The Electrochemical Behaviour of Scratched Iron Surfaces in Aqueous Solutions*, J. Electrochem. Soc., **128**, p. 33.

BURSTEIN G.T., DAVIES D.H., NEWMAN R.C. (1980) *The Electrochemical Behaviour of Freshly Generated Metal Surfaces in Aqueous Electrolytes*, Electrochem. Soc. Spring Meeting, St. Louis Navy 1980.

BURSTEIN G.T., MARSHALL P.I. (1984) *The Coupled Kinetics of Film Growth and Dissolution of Stainless Steel Repassivating in Acid Solutions*, Corrosion Science, 24, p.449.

CAPENDALE A.E. (1985) *The Influence of Water Composition on the Pitting Behaviour of a Stainless Steel*, MSc thesis, Materials Engineering Department, University of Cape Town.

CHANCE R.L., SCHREIBER T.P., FRANCE W.D. (1975) *Anomolous Effects of Temperature on the Polarization Characteristics of Type 409 Stainless Steel*, Corrosion-NACE, 31, p. 296.

CHEN W.Y.C., STEPHENS J.R. (1979) *Anodic Polarization Behaviour of Austenitic Stainless Steel Alloys with Lower Chromium Content*, Corrosion-NACE, **35**, p. 443.

CIESLAK W.R. (1986) *The Influence of Sulphide Inclusions on the Initiation of Pits in Fe-29Ni-17Co*, Corrosion-NACE, **42**, p. 111.

CIESLAK W.R., DUQUETTE D.J. (1984) *Properties of the Passive Films Formed on Ferritic Stainless Steel in Cl^-* Solutions, Corrosion-NACE, **40**, p. 545.

DAWSON J.L., FERREIRA M.G.S. (1986) *Electrochemical Studies of the Pitting of Austenitic Stainless Steel*, Corrosion Science, **26**, p. 1009.

DE BOLD T.A. (1980) *Which Corrosion Test for Stainless Steels*, ME, p. 67.

DEGERBECK J. (1973) *On Accelerated Pitting and Crevice Corrosion Tests*, J. Electrochem. Soc., **120**, p. 175.

FRANCE W.D. (1967) *A Specimen Holder for Precise Electrochemical Polarization Measurements on Metal Sheets and Foils*, J. Electrochem. Soc., **114**, p. 818.

FRANCE W.D., GREENE N.D. (1970) *Comparison of Chemically and Electrolytically Induced Pitting Corrosion*, Corrosion-NACE, **26**, p. 1.

FRANKEL G.S., STOCKERT L., HUNKELER F., BOEHNI H. (1987) *Metastable Pitting of Stainless Steel*, Corrosion-NACE, **43**, p. 429.

FRANKENTHAL R.P., PICKERING H.W. (1972) *On the Mechanism of Localized Corrosion of Iron and Stainless Steel. II. Morphological Studies*, J. Electrochem. Soc., **119**, p. 1304.

GALVELE J.R. (1976) *Transport Processes and the Mechanism of Pitting of Metals*, J. Electrochem. Soc., **123**, p. 465.

GREENE N.D. (1962) *Predicting Behaviour of Corrosion Resistant Alloys by Potentiostatic Polarization Methods*, Corrosion-NACE, **18**, p. 136.

HEINE M.A., KEIR D.S., PROYR M.J. (1965) *The Specific Effects of Chloride and Sulphate Ions on Oxide Covered Aluminium*, J. Electrochem. Soc., **112**, p. 24.

HIGGINSON A., WHITE R.T. (1983) *A Preliminary Survey of the Corrosivity of Water in Gold Mines*, Mintek Report, **M65**.

HIGGINSON A. (1984) *A Preliminary Investigation of the Initiation of Pitting Corrosion In Austenitic Stainless Steels and Nickel Based Alloys*, Mintek Report, M151.

HOAR T.P. (1967) *The Production and Breakdown of the Passivity of Metals*, Corrosion Science, 7, p. 341.

HOAR T.P., MEARS D.C., ROTHWELL G.P. (1965), Corrosion Science, 5, p. 279. As cited by Oldfield (1987).

HOFFMAN J.P. (1984) *3CR12 - An Overview of Mechanical and Corrosion Properties. Part 2 Corrosion Properties*, Proc. of the Inaugural International 3CR12 Conference, Johannesburg, p. 82.

HOSPADURAK V., PETROCELLI J.V. (1966) *The Pitting Potential of Stainless Steels in Chloride Media*, J. Electrochem., Soc., 113, p. 878.

INFORMATION LEAFLET NO. 4, (1987) *Hydro-power: A Means of Cooling and Powering Deep Mines*, Chamber of Mines Research Organisation.

JANIK-CZACHOR M. (1981) *An Assessment of the Process Leading to Pit Nucleation on Iron*, J. of Electrochem. Soc., 128, p. 513.

JOUBERT K. (1988) *Private Communication*, MSc student, Materials Engineering Department, University of Cape Town.

KEITELMAN A.D., GALVELE J.R (1982) *Pitting and Pitting Inhibition of Iron in Sodium Sulphate Solutions, Corrosion Science, 22*, p. 739.

KOLOTYRKIN J.M. (1961) *Effects of Anions on the Dissolution Kinetics of Metals*, J. Electrochem. Soc., 108, p. 209.

KRUGER J., RHYNE K. (1982) *Nuclear Chemical Waste Management*, 3, p. 205.

LECKIE H.P., UHLIG H.H. (1966) *Environmental Factors Affecting the Critical Potential for Pitting in 18-8 Stainless Steel*, J. of Electrochem. Soc., 113, p.1262.

LENEL U.R., KNOTT BR (1987) *Structure and Properties of Corrosion and Wear Resistant Cr-Mn-N Steels*, Met. Trans. A, 18A, p. 847.

LIZLOVS E.A., BOND A.P. (1975) *An Evaluation of Some Electrochemical Techniques for the Determination of Pitting Potentials of Stainless Steel*, Corrosion-NACE, 31, p. 219.

LUNARSKA E., SZKLARSKA-SMIALOWSKA Z., JANIK-CZACHOR M. (1975) *Susceptibility of Cr-Ni-Mn Steels to Pitting in Chloride Solutions*, Corrosion-NACE, **31**, p. 231.

MAN H.C., GABE D.R. (1980) *The Determination of Pitting Potentials*, Corrosion Science, 21, p.323.

MANAGER MAB (1983) Private Communication, Manager Engineering Materials Branch, Chamber of Mines Research Organisation. As cited by Capendale (1985).

MANKOWSKI J., SZKLARSKA-SMIALOWSKA (1975) *Studies on Accumulation of Chloride Ions in Pits Growing During Anodic Polarization*, Corrosion Science, **24**, p. 493.

MANNING P.E. (1983) *Comparison of Several Accelerated Laboratory Tests for the Determination of Localized Corrosion Resistance of High-Performance Alloys*, Corrosion-NACE, **39**, p. 98.

MARSHALL P.I., BURSTEIN G.T. (1984) *Effects of Alloyed Molybdenum on the Kinetics of Repassivation on Austenitic Stainless Steels*, Corrosion Science, **24**, p.463.

MITROVIC-SCEPANOVIC V., BRIGHAM R.J. (1987) *The Localized Corrosion of Stainless Steel in High Purity Sulphate Solutions*, Corrosion Science, **27**, p. 545.

MOREAU R., BRISON J. (1972) J. Men. Sci. et., **69**, p. 845. As cited by Rawat (1976).

MURSALO N., TULLMIN M., ROBINSON F.P.A. (1988) *Corrosion Behaviour of Mild Steel, 3CR12 and AISI Type 316 in Synthetic Mine Waters Containing Various Sulphate and Chloride Levels*, Unpublished Work.

NEWMAN R.C. (1983) *Protection Potentials for Pitting of Stainless Steel in Neutral Chloride Solutions*, Corrosion Science, **23**, p. 1045.

NEWMAN R.C., AJJAWI M.A.A. (1986) *A Micro-Electrode Study of the Nitrate Effect on Pitting of Stainless Steels*, Corrosion Science, **26**, p. 1057.

OKADA T. (1985) *A Theory of Pertubation-Initiated Pitting*, J. of Electrochem. Soc., **132**, p. 537.

OLDFIELD J.W. (1987) *Test Techniques for Pitting and Crevice Corrosion Resistance of Stainless Steels and Nickel-base Alloys in Chloride-containing Environments*, International Materials Reviews, **32**, p. 153.

OLDFIELD J.W., LEE T.S., KAIN R.M. (1985) *Avoiding Crevice Corrosion of Stainless Steels*, Proc. Stainless Steel '84, Chalmers University of Technology, The Institute of Metals 1985, p. 205.

PALUMBO G., KING P.J., AUST K.T. (1987) *Pitting Corrosion Behaviour of Alloy 800 in Chloride Sulphate Media*, Corrosion-NACE, 43, p. 37.

PARKINS R.N. (1985) *Significance of Pits, Crevices and Cracks in Environment Sensitive Crack Growth*, Materials Science and Technology, 1, p.480.

PESSAL N., LIU C. (1971) *Determination of Critical Pitting Potentials of Stainless Steels in Aqueous Chloride Environments*, Electrochemica Acta, 16, p. 1987.

POURBAIX M. (1965) *A Comparative Review of Electrochemical Methods of Assessing Corrosion and the Behaviour in Practice of Corrodible Material*, Corrosion Science, 5, p. 677.

POURBAIX M. (1970) *Significance of Protection Potential in Pitting and Intergranular Corrosion*, Corrosion-NACE, 26, p. 431.

POURBAIX M. et al. (1963) *Potentiokinetic and Corrosimetric Investigations of the Corrosion Behaviour of Alloy Steels*, Corrosion Science, 3, p. 240.

PRAZAK M. (1963) *Evaluation of Corrosion-Resistant Steels Using Potentiostatic Polarization Curves*, Corrosion-NACE, 19, p. 75t.

PROCTOR R. (1988) *Private Communication*, Head of the Corrosion and Protection Centre, UMIST.

RAWAT N.S. (1976) *Corrosivity of Underground Mine Atmospheres and Mine Waters. A Review and Preliminary Study*, Br. Corrosion J., 11, p.86.

RICHARDSON J.A., WOOD G.C. (1970) *A Study of the Pitting Corrosion of Al by Scanning Electron Microscopy*, Corrosion Science, 10, p. 313.

SEDRIKS A.J. (1982) *Metallurgical Aspects of Passivation of Stainless Steels*, Proc. Stainless Steel '84, Chalmers University of Technology, The Institute of Metals 1985, p. 125.

SEDRIKS A.J. (1983) *Role of Sulphide Inclusions in Pitting and Crevice Corrosion of Stainless Steels*, International Metals Reviews, 28, p. 295.

SEDRIKS A.J. (1979) *Corrosion of Stainless Steels*, The Monograph Series, Sponsored by the Electrochemical Society, Wiley Interscience Publications.

SHARLAND S.M. (1987) *A Review of the Theoretical Modelling of Crevice and Pitting Corrosion*, Corrosion Science, **27** p. 289.

SHREIR L.1. (1963) *The Potentiostat and its Application to Corrosion Studies*, Corrosion Volume 2 - Corrosion Control, **2**, p. 123.

STREHBLOW H.H., IVES M.B. (1976) *On the Electrochemical Conditions within Small Pits*, Corrosion Science, **16**, p. 317.

STREHBLOW H.H., TITZE B. (1977) *Pitting Potentials and Inhibition Potentials of Iron and Nickel for Different Aggressive and Inhibiting Anions*, Corrosion Science, **17**, p. 461.

SYRETT B.C. (1977) *PPR Curves - New Method of Assessing Pitting Corrosion Resistance*, Corrosion-NACE, **33**, p. 221.

SYRETT B.C., VISWANATHAN R., WING S.S., WITTIG J.E. (1982) *Effect of Microstructure on Pitting and Corrosion Fatigue of 14-4 PH Turbine Blade Steel in Chloride Environments*, Corrosion-NACE, **38**, p. 272.

SZKLARSKA-SMIALOWSKA Z. (1971) *Review of Literature on Pitting Corrosion since 1960*, Corrosion-NACE, **27**, p. 223.

SZKLARSKA-SMIALOWSKA Z., JANIK-CZACHOR M. (1971) *The Analysis of Electrochemical Methods for the Determination of Characteristic Potentials of Pitting Corrosion*, Corrosion Science, **21**, p. 901.

UHLIG H.H., GILMAN J.R. (1964) *Pitting of 18-8 Stainless Steel in Ferric Chloride Inhibited by Nitrates*, Corrosion-NACE, **20**, p. 289.

VERINK E.D. POURBAIX M. (1971) *Use of Electrochemical Hysterisis Techniques in Developing Alloys for Saline Exposures*, Corrosion-NACE, **27**, p. 497.

VETTER K.J., STREHBLOW H.H. Localized Corrosion (ed. R.W. Staehle et al.), Houston Tex., NACE, p. 240. As cited by Oldfield (1987).

WALKER M.S., ROWE L.C. (1969) *The Application of Electrochemical Techniques to the Study of Corrosion of Automative Trim Materials*, Corrosion-NACE, **25**, p. 47.

WHITE R.T. (1983) *A Review of Corrosion Inhibitors : Theory and Practice*, Mintek Report, **M66**.

WHITE R.T. (1985) *Water Treatment Practice in South African Gold Mines*, J. S. Afr. Inst. Min. Metall., **85**, p. 81.

WHITE R.T. (1985) *The Commissioning, Operation, and Maintenance of an On-Line Corrosion Monitoring Station for the Mining Industry*, Mintek Report, M225.

WHITE R.T., HIGGINSON A. (1985) *Factors Affecting the Corrosivity of Underground Mine Waters*, Mintek Publication, 50, p. 941.

WILDE B.E., WILLIAMS E. (1970) *The Use of Current/Voltage Curves for the Study of Localized Corrosion and Passivity Breakdown on Stainless Steels in Chloride Media*, Proc. of the 3rd Int. Conf. on Passivity of Metals, Cambridge, England, 1970.

WILLIAMS D.E., WESTCOTT C., FLEISCHMANN M. (1984) *Studies of the Initiation of Pitting Corrosion on Stainless Steels*, J. Electrochem. Soc., 180, p. 549.

MINE WATER COMPOSITIONS (after C.O.M.R.O., (1983))

IONIC SPECIES (concentration in ppm) / NAME OF MINE	pH	Total Dissolved Solids	Total Suspended Solids	Total Hardness (as $CaCO_3$)	Sulphate	Chloride	Sulphite	Sulphide	Nitrate	Free Saline Ammonia	Hypochlorite	Bicarbonate	Fluoride	Calcium	Magnesium	Sodium	Potassium	Ferrous Ion	Ferric Ion	Nickel	Copper	Langelier Index	Aluminium	Zinc	Nitrite	Conductivity (mS/m)	Total Alkalinity (as $CaCO_3$)	pH of Saturation	Calcium Hardness (as $CaCO_3$)	Magnesium Hardness (as $CaCO_3$)
MINE A	6.5	1130	26	457	425	172	*	*	49	0.7	*	44	0.4	115	25	166	6	0.1	0.3	1.05	*	-1.49	*	*	*	na	na	na	na	na
MINE B (SHAFT 1)	6.0	3502	64	811	711	1037	*	*	246	27	170	5	0.8	243	50	930	7.3	0.7	11.7	1.36	*	-2.67	2.7	0.64	12.1	460	4	na	672	139
MINE B (SHAFT 2)	6.5	3038	18	635	265	1203	*	*	144	12	157	31	1.1	182	44	790	5.5	0.2	2.9	0.21	*	-1.46	0.8	0.19	37	490	26	na	511	124
MINE C (DAY 1)	6.1	3790	7	448	153	1865	*	*	65	0.8	*	94	1.2	182	5.8	1040	12	0.1	0.1	*	*	-2.0	*	*	1.0	614	24	8.10	402	46
MINE C (DAY 2)	7.2	3520	22	414	150	1574	*	*	43	4.0	67	49	1.3	138	16	1290	7.6	0.3	2.9	0.22	*	-0.94	5.1	*	27.2	na	40	na	371	43
RAND WATER BOARD	7.4	364	32	184	102	38	*	0.3	*	0.8	*	201	0.3	48	12	37	4.5	0.1	0.2	*	*	-0.56	*	*	*	54.7	101	na	na	na
MINE D	6.5	2184	19	518	829	39	1.1	0.8	327	91	142	10	1.5	158	30	290	15.2	0.23	1.8	1.98	*	-2.02	0.3	1.77	18.6	255	8	9.52	435	83
MINE E	6.3	4975	42	1034	821	1812	*	0.9	228	36	*	39	1.0	368	28	1130	13.9	*	*	0.37	*	-1.37	*	*	6.5	700	32	7.67	961	73
MINE F	5.8	10870	4	3689	2008	2766	*	0.3	1650	55	0.1	40	0.9	1250	138	1520	70	*	*	0.46	*	-1.52	*	0.12	58	1200	33	7.32	3322	367
MINE G	6.3	4100	20	769	901	1220	*	*	191	0.8	*	14	1.0	268	18	900	31	0.1	0.1	0.61	*	-1.55	*	*	*	619	7	7	na	na
MINE I (DAY 1)	4.7	3490	4	2175	2300	36	0.8	*	22	3.9	9	2.5	0.6	620	152	69	2.3	*	*	10.7	0.23	-3.94	23	8.5	9.9	na	2	8.64	na	na
MINE I (DAY 2)	6.9	2824	4	1526	1586	36	1.0	*	9.5	3.1	2.2	49	0.7	600	6.9	70	2.4	*	1.5	*	*	-0.44	49	*	0.7	240	40	7.34	1508	18
MINE H (DAY 1)	5.5	740	204	849	760	92	1.0	2.0	194	10.6	*	4.9	0.7	276	39	111	21	0.16	0.12	1.60	*	-3.00	1.1	0.19	4.1	na	4	8.50	na	na
MINE H (DAY 2)	7.6	1820	2875	738	677	103	1.2	*	188	17.4	100	78	0.5	250	28	104	19.7	0.13	2.0	0.33	*	0.18	1.4	0.1	9.8	175	64	7.42	664	74
MINE J	6.5	6756	44	1785	2176	1564	*	*	1185	93	107	12	0.6	580	82	1480	187	0.8	1.6	1.83	*	-1.36	2.3	0.62	30.5	850	10	na	1564	221

* = LESS THAN 0.1 PPM

n.a. - NOT AVAILABLE

AISI 431 TEST PROGRAM COMPLETED

CRITICAL CHLORIDE TESTING : 100 ppm SO_4^{2-} at pH 6.2

ppm Cl-	E_{corr} (V)	$E_{br/p}$ (V)	E_{prot} (V)	i_{pass} ($\mu A/cm^2$)	Pitting
0	-0.14	0.38		40	N
20	-0.14	0.40		40	N
50	-0.15	0.12	-0.10	40	Y
100	-0.14	0.11	-0.08	20	Y
150	-0.13	0.11		3	Y

CRITICAL CHLORIDE TESTING : 500 ppm SO_4^{2-} at pH 6.2

ppm Cl-	E_{corr} (V)	$E_{br/p}$ (V)	E_{prot} (V)	i_{pass} ($\mu A/cm^2$)	Pitting
50	-0.21	0.40		4	N
100	-0.21	0.42		5	N
125	-0.20	0.41		6	N
150	-0.18	0.38		5	N
200	-0.17	0.36	-0.12	6	Y
300	-0.15	0.09	-0.12	8	Y

CRITICAL CHLORIDE TESTING : 1000 ppm SO_4^{2-} at pH 6.2
(data corrected for XY recorder calibration error)

ppm Cl-	E_{corr} (V)	$E_{br/p}$ (V)	E_{prot} (V)	i_{pass} ($\mu A/cm^2$)	Pitting
300	-0.26	0.40		7	N
330	-0.20	0.50		20	N
340	-0.18	0.46		40	N
350	-0.22	0.30		10	N
360	-0.15	0.30	+0.10	20	Y
380	-0.18	0.18	+0.13	20	Y
400	-0.20	0.12	-0.07	8	Y

CRITICAL CHLORIDE TESTING : 2000 ppm SO_4^{2-} at pH 6.2

ppm Cl-	E_{corr} (V)	$E_{br/p}$ (V)	E_{prot} (V)	i_{pass} ($\mu A/cm^2$)	Pitting
300	-0.26	0.56		10	N
400	-0.24	0.50		30	N
500	+0.16	0.54		40	N
600	-0.25	0.26	+0.08	40	Y
700	-0.24	0.35	+0.02	10	Y

AISI 431 TEST PROGRAM COMPLETED

CRITICAL CHLORIDE TESTING : 500 ppm NO_3^- at pH 6.2

ppm Cl-	E_{corr} (V)	$E_{br/p}$ (V)	E_{prot} (V)	i_{pass} ($\mu A/cm^2$)	Pitting
300	-0.15	0.50		0.8	N
400	-0.16	0.70		0.8	N
500	-0.17	0.48		0.8	N
600	-0.14	0.34	-0.07	0.7	Y
700	-0.13	0.37	+0.00	1.0	Y
800	-0.12	0.24	+0.04	1.0	Y

CRITICAL CHLORIDE TESTING : 500 ppm NO_3^- + 100 ppm SO_4^{2-} at pH 6.2

ppm Cl-	E_{corr} (V)	$E_{br/p}$ (V)	E_{prot} (V)	i_{pass} ($\mu A/cm^2$)	Pitting
400	-0.24	0.48		0.8	N
500	-0.27	0.45		0.8	N
600	-0.28	0.46		1.0	N
700	-0.25	0.31	-0.03	1.0	Y
800	-0.23	0.38	-0.01	1.0	Y
900	-0.21	0.31	+0.05	1.0	Y

CRITICAL CHLORIDE TESTING : 500 ppm NO_3^- + 500 ppm SO_4^{2-} at pH 6.2

ppm Cl-	E_{corr} (V)	$E_{br/p}$ (V)	E_{prot} (V)	i_{pass} ($\mu A/cm^2$)	Pitting
600	-0.15	0.50		1.0	N
700	-0.14	0.52		1.0	N
800	-0.15	0.50		1.0	N
900	-0.14	0.40	-0.05	1.1	Y
1000	-0.15	0.40	+0.05	1.1	Y

CRITICAL CHLORIDE TESTING : 500 ppm NO_3^- + 1000 ppm SO_4^{2-} at pH 6.2

ppm Cl-	E_{corr} (V)	$E_{br/p}$ (V)	E_{prot} (V)	i_{pass} ($\mu A/cm^2$)	Pitting
900	-0.14	0.58		1.2	N
1000	-0.13	0.59		1.2	N
1100	-0.14	0.58	+0.11	1.2	Y
1200	-0.14	0.48	+0.06	1.2	Y
1300	-0.13	0.40	+0.04	1.3	Y

CRITICAL CHLORIDE TESTING : 500 ppm NO_3^- + 1500 ppm SO_4^{2-} at pH 6.2

ppm Cl-	E_{corr} (V)	$E_{br/p}$ (V)	E_{prot} (V)	i_{pass} ($\mu A/cm^2$)	Pitting
0	-0.26	0.55		1.0	N
1100	-0.31	0.54		1.2	N
1125	-0.28	0.45	+0.13	1.4	Y
1150	-0.28	0.52	+0.00	1.4	Y
1200	-0.30	0.50	+0.07	1.1	Y
1250	-0.28	0.43	-0.03	1.2	Y
1300	-0.31	0.48	+0.07	1.2	Y
1400	-0.29	0.41	-0.13	1.2	Y

AISI 431 TEST PROGRAM COMPLETED

CRITICAL CHLORIDE TESTING : 1000 ppm NO_3^- + 200 ppm SO_4^{2-} at pH 6.2

ppm Cl-	E_{corr} (V)	$E_{br/p}$ (V)	E_{prot} (V)	i_{pass} ($\mu A/cm^2$)	Pitting
500	-0.32	0.51		1	N
700	-0.31	0.57		1	N
900	-0.36	0.52		1	N
1100	-0.35	0.46		1	N
1200	-0.31	0.46		1	N
1250	-0.27	0.21	-0.05	2	Y
1300	-0.27	0.16	-0.15	1	Y
1350	-0.27	0.15	-0.06	1	Y
1400	-0.32	0.25	-0.05	2	Y
1500	-0.34	0.30	-0.15	1	Y
1700	-0.34	0.31	-0.07	1	Y

CRITICAL CHLORIDE TESTING : 1000 ppm NO_3^- + 500 ppm SO_4^{2-} at pH 6.2
(data corrected for XY recorder calibration error)

ppm Cl-	E_{corr} (V)	$E_{br/p}$ (V)	E_{prot} (V)	i_{pass} ($\mu A/cm^2$)	Pitting
1200	-0.31	0.60		1	N
1300	-0.30	0.56		1	N
1400	-0.29	0.43		1	N
1450	-0.28	0.22	-0.04	1	Y
1500	-0.31	0.09	+0.03	1	Y
1550	-0.30	0.17	+0.02	1	Y
1600	-0.32	0.13	-0.05	1	Y
1600	-0.34	0.12	-0.01	1	Y
1700	-0.30	0.11	-0.10	1	Y

CRITICAL CHLORIDE TESTING : 1000 ppm NO_3^- + 1000 ppm SO_4^{2-} at pH 6.2

ppm Cl-	E_{corr} (V)	$E_{br/p}$ (V)	E_{prot} (V)	i_{pass} ($\mu A/cm^2$)	Pitting
1400	-0.36	0.65		1	N
1500	-0.32	0.60		1	N
1550	-0.38	0.65		1	N
1600	-0.35	0.68		1	Y
1650	-0.36	0.12		1	Y
1700	-0.32	0.38	-0.14	1	Y
1800	-0.32	0.45	-0.05	1	Y

CRITICAL CHLORIDE TESTING : 1000 ppm NO_3^- + 1500 ppm SO_4^{2-} at pH 6.2

ppm Cl-	E_{corr} (V)	$E_{br/p}$ (V)	E_{prot} (V)	i_{pass} ($\mu A/cm^2$)	Pitting
0	-0.29	0.54		1	N
1000	-0.29	0.50		1	N
1500	-0.28	0.48		1	N
2000	-0.29	0.51		1	N
2025	-0.30	0.21	-0.12	1	Y
2050	-0.28	0.31	-0.16	1	Y
2100	-0.29	0.28	+0.06	1	Y
2500	-0.28	0.32	+0.03	1	Y

AISI 431 TEST PROGRAM COMPLETED

CRITICAL CHLORIDE TESTING : 1000 ppm NO_3^- + 1000 ppm SO_4^{2-} at pH 3.8

ppm Cl-	E_{corr} (V)	$E_{br/p}$ (V)	E_{prot} (V)	i_{pass} ($\mu A/cm^2$)	Pitting
0	-0.28	0.60		1	N
500	-0.30	0.66		1	N
600	-0.23	0.64		1	N
900	-0.28	0.64		1	N
1000	-0.30	0.58		1	Y
1100	-0.34	0.56		1	Y
1200	-0.29	0.55		1	Y
1400	-0.29	0.50		1	Y
1500	-0.27	0.24	-0.18	1	Y

CRITICAL CHLORIDE TESTING : 1000 ppm NO_3^- + 1000 ppm SO_4^{2-} at pH 9.4

ppm Cl-	E_{corr} (V)	$E_{br/p}$ (V)	E_{prot} (V)	i_{pass} ($\mu A/cm^2$)	Pitting
0	-0.21	0.65		1	N
500	-0.16	0.65		1	N
1000	-0.25	0.59		1	N
1800	-0.20	0.56		1	N
1900	-0.18	0.46	-0.06	1	Y
2000	-0.23	0.21	-0.10	1	Y
2000	-0.23	0.27	-0.07	1	Y
2100	-0.27	0.20	-0.01	1	Y
2200	-0.24	0.24	-0.11	1	Y
3000	-0.24	0.18	-0.10	1	Y
4000	-0.22	0.21	+0.02	0.5	Y
5000	-0.21	0.09	-0.07	1	Y

ALLOY 1210 TEST PROGRAM COMPLETED

E - pH TESTING : 500 ppm SULPHATE

pH	E_{corr} (V)	E_F (V)	E_{br} (V)	i_{pass} ($\mu A/cm^2$)	Pitting
2.20	-0.68	+0.00	0.74	2	N
3.00	-0.70	+0.00	0.58	1	N
5.00	-0.88	-0.70	0.54	1	N
6.00	-0.88	-0.70	0.42	1	N
7.15	-1.00	-0.46	0.34	40	N
8.00	-0.92	-0.60	0.38	20	N
9.18	-0.86	-0.74	0.28	6	N
10.20	-0.88		0.18	5	N
11.25	-0.94		0.08	7	N

CRITICAL CHLORIDE TESTING : 200 ppm SO_4^{2-} + 500 ppm NO_3^- at pH 6.2

ppm Cl-	E_{corr} (V)	$E_{br/p}$ (V)	E_{prot} (V)	i_{pass} ($\mu A/cm^2$)	Pitting
0	-0.24	+0.75		1	N
200	-0.35	+0.74		2	N
500	-0.23	+0.76		1	N
525	-0.20	+0.05		1	Y
600	-0.13	+0.05		4	Y
700	-0.28	+0.00		2	Y
800	-0.34	-0.09		1	Y
1000	-0.40	+0.07		1	Y

CRITICAL CHLORIDE TESTING : 1000 ppm SO_4^{2-} + 500 ppm NO_3^- at pH 6.2

ppm Cl-	E_{corr} (V)	$E_{br/p}$ (V)	E_{prot} (V)	i_{pass} ($\mu A/cm^2$)	Pitting
0	-0.34	+0.76		0.8	N
500	-0.32	+0.74		1	N
550	-0.32	+0.24	-0.26	1	Y
650	-0.32	+0.08	+0.03	1	Y
700	-0.30	+0.25		1	Y
800	-0.36	-0.10	-0.17	1	Y
900	-0.33	-0.11	-0.17	1	Y
1000	-0.33	-0.10	-0.17	1	Y

CRITICAL CHLORIDE TESTING : 2000 ppm SO_4^{2-} + 500 ppm NO_3^- at pH 6.2

ppm Cl-	E_{corr} (V)	$E_{br/p}$ (V)	E_{prot} (V)	i_{pass} ($\mu A/cm^2$)	Pitting
0	-0.18	+0.74		3	N
500	-0.20	+0.70		2	N
900	-0.23	+0.76		3	N
925	-0.21	+0.46		1	Y
950	-0.27	-0.12		2	Y
1000	-0.25	+0.08	-0.17	1	Y

3CR12 TEST PROGRAM COMPLETED

E - pH TESTING : 500 ppm SULPHATE

pH	E_{corr} (V)	E_F (V)	E_{br} (V)	i_{pass} ($\mu A/cm^2$)	Pitting
2.00	-0.42	+0.32	0.68	10	N
3.00	-0.60	+0.04	0.64	5	N
4.00	-0.64	+0.06	0.56	5	N
4.80	-0.89	-0.43	0.38	7	N
5.50	-0.91	-0.58	0.44	7	N
6.70	-0.88	-0.62	0.50	6	N
7.70	-0.88	-0.68	0.48	7	N
9.00	-0.90	-0.74	0.40	6	N
10.00	-0.92	-0.68	0.38	7	N

CRITICAL CHLORIDE TESTING : 200 ppm SO_4^{2-} + 500 ppm NO_3^- at pH 6.2

ppm Cl-	E_{corr} (V)	$E_{br/p}$ (V)	E_{prot} (V)	i_{pass} ($\mu A/cm^2$)	Pitting
0	-0.29	0.75		3	N
500	-0.31	0.73		2	N
650	-0.36	0.68		2	N
700	-0.26	0.77		2	N
700	-0.30	0.29		2	Y
725	-0.29	0.28	+0.03	2	Y
750	-0.29	0.64	+0.10	2	Y

CRITICAL CHLORIDE TESTING : 1000 ppm SO_4^{2-} + 500 ppm NO_3^- at pH 6.2

ppm Cl-	E_{corr} (V)	$E_{br/p}$ (V)	E_{prot} (V)	i_{pass} ($\mu A/cm^2$)	Pitting
0	-0.32	0.74		2	N
700	-0.29	0.54		3	N
700	-0.30	0.70		2	N
750	-0.30	0.72		3	N
800	-0.28	0.49	-0.01	2	Y
800	-0.36	0.42	-0.04	3	Y
900	-0.31	0.36	+0.00	2	Y
1000	-0.28	0.46	+0.01	2	Y
1100	-0.29	0.28	-0.04	2	Y

CRITICAL CHLORIDE TESTING : 2000 ppm SO_4^{2-} + 500 ppm NO_3^- at pH 6.2

ppm Cl-	E_{corr} (V)	$E_{br/p}$ (V)	E_{prot} (V)	i_{pass} ($\mu A/cm^2$)	Pitting
0	-0.29	0.72		1	N
500	-0.32	0.76		1	N
600	-0.30	0.74		1	N
700	-0.30	0.76		1	N
750	-0.30	0.74		1	N
800	-0.25	0.07		1	Y
900	-0.29	0.08		1	Y

ALLOY 825 TEST PROGRAM COMPLETED

E-pH TESTING : 500 ppm SULPHATE

pH	E_{corr} (V)	E_F (V)	E_{br} (V)	i_{pass} ($\mu A/cm^2$)	Pitting
2.10	-0.64				N
3.00	-0.62				N
4.00	-0.65				N
5.00	-0.80				N
6.00	-0.80	-0.72	-0.68	3	N
7.00	-0.84	-0.72	-0.56	1	N
8.00	-0.88	-0.72	-0.60	1	N
9.30	-0.88	-0.74	+0.32	2	N
10.40	-0.92		+0.34	2	N

CRITICAL CHLORIDE TESTING : 200 ppm SO_4^{2-} + 500 ppm NO_3^- at pH 6.2

ppm Cl-	E_{corr} (V)	$E_{br/p}$ (V)	E_{prot} (V)	i_{pass} ($\mu A/cm^2$)	Pitting
0	-0.25	+0.75		2	N
100	-0.35	+0.75		2	N
125	-0.24	+0.32		8	Y
150	-0.30	+0.12		10	Y
200	-0.31	+0.20		6	Y
500	-0.25	+0.13		5	Y

CRITICAL CHLORIDE TESTING : 1000 ppm SO_4^{2-} + 500 ppm NO_3^- at pH 6.2

ppm Cl-	E_{corr} (V)	$E_{br/p}$ (V)	E_{prot} (V)	i_{pass} ($\mu A/cm^2$)	Pitting
0	-0.31	-0.22		6	N
50	-0.28	+0.31		1	N
100	-0.28	-0.20		1	N
200	-0.25	+0.22		1	Y
300	-0.28	+0.07		1	Y
700	-0.47	-0.47			

CRITICAL CHLORIDE TESTING : 2000 ppm SO_4^{2-} + 500 ppm NO_3^- at pH 6.2

ppm Cl-	E_{corr} (V)	$E_{br/p}$ (V)	E_{prot} (V)	i_{pass} ($\mu A/cm^2$)	Pitting
0	-0.39	-0.39			N
100	-0.30	-0.30			N
200	-0.35	+0.75		2	Y
300	-0.38	-0.30		1	Y
500	-0.40	-0.40			Y
700	-0.43	-0.43			Y

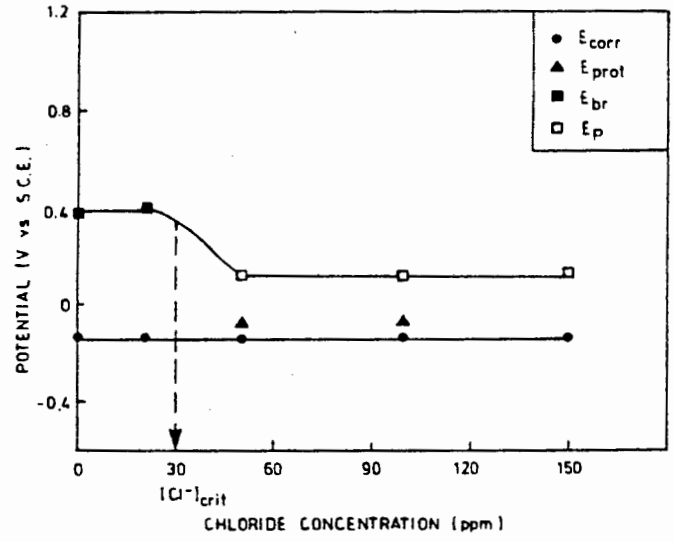

Figure C.1 : E_{corr} and E_{br} of AISI 431 in 100 ppm SO_4^{2-} versus chloride concentration at pH 6.2.

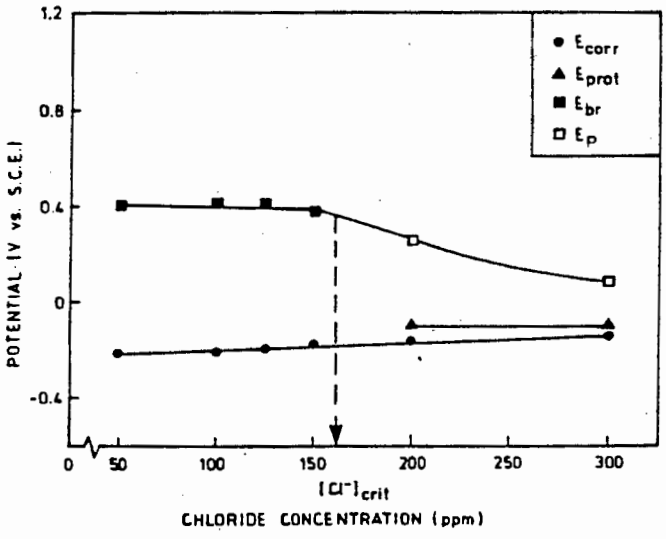

Figure C.2 : E_{corr} and E_{br} of AISI 431 in 500 ppm SO_4^{2-} versus chloride concentration at pH 6.2.

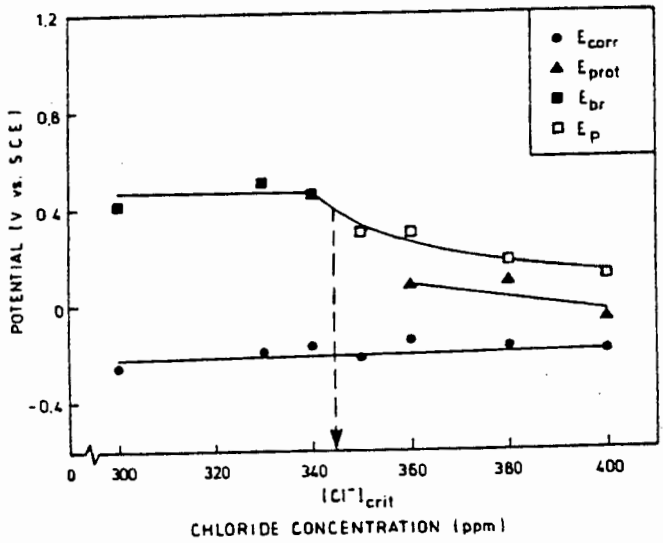

Figure C.3 : E_{corr} and E_{br} of AISI 431 in 1000 ppm SO_4^{2-} versus chloride concentration at pH 6.2.

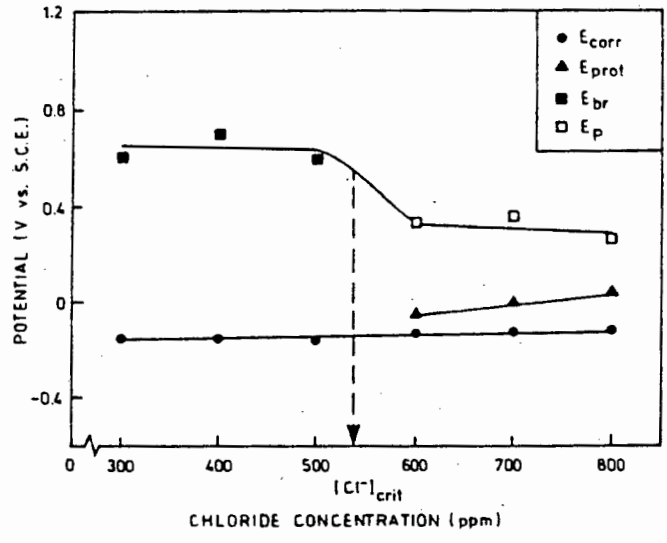

Figure C.4 : E_{corr} and E_{br} of AISI 431 in 500 ppm NO_3^- versus chloride concentration at pH 6.2.

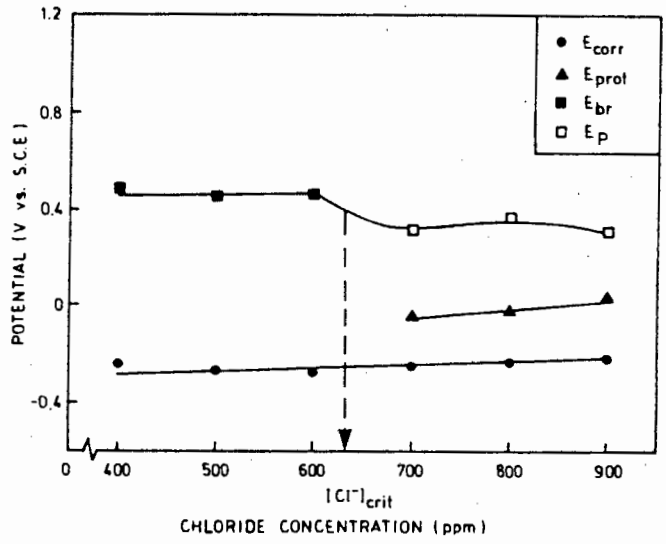

Figure C.5 : E_{corr} and E_{br} of AISI 431 in 100 ppm SO_4^{2-} + 500 ppm NO_3^- versus chloride concentration at pH 6.2.

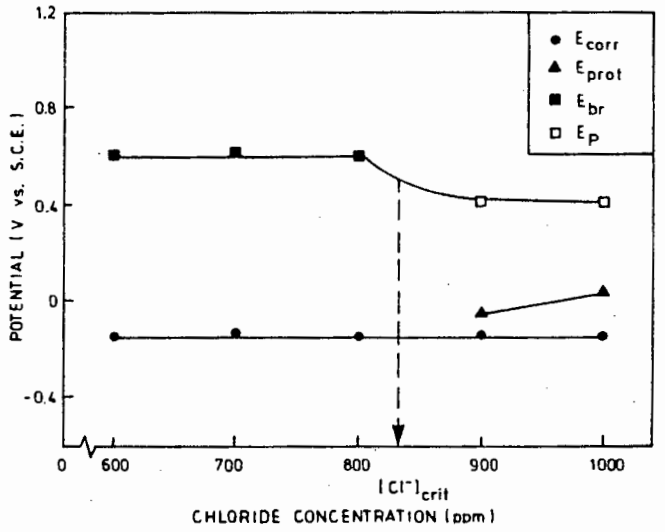

Figure C.6 : E_{corr} and E_{br} of AISI 431 in 500 ppm SO_4^{2-} + 500 ppm NO_3^- versus chloride concentration at pH 6.2.

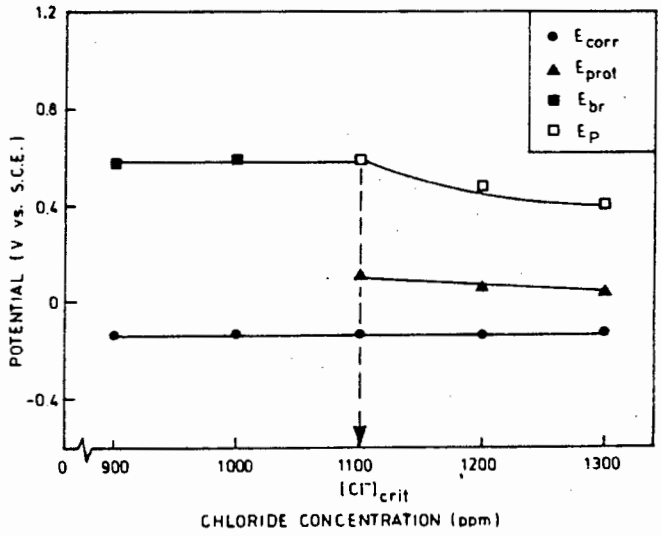

Figure C.7 : E_{corr} and E_{br} of AISI 431 in 1000 ppm SO_4^{2-} + 500 ppm NO_3^- versus chloride concentration at pH 6.2.

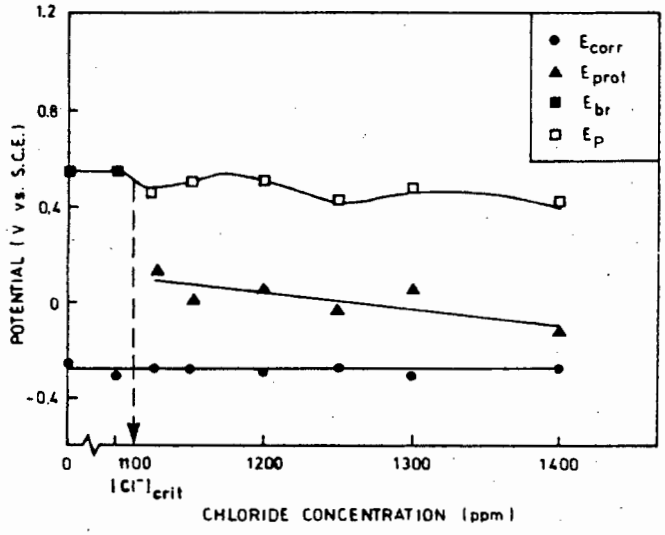

Figure C.8 : E_{corr} and E_{br} of AISI 431 in 1500 ppm SO_4^{2-} + 500 ppm NO_3^- versus chloride concentration at pH 6.2.

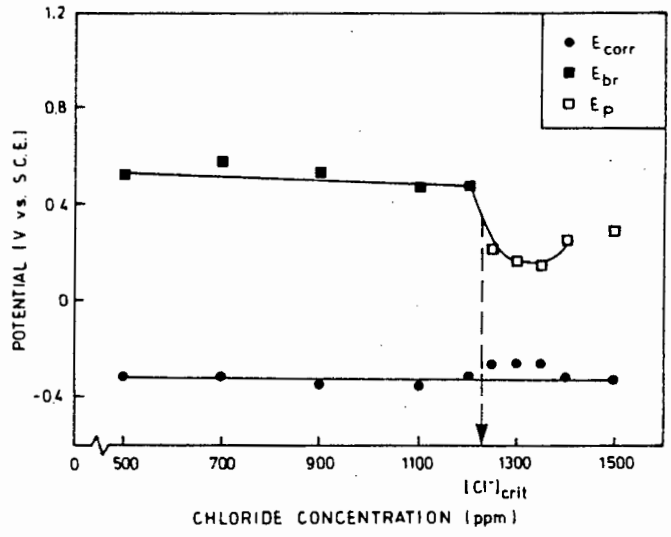

Figure C.9 : E_{corr} and E_{br} of AISI 431 in 200 ppm SO_4^{2-} + 1000 ppm NO_3^- versus chloride concentration at pH 6.2.

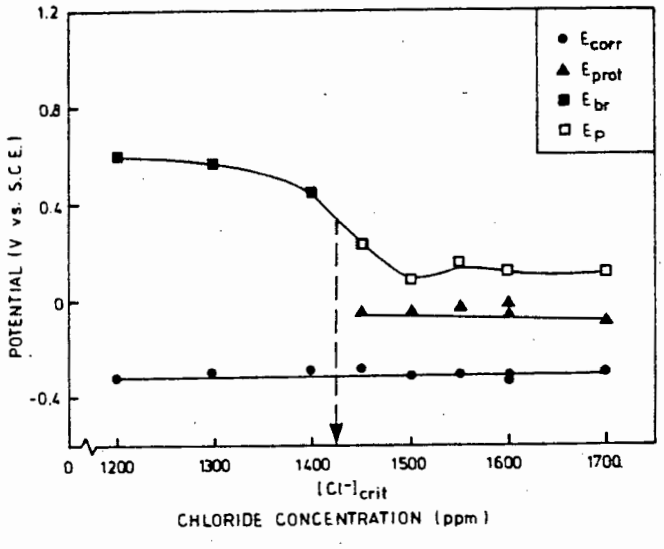

Figure C.10 : E_{corr} and E_{br} of AISI 431 in 500 ppm SO_4^{2-} + 1000 ppm NO_3^- versus chloride concentration at pH 6.2.

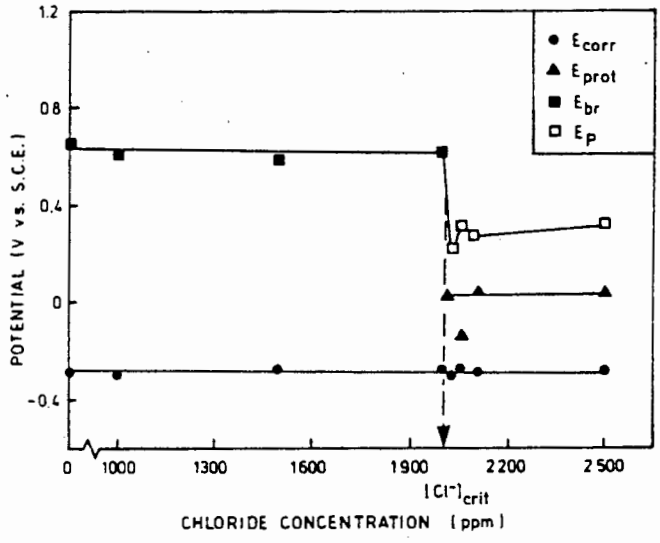

Figure C.11 : E_{corr} and E_{br} of AISI 431 in 1500 ppm SO_4^{2-} + 1000 ppm NO_3^- versus chloride concentration at pH 6.2.